2017

Technological advancements towards paper-based biomolecular diagnostics

BOSTON UNIVERSITY

COLLEGE OF ENGINEERING

Dissertation

TECHNOLOGICAL ADVANCEMENTS TOWARDS PAPER-BASED BIOMOLECULAR DIAGNOSTICS

by

DANA BRAFF

B.S., Massachusetts Institute of Technology, 2012
M.S., Boston University, 2016

Submitted in partial fulfillment of the

requirements for the degree of

Doctor of Philosophy

2017

Approved by

First Reader

Ahmad S. Khalil, Ph.D.
Assistant Professor of Biomedical Engineering

Second Reader

James J. Collins, Ph.D.
Termeer Professor of Medical Engineering and Science
Massachusetts Institute of Technology

Third Reader

Michael A. Lobritz, M.D, Ph.D.
Instructor in Medicine
Massachusetts General Hospital

Fourth Reader

Wilson W. Wong, Ph.D.
Assistant Professor of Biomedical Engineering

Fifth Reader

James E. Galagan, Ph.D.
Associate Professor of Biomedical Engineering
Boston University College of Engineering

Associate Professor of Microbiology
Boston University, School of Medicine

DEDICATION

לאמא

ACKNOWLEDGMENTS

I am incredibly fortunate to have been surrounded by a wonderfully supportive community, without whom I would not be the person I am today. Thank you:

To my advisors, Jim and Mo—for your guidance, patience, advice, and unwavering support. Through multiple project changes, lab moves, and, more recently, career decisions, I can't thank you enough for your confidence in me, your mentorship, and for providing me with the opportunity to pursue a PhD in your labs. Needless to say, I couldn't have done this without you.

To Dr. Dr. Mike Lobritz –for your patience and understanding in guiding me from my first project in the lab through to my last. I am incredibly grateful for the time and effort you put in to helping me learn and grow as a scientist, and I sincerely appreciate your foresight in pushing me to pick a project, stick with it, and accomplish something.

To Wilson Wong and James Galagan—for serving as last-minute additions to my committee. I began my PhD in your BE605 class, so it is fitting that I also end my PhD with your generous support and guidance.

To Keith and Nina—for teaching me all about cell-free paper-based systems.

To Melina and Melissa—for giving me the kick-start I needed in picking up a new project. You are both absolutely wonderful to work with and I learned so much from each

of you.

To the Collins Lab Postdocs—for the community you fostered. I've learned the most, collectively, from all of you and I appreciate the time you took to mentor, inspire, and support me and my fellow grad students. In particular: Nichole, Rebecca, Laura, Caroline, and Prerna—for being kind and understanding, RNO—despite the grouchiness, and Shims—for the puns.

To the Khalil Lab Grad Students—for always being excited to see me, and giving me helpful feedback and advice, even after the move to MIT.

To all my friends—for your support in many forms throughout the years. Roomies past and present (Jenny, Luly, Dan, Lucy, Brian, Saloni, Kartiek, Ivy, and Ben), Premed, KF, Ania and Vania, Danielle, and many more—I couldn't have done this without you all.

To my family—for everything. I love you.

TECHNOLOGICAL ADVANCEMENTS TOWARDS PAPER-BASED BIOMOLECULAR DIAGNOSTICS

DANA BRAFF

Boston University College of Engineering, 2017

Major Professor: Ahmad S. Khalil, Ph.D., Assistant Professor of Biomedical Engineering

ABSTRACT

Clinically tractable diagnostics must be low-cost, rapid, sensitive, easy to use, and adaptable to new targets. With its rational design, synthetic biology holds promise for developing diagnostic technologies that can address these needs. In particular, progress in synthetic biology has led to improved circuit-building abilities and a large collection of biomolecular sensors. However, these technologies fundamentally require transcription and translation, limiting their applicability to cellular contexts

In vitro cell-free expression systems that contain transcription and translation machinery provide the environment necessary for biologically-based technologies to function independently of living cells. Our lab recently developed a paper-based system for cell-free gene expression, which utilizes cell-free extracts that are freeze-dried on to paper and other porous substrates to allow for long-term preservation of synthetic circuits at room temperature. Our platform represents a scalable, cost-effective technology that is easy to use and is compatible with synthetic biology tools.

In this dissertation, I present several advancements to this diagnostic platform that are geared towards improving the system's clinical tractability. In the context of developing a diagnostic for Zika virus that could be deployed in low-resource settings, I

demonstrate improvements to diagnostic sensitivity and rapid sample processing that allow for detection of low femtomolar quantities of active virus directly from blood plasma samples. I also describe preliminary results towards a streamlined one-pot amplification-sensing reaction, and propose the development of a paper-based diagnostic for antibiotic susceptibility testing.

TABLE OF CONTENTS

LIST OF TABLES

LIST OF FIGURES

LIST OF ABBREVIATIONS

AST ..... antibiotic susceptibility testing

Cas9 ..... CRISPR associated protein 9

CDC ..... Centers for Disease Control and Prevention

CFPS ..... cell-free protein synthesis

CPRG ..... chlorophenol red-β-D-galactopyranoside

CRISPR ..... clustered regularly interspaced short palindromic repeats

DNA ..... deoxyribonucleic acid

dNTP ..... deoxyribose nucleoside triphosphate

E. coli ..... *Escherichia coli*

NASBA ..... nucleic acid sequence based amplification

NASBACC ..... NASBA-CRISPR cleavage

NTP ..... nucleoside triphosphate

PAM ..... protospacer adjacent motif

PCR ..... polymerase chain reaction

POC ..... point-of-care

RBS ..... ribosome binding site

RNA ..... ribonucleic acid

SD ..... standard deviation

SHERLOCK ..... Specific High-sensitivity Enzymatic Reporter unLOCKing

TXTL ..... transcription-translation

WHO ..... World Health Organization

CHAPTER ONE: BACKGROUND & INTRODUCTION

1.1 Synthetic biology

Synthetic biologists have developed tools for rationally engineering biological systems by studying and repurposing the design principles that underlie native gene networks (Khalil and Collins 2010; Cameron, Bashor et al. 2014). Early efforts in synthetic biology focused on the development of model transcriptional networks to recapitulate and understand native gene regulation (Elowitz and Leibler 2000; Gardner, Cantor et al. 2000; Basu, Gerchman et al. 2005; Stricker, Cookson et al. 2008). These works advanced our ability to engineer complex behavior, such as memory encryption and oscillatory gene expression, and catalyzed advancements in the rapid design and implementation of synthetic gene networks (Hasty, Dolnik et al. 2002; Canton, Labno et al. 2008; Gibson, Young et al. 2009; Lu, Khalil et al. 2009; Salis, Mirsky et al. 2009; Danino, Mondragon-Palomino et al. 2010; Egbert and Klavins 2012; Casini, Storch et al. 2015; Chen, Kim et al. 2015). The field has since moved towards repurposing natural biological processes for tunable and targetable synthetic gene regulation (Qi, Larson et al. ; Isaacs, Dwyer et al. 2004; Mutalik, Guimaraes et al. 2013; Green, Silver et al. 2014). The innate biochemistry of microorganisms has been harnessed in the biosynthesis of organic compounds, such as the antimalarial drug artemisinin (Ro, Paradise et al. 2006) and various opioids (Galanie, Thodey et al. 2015). Strides have also been made in engineering genetic networks for direct clinical applications, such as customized cancer treatments and nonconventional cell therapies (Ruder, Lu et al. 2011; Weber and Fussenegger 2012).

1.2 Diagnostic applications for synthetic biology tools

Synthetic biology platforms have been particularly useful for medical diagnostic purposes (Slomovic, Pardee et al. 2015). Biomolecular genetic circuits have been developed for whole-cell bio-sensing and *in vivo* diagnostics, including tumor imaging and mammalian gut monitoring. To further these diagnostic applications, natural biomolecular sensing capabilities have been mined and utilized as relevant reporting tools. For example, natural *E. coli* nitric oxide sensors have been reconfigured to allow for *in vivo* detection of nitric oxide levels that are indicative of inflammation (Archer, Robinson et al. 2012). Synthetic biologists are actively working to expand the repertoire of molecular sensors. The development of chimeric transcription factors that connect a desired signal to a known transcriptional output has proven successful in engineering novel ligand-inducible expression systems that respond to factors such as amino acids and light (Utsumi, Brissette et al. 1989; Tabor, Salis et al. 2009; Shis, Hussain et al. 2014). This progress has led to a large collection of DNA, RNA, and protein-based sensors for many industrially and clinically relevant inputs, including small molecules and pathogen markers. Clinically tractable diagnostics must be low-cost, rapid, sensitive, easy to use, and adaptable to new targets. With their rational design, synthetic biology platforms hold promise for diagnostic technologies that can address these needs.

1.2.1 Bacteriophage-based diagnostics

Phages are ideal vectors for diagnostic applications due to their highly specific targeting capabilities (Schofield, Sharp et al. 2012; Tawil, Sacher et al. 2014). Early

phage diagnostics took the form of plaque assays that identified bacteria based on their clearance by known phage species (Lu and Koeris 2011; Smartt and Ripp 2011; Schofield, Sharp et al. 2012; Tawil, Sacher et al. 2014). With time, phage-based diagnostics evolved to rely on genetic modifications to enhance signal amplification and shorten the time required to obtain a readable output (Lu, Bowers et al. 2013).

Phage infection markers have taken the form of standard fluorescent, bioluminescent, and colorimetric readouts (Figure 1) (Loessner, Rees et al. 1996; Tanji, Furukawa et al. 2004; Schofield, Molineux et al. 2009; Smartt and Ripp 2011; Schofield, Bull et al. 2012; Tawil, Sacher et al. 2014). In other approaches, external phage proteins have been genetically modified to allow for detection through auxiliary methods. In a demonstration of this methodology, Edgar *et al.* engineered phages to express a biotinylated capsid protein for direct detection by streptavidin-coated quantum dots, allowing identification of as few as ten bacterial cells per milliliter in one hour (Edgar, McKinstry et al. 2006). While modern-day clinical use of phage-based therapeutics has been dampened by strict regulatory requirements, commercial diagnostic applications of phages have had considerable success, with several such platforms available for use in laboratory and food-industry settings (Lu and Koeris 2011; Schofield, Sharp et al. 2012; Lu, Bowers et al. 2013; Nakonieczna, Cooper et al. 2015).

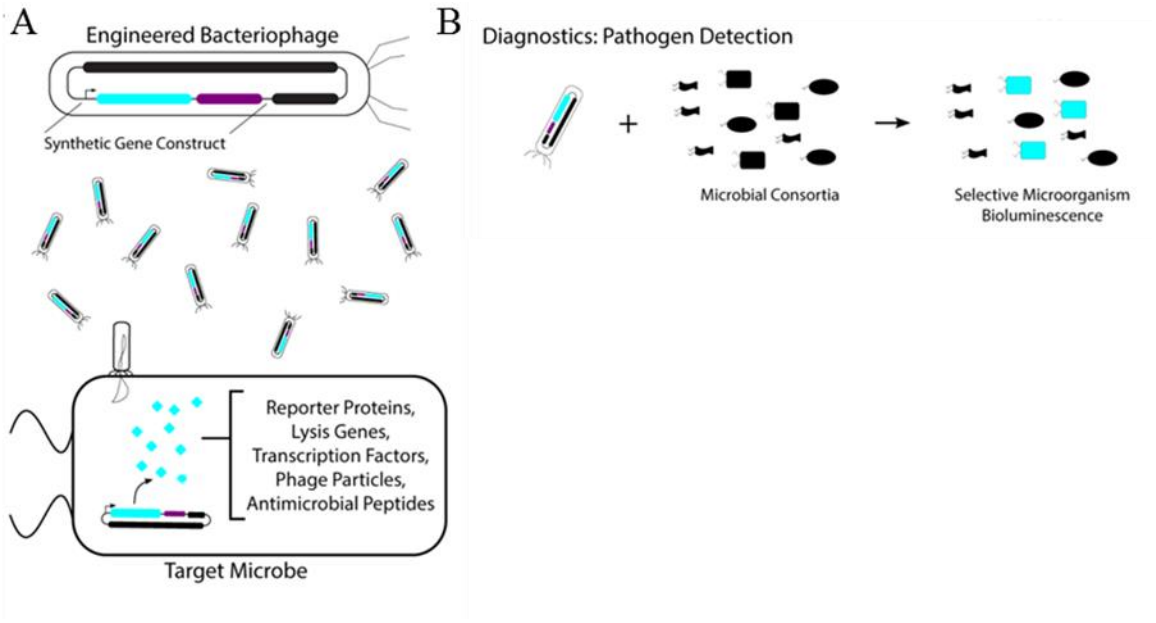

Figure 1. Engineered bacteriophage for diagnostic applications.
(A) The ability of phage to infect and replicate within a host microorganism has made them a popular technology platform. An engineered phage can induce the expression of heterologous constructs in a specific population of microbes for therapeutic and diagnostic applications. (B) By inducing microbial expression of reporter proteins, an engineered phage can facilitate bioluminescence that enables precise and sensitive detection of a microorganism. Figure taken from (Braff, Shis et al. 2016).

1.2.2 Synthetic probiotics as living diagnostics

Although most diagnostics have been developed for *in vitro* use, there has been a push toward the development of *in vivo* living diagnostic platforms. Much like therapeutic probiotics that secrete antimicrobial agents upon pathogen detection, diagnostic bacteria could persistently monitor the microbiome for a particular cue and respond with reporter expression.

Diagnostic probiotics must be able to encode long-term synthetic memory. A memory device ensures that the diagnostic microbe will "remember" transient

environmental events even after the trigger has disappeared, and that the microbe will convey accurate diagnostic information over the course of multiple cellular generations (Figure 2). Early efforts to engineer genetic memory focused on the creation of bistable toggle switches that flipped between two protein expression states in response to exogenous inducers (Gardner, Cantor et al. 2000), and native cellular networks such as the SOS signaling pathway responding to DNA damage (Kobayashi, Kærn et al. 2004). More recently, efforts to engineer biological memory transitioned to the use of DNA modification in order to overcome inherent stochasticity in gene expression and relieve the metabolic load imposed on the host microbe in sustaining circuit operation. Orthogonal integrases that can irreversibly flip DNA segments have been engineered to encode genetic memory (Friedland, Lu et al. 2009; Yang, Nielsen et al. 2014), and recombinase-based systems have been used to record the magnitude and duration of trigger exposure through regulated co-expression of recombinase and retron elements that modify genomic DNA (Farzadfard and Lu 2014).

Improvements in the design of synthetic cellular memory have led to the prospect of building reliable diagnostic probiotics for use *in vivo*. Researchers have endowed *E. coli* with a synthetic memory circuit that enables probiotic tracking of antibiotic exposure from within a mouse gut (Kotula, Kerns et al. 2014), and the human commensal microbe *Bacteroides thetaiotamicron*, has been instilled with integrase-based memory constructs that can operate *in vivo* to track external stimuli (Mimee, Tucker et al. 2015). These efforts demonstrate the budding feasibility of using engineered probiotics to persistently monitor the gut microbiome.

Thus far, most synthetic probiotics have been proof-of-concept models designed to respond to exogenous inducers rather than to host factors indicative of a diseased state or pathogen presence (Holmes, Kinross et al. 2012). Mining natural bacterial pathways can help develop more relevant sensing capabilities, such as the detection of nitric oxide levels that are indicative of gut inflammation (Archer, Robinson et al. 2012). To further expand the repertoire of pathogen sensors, development of chimeric transcription factors that connect a desired signal to a known transcriptional output may be a productive strategy (Shis, Hussain et al. 2014; Chan, Lee et al. 2016). Such efforts have been successful in engineering novel ligand-inducible expression systems that respond to factors such as amino acids and light (Utsumi, Brissette et al. 1989; Tabor, Salis et al. 2009). Expanding the ability of engineered probiotics to sense their environment will greatly improve their clinical relevance as diagnostic and therapeutic agents.

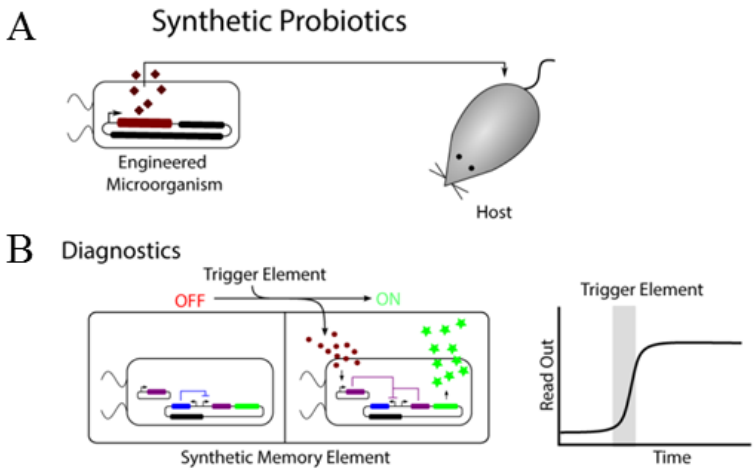

Figure 2. Synthetic probiotics for diagnostic applications.
(A) Engineered microorganisms can be deployed *in vivo* to provide prophylactic, therapeutic, and diagnostic benefits. (B) By modifying probiotic microbes to express synthetic gene circuits that facilitate cellular memory, probiotics can be used to persistently monitor the host and report on the presence of a molecule or signal of interest. Figure taken from (Braff, Shis et al. 2016).

1.2.3 Cell-free and paper-based platforms

Although phages and engineered probiotics are suitable for a wide range of diagnostic applications, other biologically-based diagnostic platforms are less tractable *in vivo*. Progress in synthetic biology has led to improved circuit-building abilities and a large collection of RNA and DNA sensors; however, these technologies fundamentally require transcription and translation, limiting their applicability to cellular contexts (Isaacs, Dwyer et al. 2004; Khalil, Lu et al. 2012; Green, Silver et al. 2014; Slomovic and Collins 2015).

In vitro cell free expression systems that contain transcription and translation machinery provide the environment necessary for biologically-based technologies to function independently of living cells (Carlson, Gan et al. 2012). Cell-free transcription and translation (TXTL) systems have been used for *in vitro* protein synthesis for research purposes for many years (Hodgman and Jewett 2012; Smith, Wilding et al. 2014). These systems may be comprised of crude cell extract or they may be reconstituted *de novo* from purified cellular transcription and translation enzymes. Though cell-free systems are available commercially, there has been a recent effort to ease in-house production of crude cell extracts in laboratory settings (Sun, Hayes et al. 2013; Kwon and Jewett 2015).

Cell free protein synthesis (CFPS) expression systems have recently been recognized for their ability to support more complicated gene networks (Roberts and Paterson 1973; Endo and Sawasaki 2006; Hodgman and Jewett 2012; Smith, Wilding et al. 2014). Synthetic gene circuits have been shown to operate well within these systems, often with the added benefit of reduced cross-talk and minimal off-target effects. Further,

the more precise control of conditions offered by *in vitro* expression systems has enabled the high-throughput tuning of synthetic constructs (Hodgman and Jewett 2012; Sun, Hayes et al. 2013; Sun, Yeung et al. 2013; Smith, Wilding et al. 2014). Despite these advancements, the application of cell-free methods has been limited to laboratory settings due to strict storage requirements, including the need for refrigeration.

To mitigate these constraints, Pardee *et al.* developed a paper-based system for cell-free gene expression, providing a simple platform for the real-world application of engineered genetic systems (Figure 3) (Pardee, Green et al. 2014). This paper-based technology utilizes cell-free extracts freeze-dried on paper and other porous substrates to allow for long-term preservation of synthetic circuits at room temperature. The system is low-cost, at about $0.04 to $0.65 per reaction, and can be interfaced with an electronic optical reader for optimal performance in low-resource settings (Figure 3B). In a noteworthy demonstration, RNA toehold switch sensors were used to develop a paper-based colorimetric diagnostic that was able to rapidly detect and distinguish between the Sudan and Zaire Ebola strains from the 2014 outbreak (Green, Silver et al. 2014; Pardee, Green et al. 2014; Carroll, Matthews et al. 2015). The paper-based system has also been shown to integrate well with non-RNA sensor modalities such as ligand-inducible promoters and FRET-based nanosensors, and to allow for complex circuitry that encodes molecular-based logic. This platform is primed for antimicrobial diagnostic development and represents a scalable, cost-effective technology that is sensitive, easy to use, and compatible with synthetic biology tools.

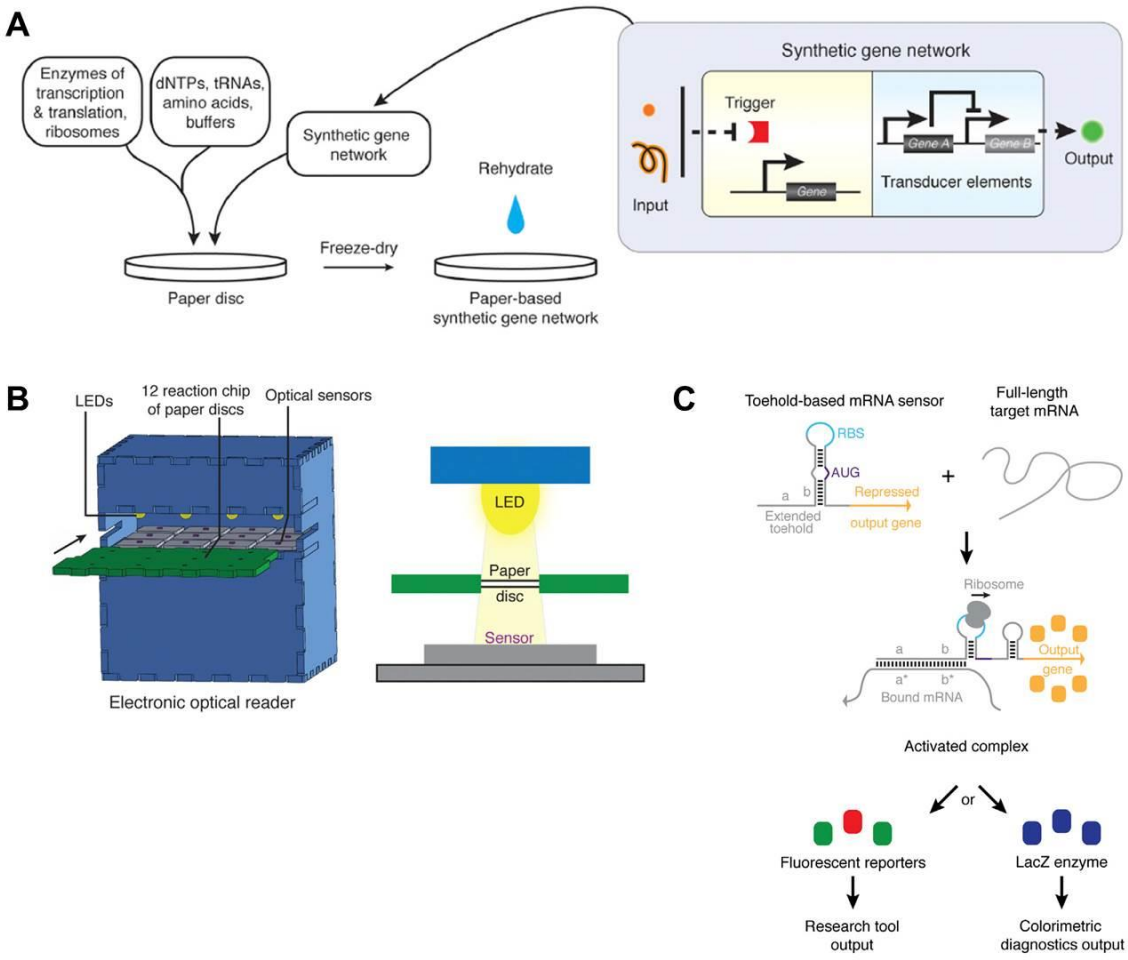

Figure 3. Cell-free paper-based platform for real world applications of synthetic gene networks.

(A) Components necessary for transcription and translation are freeze-dried along with synthetic gene networks on to a paper substrate. These components can be stored at room temperature and utilized for diagnostic purposes upon rehydration. (B) A low-cost electronic optical reader was developed to read and process colorimetric signals from cell-free paper-based reactions. (C) Toehold switches are second-generation riboregulator elements that can be designed to sense full-length mRNA sequences. In the inactive complex, translation of the output gene is inhibited by secondary structure of the toehold. When target mRNA is present, the toehold switch adopts an alternate conformation that allows for translation of the reporter gene. Reporter genes can take the form of fluorescent and colorimetric outputs. Figure modified from (Pardee, Green et al. 2014).

1.3 Dissertation overview

In this dissertation I describe several advancements to the paper-based cell-free platform that are geared towards improving the system's clinical tractability.

The next two chapters (Chapters 2 and 3) focus on developments in diagnostic sensitivity and sample processing in the context of building a diagnostic for Zika virus that could be deployed in low-resource settings. As such, the next section of this chapter (Section 1.4) provides background information on the Zika diagnostic that will be referenced throughout the dissertation. All text and figures describing the Zika work are adapted from (Pardee, Green et al. 2016).

The following chapters focus on next-step advancements to the paper-based platform, including developing a one-pot amplification-sensing reaction to improve both speed and sensitivity (Chapter 4) and a proposal for developing a paper-based diagnostic for antibiotic susceptibility testing (Chapter 5). All methods are described in detail in Chapter 6.

1.4 Rapid, low-cost detection of Zika virus using programmable biomolecular components

The emerging outbreak of Zika virus in the Americas has brought this once obscure pathogen to the forefront of global healthcare. Mostly transmitted by *Aedes aegypti* and *Aedes albopictus* mosquitoes, Zika virus infections have been further spread by international travel, and have expanded to large, heavily populated regions of South, Central and North America (Bogoch et al., 2016). Correlations between the increase in

Zika virus infections and the development of fetal microcephaly (Calvet et al., 2016; Galindo-Fraga et al., 2015; Victora et al., 2016) and Guillain–Barré syndrome have resulted in the declaration of a public health emergency by the World Health Organization (WHO) and a call for fast-tracked development of Zika virus diagnostics (Oehler et al., 2014; Smith and Mackenzie, 2016; WHO, 2016).

Synthetic biology is an emerging discipline that has great potential to respond to such pandemics. The increasing ability of synthetic biologists to repurpose and engineer natural biological components for practical applications has led to new opportunities for molecular diagnostics (Kotula et al., 2014; Lu et al., 2013; Slomovic et al., 2015). We previously developed two biotechnologies that dramatically lower the cost of and technical barriers to the development of synthetic biology-based diagnostics. The first technology, programmable RNA sensors called toehold switches, can be rationally designed to bind and sense virtually any RNA sequence (Green et al., 2014). The second technology, a freeze-dried, paper-based, cell-free protein expression platform, allows for the deployment of these toehold switch sensors outside of a research laboratory by providing a sterile and abiotic method for the storage and distribution of genetic circuits at room temperature (Pardee et al., 2014). We combined these technologies to create a platform for rapidly and inexpensively developing and deploying diagnostic sensors.

In the context of the Zika virus outbreak, the paper-based sensors offer a solution to the critical challenges facing diagnosis of the virus. Standard serological approaches, such as antibody detection, are limited in diagnostic value due to cross-reactivity in patients that have previously been infected by other flaviviruses circulating in the region.

As a result, accurate diagnosis requires nucleic acid-based detection methods, such as PCR and isothermal nucleic acid amplification (Lanciotti et al., 2008; de M Campos et al., 2016; Tappe et al., 2014; Zammarchi et al., 2015). However, such techniques are relatively expensive, require technical expertise to run and interpret, and utilize equipment that is incompatible with use in remote and low-resource locations where surveillance and containment are critically needed.

Here, we demonstrate the rapid development of a diagnostic workflow for sequence-specific detection of Zika virus that can be employed in low-resource settings (Figure 4). We have addressed limitations in the practical deployment of nucleic acid-based molecular diagnostics by combining isothermal RNA amplification with toehold switch sensors on our freeze-dried, paper-based platform. We automate the amplification primer and sensor design process using *in silico* design algorithms and demonstrate a high-throughput pipeline to assemble and test 48 Zika sensors in less than seven hours. Clinically relevant sensitivity is attained using our amplification and detection scheme, and we report no significant detection of the closely related Dengue virus. To further increase diagnostic capabilities, we develop a CRISPR/Cas9-based module that discriminates between Zika genotypes at single-base resolution. Finally, we employ a simple sample-preparation protocol to reliably extract viral RNA, and demonstrate robust detection with this scheme on active Zika virus samples.

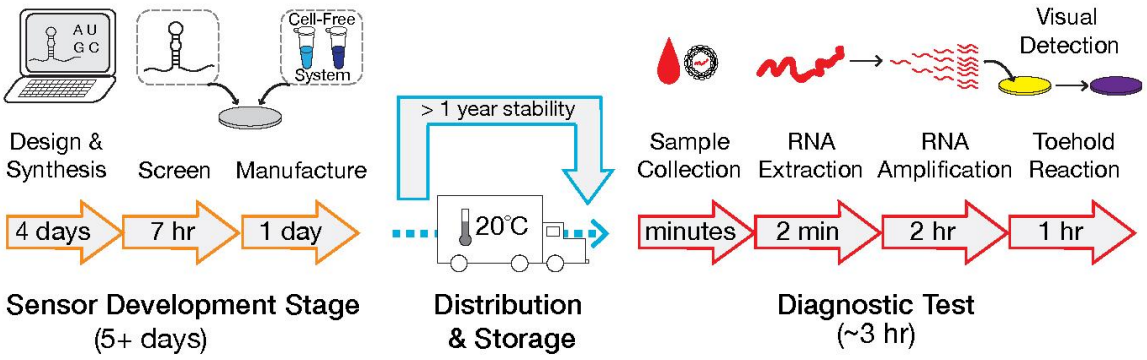

Figure 4. Workflow for the rapid prototyping of paper-based biomolecular sensors for portable and low-cost diagnostics.
Using sequence information from online databases, primers for isothermal RNA amplification and toehold switch-based RNA sensors were designed *in silico* using purpose-built algorithms. Once synthesized, the resulting sequence-specific toehold sensors can be assembled and validated in less than seven hours. In under a day, validated sensors can be embedded into paper and freeze-dried along with a cell-free transcription and translation system to be deployed in the field as stable diagnostics. For the diagnostic test, extracted RNA is isothermally amplified via NASBA and used to rehydrate the freeze-dried paper sensors. The detection of the appropriate trigger RNA is indicated by a color change in the paper disc from yellow to purple. Figure taken from (Pardee, Green et al. 2016).

1.4.1 *In silico* toehold switch design for Zika virus detection

RNA-based sensors have been optimized and employed by synthetic biologists in many cellular engineering and diagnostic pursuits. Riboregulators are an example of such RNA-based devices that confer tunable control of gene expression by induced secondary structure changes that allow for transcript translation in response to the binding of a trans-acting RNA (Isaacs, Dwyer et al. 2004; Callura, Dwyer et al. 2010; Callura, Cantor et al. 2012). Though they have been used as biological devices to study microbial toxin-antitoxin systems (Callura, Dwyer et al. 2010) and to gain insight into the underlying mechanisms of action of antibiotic treatments (Dwyer, Kohanski et al. 2007; Kohanski, Dwyer et al. 2007), riboregulators can also serve as simple molecular reporters for the

presence of RNA sequences by inducing expression of reporter proteins (Pardee, Green et al. 2014).

Green et al. recently developed a second-generation riboregulator variant that enables tunable regulation of endogenous RNA transcripts and can also be employed in microbial screens and transcript detection (Figure 3C) (Green, Silver et al. 2014). Notably, toehold switch sensors have been utilized as diagnostic devices on the paper-based platform, demonstrating high sensitivity and rapid readout capabilities in the detection of medically interesting RNAs, such as Ebola transcripts and antibiotic resistance markers (Pardee, Green et al. 2014). These sensors display a high level of orthogonality and can be easily and rapidly designed and tested. Toehold switches thus lend themselves to a wide array of medical diagnostic applications, particularly in conjunction with the paper-based platform.

Toehold switch sensors are programmable synthetic riboregulators that control the translation of a gene via the binding of a *trans*-acting trigger RNA. The switches contain a hairpin structure that blocks gene translation in *cis* by sequestration of the ribosome binding site (RBS) and start codon. Upon a switch binding to a complementary trigger RNA, sequestration of the RBS and start codon is relieved, activating gene translation (Figure 5A and 5B) (Green et al., 2014). To allow for colorimetric detection of trigger RNA sequences, the sensors can be designed to regulate translation of the enzyme LacZ, which mediates a color change by converting a yellow substrate (chlorophenol red-β-D-galactopyranoside, CPRG) to a purple product (chlorophenol red).

Toehold switch sensors for sequence-based detection of Zika virus were generated

using a modified version of the previously developed *in silico* design algorithm (Supplemental Information, (Pardee, Green et al. 2016)). The modified algorithm screened the genome of the Zika strain prevalent in the Americas (Genbank accession number: KU312312) for regions compatible with RNA amplification and toehold switch activation. The selected Zika genome regions were then computationally filtered to eliminate potential homology to the human transcriptome and to a panel of closely related viruses, including Dengue and Chikungunya. A total of 24 unique regions of the Zika genome compatible with downstream sensing efforts were identified.

Two toehold switches, each utilizing a different design scheme, were designed for each region, resulting in a total of 48 sensors. The first design scheme, termed the A series, utilizes a modification to the original toehold switch (Green et al., 2014) that reduces the size of the loop domain from 18-nts to 11-nts (Figure 5A) to discourage loop-mediated docking of the ribosome and therefore reduce leakage in the OFF state. The second design scheme, termed the B series, features a 12-nt loop and incorporates a more thermodynamically stable stem in order to lower OFF state gene expression (Figure 5B).

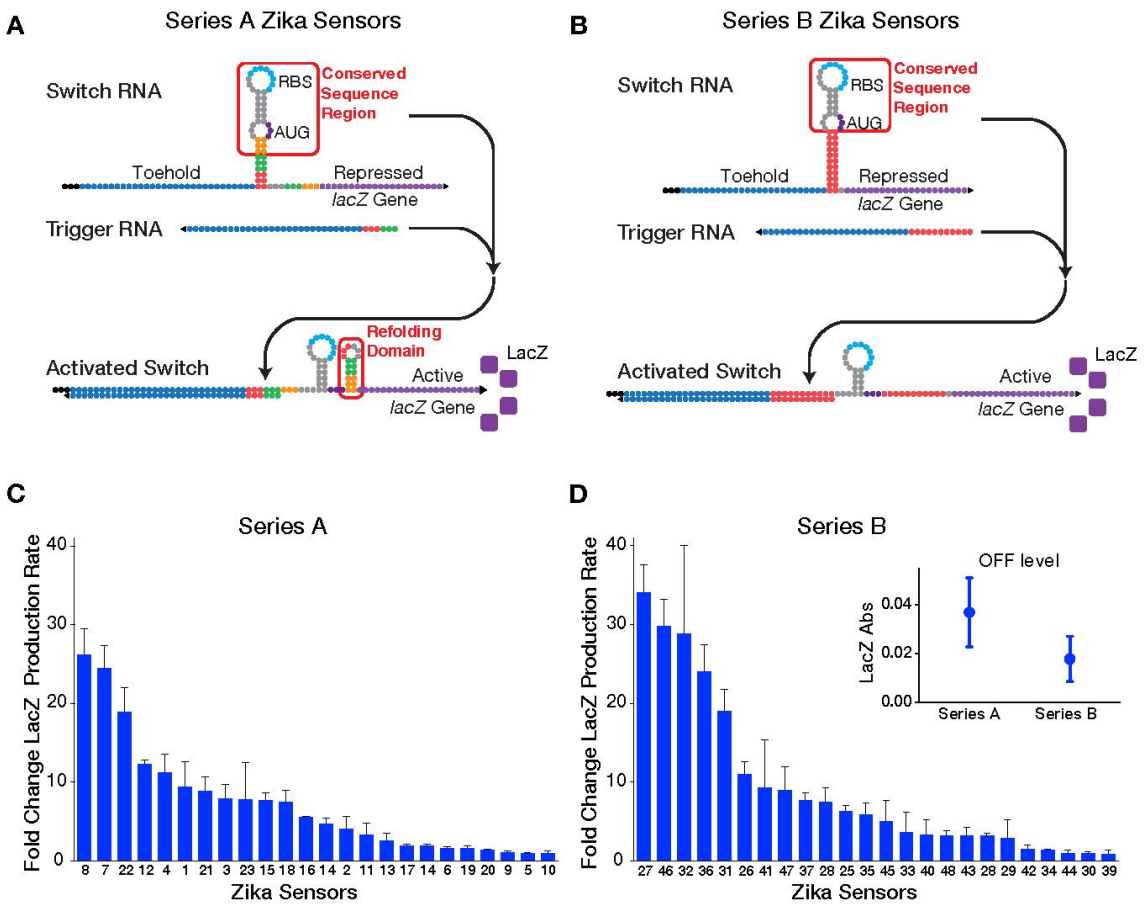

Figure 5. Rapid prototyping of 48 paper-based RNA toehold sensors for Zika virus detection.

(A) Series A toehold switch sensor schematic. The sensor design from Green *et al*. (2014) was modified with a shortened 11-nt loop sequence to reduce leakage of output gene expression. (B) Series B toehold switch sensor and schematic. Based on the same Zika genomic region as the A series, these sensors include a 12-nt loop and lack of the refolding domain. These modifications were made to further reduce LacZ reporter leakage in the OFF state. (C) Maximum fold change in the rate of LacZ production for the Series A Zika virus RNA sensors during the first 90 min at 37°C. Fold change of LacZ production rate is determined from the slope of absorbance at 570 nm over time (sensor alone vs. sensor with 3000 nM RNA trigger). Sensors are ordered according to fold change. (D) Maximum fold change in the rate of LacZ production for the Series B Zika virus RNA sensors during the first 90 min at 37°C. Error bars represent SD from three replicates. Inset: average LacZ absorbance of the OFF state at 60 min indicates an overall reduction in LacZ reporter leakage for the Series B sensors. Error bars represent SD across the 24 sensors. See also Figure S1 and Table S1. Figure taken from (Pardee, Green et al. 2016).

1.4.2 Rapid *in vitro* sensor assembly and screening for Zika virus

In vitro assembly and initial screening of all 48 sensors took place in a seven-hour time period, with low costs associated with sensor development (DNA input $20 USD/sensor) and testing ($0.10 – $1/test). All 48 sensors and 24 targeted genomic regions were assembled in-house using *in vitro* protocols. Toehold switches were constructed by ligating the sensors (~130 nt) to a LacZ reporter element in a single two-hour PCR-based step. Sensor performance screening to assess each sensor against its respective trigger RNA element (Zika genome fragment) was completed using low volume, cell-free transcription and translation reactions on paper. We found that 25 (52%) of the 48 sensors produce a fold change of five or greater in the presence of the appropriate trigger element (128 – 178 nucleotide regions of the Zika genome; Figures 5C, 5D and S1 from (Pardee, Green et al. 2016)). The top-ranked sensors exhibited activation as high as 34-fold over sensor alone (sensor 27B), and were activated in as quickly as 20 minutes after incubation at 37°C (sensors 7A and 8A). For all sensors, maximum fold change occurred within the first 90 minutes. Averaging the LacZ output from sensors not exposed to trigger RNA confirmed that the low background design of the series B toehold switch sensors successfully reduced signal leakage (Figure 5D inset).

CHAPTER TWO: ADVANCEMENTS IN SENSITIVITY AND DETECTION

2.1 Introduction

Our first area of focus in building on the paper-based diagnostic's clinical relevance was to improve the diagnostic sensitivity of the toehold sensors. Our goal was to develop a simple method for signal amplification that would be compatible with applications in low-resource settings. As such, we decided to focus on a technique called NASBA (nucleic acid sequence based amplification). NASBA is an isothermal RNA amplification process that requires minimal temperature cycling and could thus be easily integrated into a diagnostic workflow in low-resource areas (Cordray and Richards-Kortum, 2012).

This chapter focuses on the development and demonstration of a NASBA protocol that is compatible with our paper-based toehold sensors. The following section (Section 2.2) delineates preliminary experiments that demonstrate the compatibility of the NASBA amplification scheme with paper-based toehold detection. The next section (Section 2.3) outlines a demonstration of this amplification scheme in the context of the Zika diagnostic.

2.2 Preliminary NASBA experiments and results

2.2.1 NASBA overview

NASBA is a promising candidate for use with our diagnostic scheme because it is known to be extremely sensitive and has a proven track record in field-based diagnostic applications (Cordray and Richards-Kortum, 2012). The amplification process begins

with reverse transcription of a target RNA that is mediated by a sequence-specific reverse primer to create an RNA/DNA duplex. RNase H then degrades the RNA template, allowing a forward primer containing the T7 promoter to bind and initiate elongation of the complementary strand, generating a double-stranded DNA product. T7-mediated transcription of the DNA template then creates copies of the target RNA sequence. Importantly, each new target RNA can be detected by the toehold switch sensors and also serve as starting material for further amplification cycles. NASBA requires an initial heating step (65°C), followed by isothermal amplification at 41°C (Figure 6) (Guatelli et al., 1990).

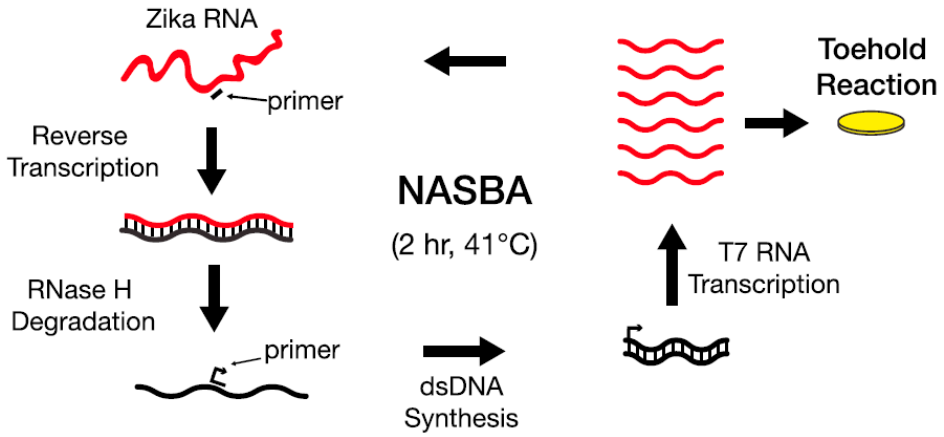

Figure 6. NASBA-mediated RNA amplification.
NASBA begins with reverse transcription of a target RNA, mediated by a sequence-specific reverse primer to create an RNA/DNA duplex. RNase H then degrades the RNA template, allowing a forward primer containing the T7 promoter to bind and initiate elongation of the complementary strand, generating a double-stranded DNA product. T7-mediated transcription of the DNA template then creates copies of the target RNA sequence. Each new target RNA can be detected by the toehold switch sensors and also serve as starting material for further amplification cycles. Figure taken from (Pardee, Green et al. 2016).

2.2.2 NASBA produces RNA that is compatible with toeholds

Our first goal was to demonstrate compatibility of the NASBA amplification product with the toehold sensors. Our preliminary experiments were performed with toehold sensors for the Kanamycin resistance gene using two different sets of NASBA primers. We were able to confirm that the NASBA-amplified RNA products from both sets of NASBA primers were compatible with activating the toehold switches (Figure 7). All experiments in this section were done in collaboration with Melina Fan.

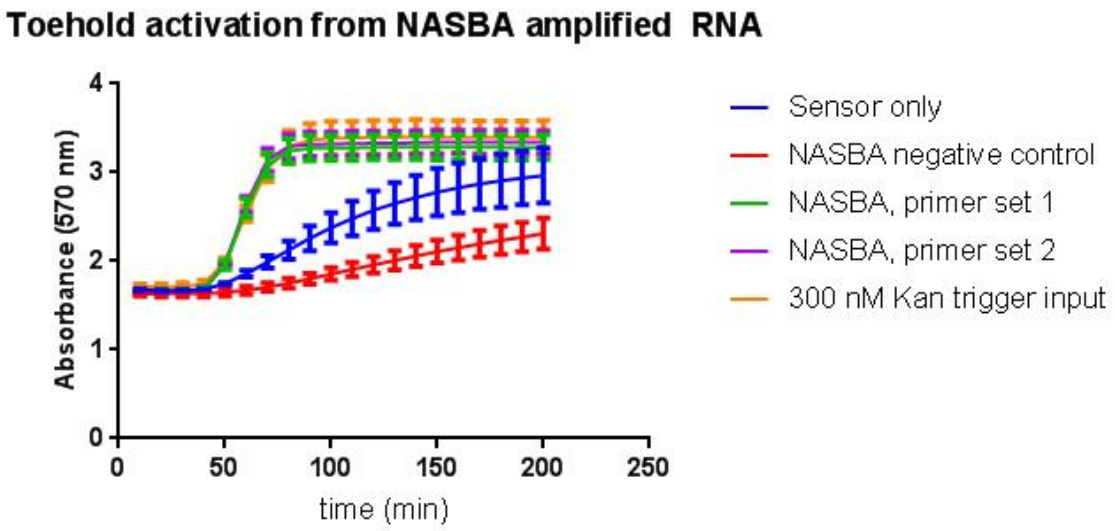

Figure 7. Toehold activation from NASBA-amplified RNA.
NASBA was performed on trigger RNA using two different sets of primers. Both primer sets were able to mediate sufficient RNA amplification for triggering the paper-based toehold switches.

2.3 Assessing and improving Zika sensor sensitivity

We then proceeded to test the NASBA protocol on the Zika sensors. We selected top performing sensors from both the A and B series for trigger RNA titration experiments, and found that all chosen sensors were activated with as little as 30 nM of trigger RNA (Figure 8A). The sensors displayed a linear response to RNA concentration, providing semi-quantitative information on input trigger RNA values (Figure S2A from (Pardee, Green et al. 2016)). Additionally, our top three sensors were shown to be highly orthogonal to each other when challenged with a high dose of trigger RNA from off-target Zika sequences (3000 nM) (Figure S2B from (Pardee, Green et al. 2016)).

Though the sensors displayed specificity for their respective Zika RNA trigger, they were unable to detect clinically relevant RNA concentrations. Zika viral loads have been documented up to 202 x 10^6 copies/ml (365 fM) in urine (Gourinat et al., 2015). However, viral loads in saliva and serum are reportedly even lower, with 3 x 10^6 copies/mL (4.9 fM) (Barzon et al., 2016) reported in patient saliva and 2.5 x 10^6 copies/ml (4.1 fM) (Zika experimental science team) and 7.2 x 10^5 copies/ml (1.2 fM) (Lanciotti et al., 2008) in primate and patient serum respectively. Accordingly, to increase the sensitivity of our diagnostic platform, we incorporated an isothermal RNA amplification technique known as NASBA into our workflow (Figure 6).

NASBA was performed on trigger RNA corresponding to Zika genomic regions for sensors 27B and 32B. Trigger RNAs were spiked into either water or human serum (7%) to more closely mimic clinical samples. NASBA reactions were run for two hours and then applied to freeze-dried, paper-based sensors. We saw detection with Zika

sensors from NASBA reactions initiated with as little as 3 fM of trigger RNA (Figure 8B), a value well within the range of reported patient viral loads. Zika sensor detection of NASBA-amplified trigger RNA proved to be reliable on samples spiked into either serum or water (Figure 9A). Additionally, for reactions initialized with high concentrations of trigger RNA (>300 fM), NASBA reaction times could be reduced to as little as 30 minutes (Figure 9B). NASBA reagents are compatible with freeze-drying (Figure 9C) and could therefore be easily deployed and utilized alongside our paper-based sensors. We also demonstrated that NASBA can be run in the absence of the initial heating step (65°C) (Figure 9D), further reducing the technical and power requirements for deployment.

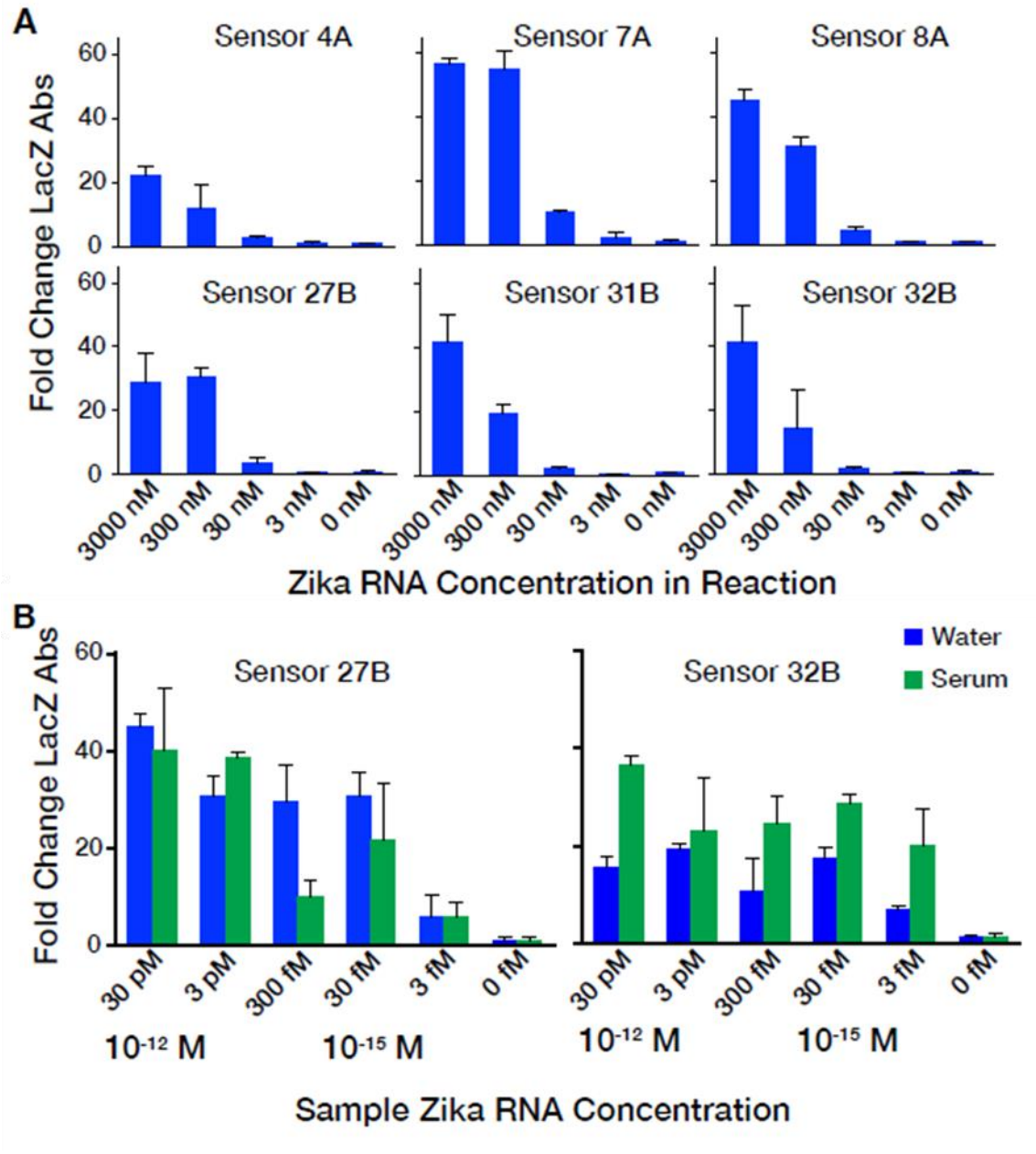

Figure 8. Isothermal RNA amplification improves sensitivity of toehold switch sensors to allow for detection of femtomolar concentrations of Zika virus fragments.
(A) Sensitivity of six of the best performing Zika Series A and B sensors without RNA amplification. Fold change is calculated from absorbance (570 nm) after 30 min at 37°C. Error bars represent SD from three replicates. (B) Zika RNA fragments diluted in water or 7% human serum were amplified using NASBA with input concentrations ranging from 30 pM down to 3 fM. A 1:7 dilution of the NASBA reaction in water was then used to rehydrate freeze-dried, paper-based reactions containing sensors 27B and 32B. Fold change is calculated as described in (A) after 30 min at 37°C. Figure taken from (Pardee, Green et al. 2016).

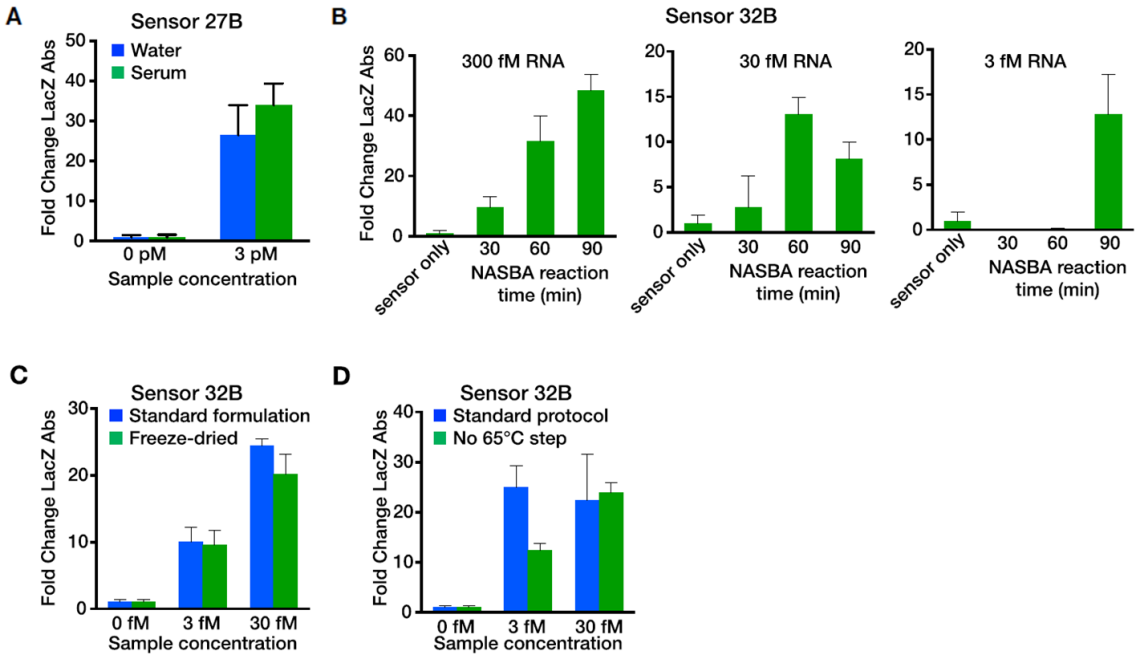

Figure 9. Further analysis on NASBA-mediated sensor sensitivity.
(A) Reproducibility of NASBA reactions. Samples of Zika RNA in water or 7% human serum were amplified in three independent 2 hr NASBA reactions. Each NASBA reaction was diluted 1:7 in water and used to rehydrate three freeze-dried, paper-based reactions containing sensor 27B for a total of nine replicates. Fold change was calculated from absorbance (570 nm) after 30 min at 37^0C. Error bars represent SD from nine replicates for the 3pM sample and three replicates for the 0pM sample. (B) Effect of NASBA reaction time on sensitivity. Samples of Zika RNA in 7% human serum were amplified in NASBA reactions for 30, 60, and 90 min. Diluted NASBA reactions (1:7) were tested with sensor 32B. Fold change was calculated as above. Error bars represent SD of three replicates. (C) NASBA with freeze-dried reagents. Samples of Zika RNA in 7% human serum were amplified by NSABA reagents in the standard formulation and by reagents freeze-dried in-house. Fold change and error bars were calculated as above after 60 min. (D) Removing the 65^0C step from NASBA protocol. Samples of Zika RNA in 7% human serum incubated at 95^0C for two minutes, mimicking viral lysis, and then amplified by NASBA according to the standard procedure without the 65^0C step. Fold change and error bars were calculated as above after 60 min. Figure taken from (Pardee, Green et al. 2016).

2.3.1 Moving towards a field-ready diagnostic platform

To move our experiments toward conditions more representative of those found in clinics worldwide, we focused on three key efforts: (1) testing sensor specificity against related viruses that share clinical symptoms, partial homology, and geographic range with Zika virus, (2) building a second-generation portable, battery-powered reader to provide lab-quality results in low-resource environments, and (3) developing a low-cost and tractable method for viral RNA extraction (Chapter 3).

Although our sensor design algorithm screened for Zika genomic sequences that are mostly distinct from those of related viruses, the targeted Zika sequences do share substantial similarity (51%–59%) with their Dengue virus counterparts (Figure S3A and S3B from (Pardee, Green et al. 2016)). To test the Zika sensors for possible cross-reactivity, we exposed the sensors to regions of the Dengue genome that share a degree of homology with regions targeted in the Zika genome. Sensors 27B and 32B were treated with high concentrations of RNA amplicons (3000 nM) from either Zika or Dengue genomic regions. As seen in Figure 10A, Dengue RNA sequences failed to activate the toehold switch sensors. We also tested our NASBA primer sets for specificity to their targeted Zika sequences by applying the NASBA-mediated amplification and paper-based detection scheme to 300 fM inputs of the Dengue and Zika RNA in human serum (7%). Again, we did not see a response to the Dengue RNA sequences, demonstrating robust sequence specificity in our amplification and detection scheme (Figure 10B).

As part of our efforts to advance the paper-based sensor platform toward field-ready diagnostics, we designed a second-generation portable electronic reader to serve as

an accessible, low-cost companion technology that provides robust and quantitative measurements of sensor outputs. The electronic reader was assembled using readily available consumer components, open-source code, and laser-cut acrylic housing, with a total cost of just under $250 (Figure S4 from (Pardee, Green et al. 2016)). The reader is powered by a lithium ion battery (18.5 hours) that can be re-charged via micro USB, and houses onboard data storage (4 GB) to resolve the need for an attached laptop during diagnostic reads (Pardee et al., 2014). To achieve sensitive detection of toehold switch signal output, an acrylic chip that holds the freeze-dried, paper-based reactions is placed into the reader between an LED light source (570 nm) and electronic sensors (Figure S4B from (Pardee, Green et al. 2016)). Using onboard electronics, each sample is read 29 times per minute, providing low-noise measurements of changes in light transmission due to LacZ-mediated color change.

To demonstrate the utility of the companion reader, we monitored detection of 1 fM and 3 fM of Zika RNA amplicons that had been amplified in NASBA reactions for 2.5 hours. The reader detected significant signal from both samples, which are within the reported range of Zika virus in patient serum (1.2 fM) and urine (365 fM) (Gourinat et al., 2015; Lanciotti et al., 2008), after just over 20 minutes (Figure 10C).

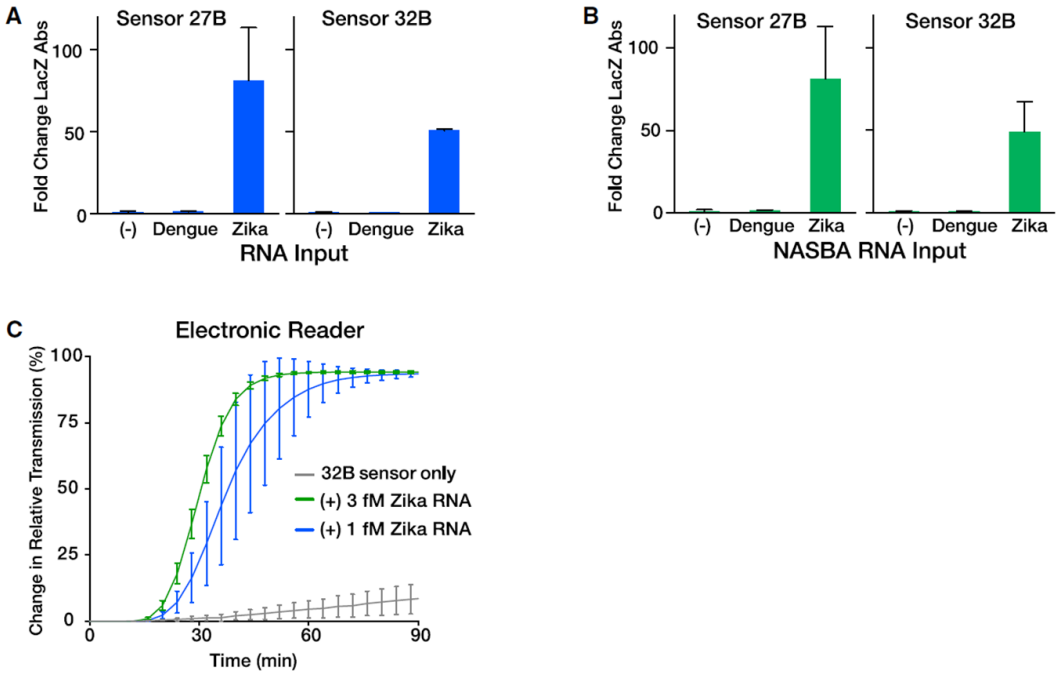

Figure 10. Moving towards a field-ready diagnostic for Zika virus.
(A) Sequence specificity of Zika virus sensors 27B and 32B. Sensors were challenged with 3,000 nM of RNA corresponding to target sequences from the Zika virus or the homologous region of the Dengue virus. Fold change is calculated from absorbance (570 nM) at 60 min after rehydration and incubation of freeze-dried, paper-based reactions at 37^0C. Error bars represent SD from three replicates. (B) Zika virus sensors 27B and 32B were tested for specificity using NASBA reaction products derived from 300 fM input RNA corresponding to target genomic regions of the Zika or Dengue viruses in 7% human serum. Fold change was calculated as in (A). (C) Using the portable electronic reader, time-course data were collected for Zika virus sensor 32B in the presence of RNA amplified from 1 fM or 3 fM inputs of trigger RNA in 7% human serum. To increase sensitivity, NASBA reactions were run for 2.5 hr. Graphs plot the relative absorbance of 570 nm wavelength light compared to background, which was collected every minute from freeze-dried, cell-free reactions embedded into paper. Figure taken from (Pardee, Green et al. 2016).

2.4 Discussion

To the best of our knowledge, this is the first report where NASBA, or any RNA amplification scheme, has been linked to a downstream synthetic gene network as an output detection method. This innovative development addresses several key technical

and economic challenges in the employment of isothermal amplification methods in the field (Cordray and Richards-Kortum, 2012). Namely, although NASBA has exceptional sensitivity to low-level infections (Casper et al., 2007; Cordray and Richards-Kortum, 2012; Ulrich et al., 2010), the technique is costly ($5–$20/test) and susceptible to contamination that can lead to off-target products and false positives (Cordray and Richards-Kortum, 2012). Our diagnostic scheme addresses both of these points and brings NASBA closer towards application in low-resource settings. The low volume paper-based reactions only use a fraction of a microliter of NASBA product ($0.51/μl), significantly reducing the total cost of NASBA per test. Additionally, linking NASBA to a synthetic gene network for signal detection allows for rapid and sensitive output reads in a cost-effective manner ($0.10 – $1/test) that is practical for use in low-resource settings. Our ability to eliminate the initial 65°C heating step (Figure 10D) traditionally used in NASBA reactions streamlines the diagnostic protocol for in-field use and reduces the requirements of the hardware necessary for monitoring results. Finally, we have shown that NASBA reagents can be freeze-dried (Figure 10C) and therefore could be distributed around the world at room temperature alongside our toehold switch sensors.

CHAPTER THREE: ADVANCEMENTS IN SAMPLE PROCESSING

3.1 Introduction

In this chapter, I discuss advancements made towards rapid and simple sample processing procedures that are compatible for use in low-resource settings, with a focus on processing blood serum and blood plasma patient samples. The next two sections (Sections 3.2 and 3.3) discuss procedures to minimize reaction inhibitors and access RNA within viral capsids and bacterial cells. The last sections (Sections 3.4 and 3.5) discuss the validation of these procedures in the context of the Zika virus diagnostic.

3.2 RNA amplification and toehold detection from serum samples

Certain components within blood are known to inhibit PCR (Schrader et al., 2012) and similarly affect all nucleic acid based diagnostics, including NASBA. However, we found that a simple dilution of serum or plasma into water sufficiently removes this effect in our diagnostic scheme (Figure 11). This dilution procedure is minimally time and cost intensive, allowing for its use in low-resource settings.

We therefore used diluted human serum (7%) as a matrix for our exploratory experiments, and diluted viremic plasma samples (10%) for our final validation experiment for the Zika diagnostic. The dilution step does affect the overall sensitivity of the diagnostic platform, but we have shown that increasing the NASBA reaction time can sufficiently compensate for this (Pardee, Green et al. 2016).

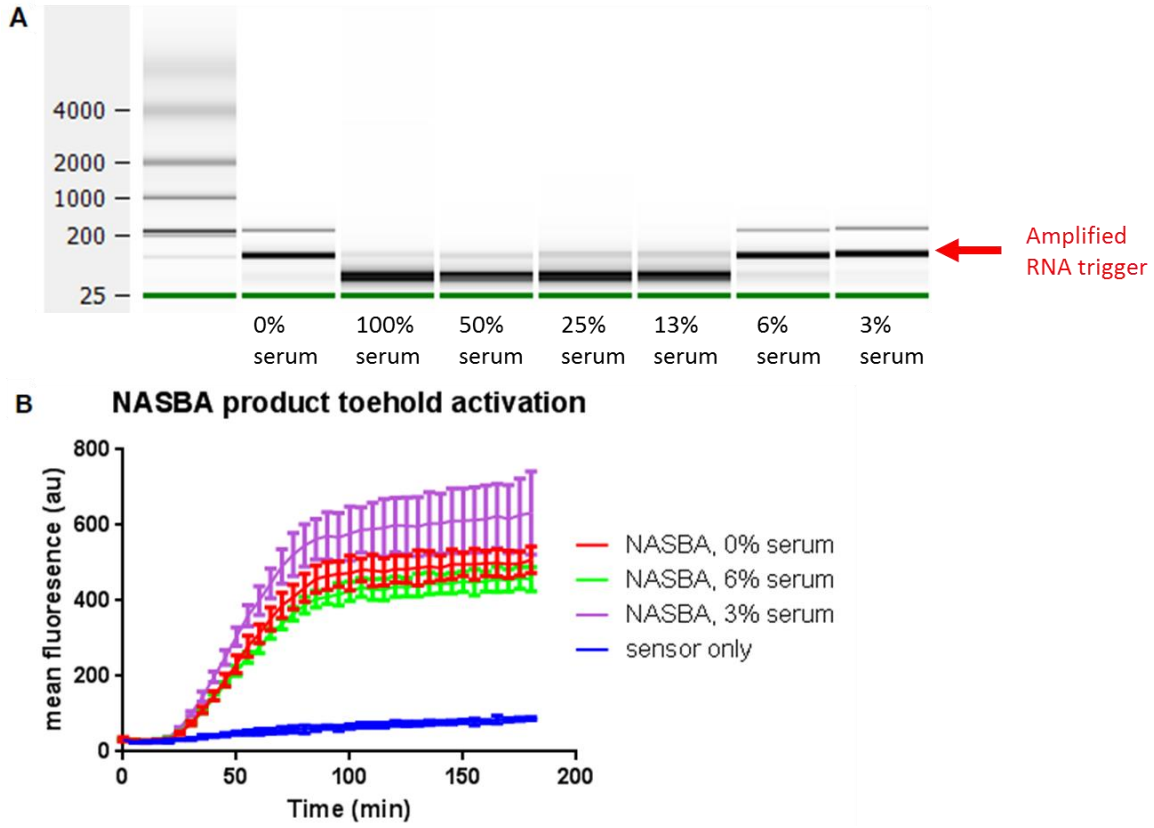

Figure 11. Effect of serum on NASBA reaction.
(A) NASBA was performed on trigger RNA spiked into a background of water (0% serum) or serum diluted into water (100%, 50%, 25%, 13%, 6%, and 3% final concentration of serum). NASBA outputs were run on an Agilent Bioanalyzer for analysis, which confirmed that NASBA amplification was able to proceed in solutions of 6% serum or less. (B) NASBA reactions for 0% serum, 3% serum, and 6% serum background were used as inputs into a paper-based toehold reaction. All three NASBA reactions were able to successfully activate the toehold reaction.

3.3 Sample boiling to release RNA

Our next challenge was to develop a technique to release RNA from the viral capsid using simple methodology compatible with low-resource environments. To this end, we tested the efficacy of boiling viral samples to break down the capsid. For initial development, we engineered lentivirus, which is also an RNA virus, to encapsulate the regions of either the Zika or Dengue genomes that correspond to the sensor 32B target

sequence (Figure S3B from (Pardee, Green et al. 2016)). These proxy Zika and Dengue viruses were spiked into human serum (7%) at a final concentration of 3 fM, and heated to 95°C for either one or two minutes. The resulting lysates were then immediately used to initiate NASBA reactions, in order to simulate what might be recovered from a patient sample. Boiling the viral samples for one minute was sufficient to release detectable amounts of RNA in our amplification and toehold switch detection scheme (Figure 12B). NASBA reactions from two-minute boiled samples were also monitored for sensor activation on the portable electronic reader. We detected strong sensor activation in less than 30 minutes from 3 fM of lentivirus carrying Zika RNA. We were also able to demonstrate clear discrimination between lentiviruses containing Zika and Dengue RNA sequences (Figure 12A).

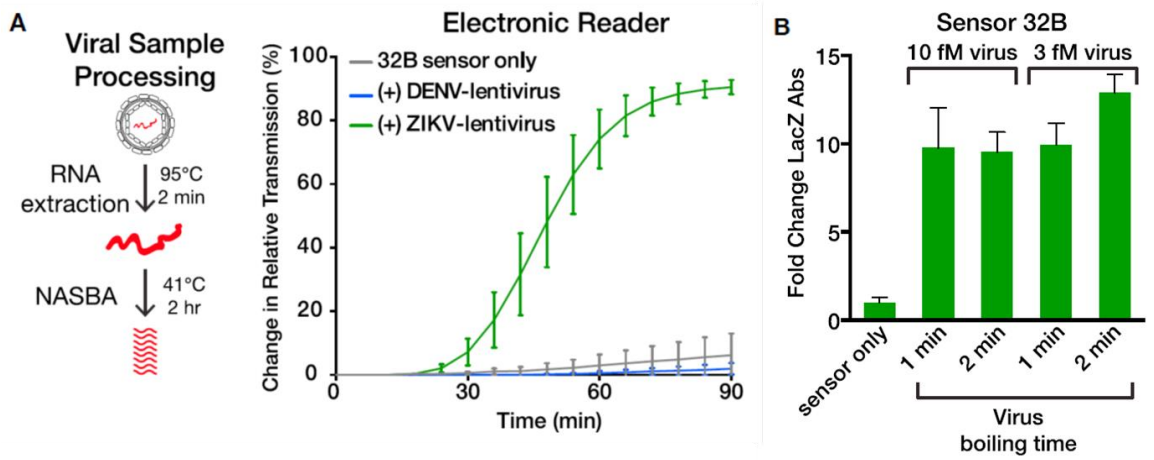

Figure 12. Incorporating viral sample processing into the diagnostic workflow.
(A) Lentivirus was packaged with Zika RNA or homologous Dengue RNA fragments targeted by sensor 32B. Three femtomolar of virus was spiked into 7% human serum and heated to 95°C for 2 min to extract viral RNA. The boiled lysate was used to initiate NASBA-mediated RNA amplification. A 1:7 dilution of the 2hr NASBA reaction in water was then used to rehydrate freeze-dried paper-based reactions. Time-course data were collected on the portable electronic reader. (B) Effect of boiling time on RNA extraction. Lentivirus was packaged with the Zika virus RNA fragment corresponding to sensor 32B. Virus was diluted to 10 and 3 fM target RNA in 7% human serum. 25 µL of virus was heated to 95°C for 1 and 2 min. One µL was then used to initiate NASBA-mediated RNA amplification. A 1:7 dilution of 2 hour NASBA reactions in water was then used to rehydrate freeze-dried, paper-based reactions. Fold change was calculated from absorbance (570 nm) after 60 min at 37°C. Error bars represent SD of three replicates. Figure taken from (Pardee, Green et al. 2016).

We are also working to expand the boiling procedure to other, non-viral biological entities. Preliminary tests for boiling bacterial samples to extract *E. coli* RNA have been promising (Figure 13), however, more experiments are required to test for extraction consistency, detection from genomically encoded RNA (rather than RNA expressed off of a plasmid), and detection from other bacterial species, including gram-positive organisms.

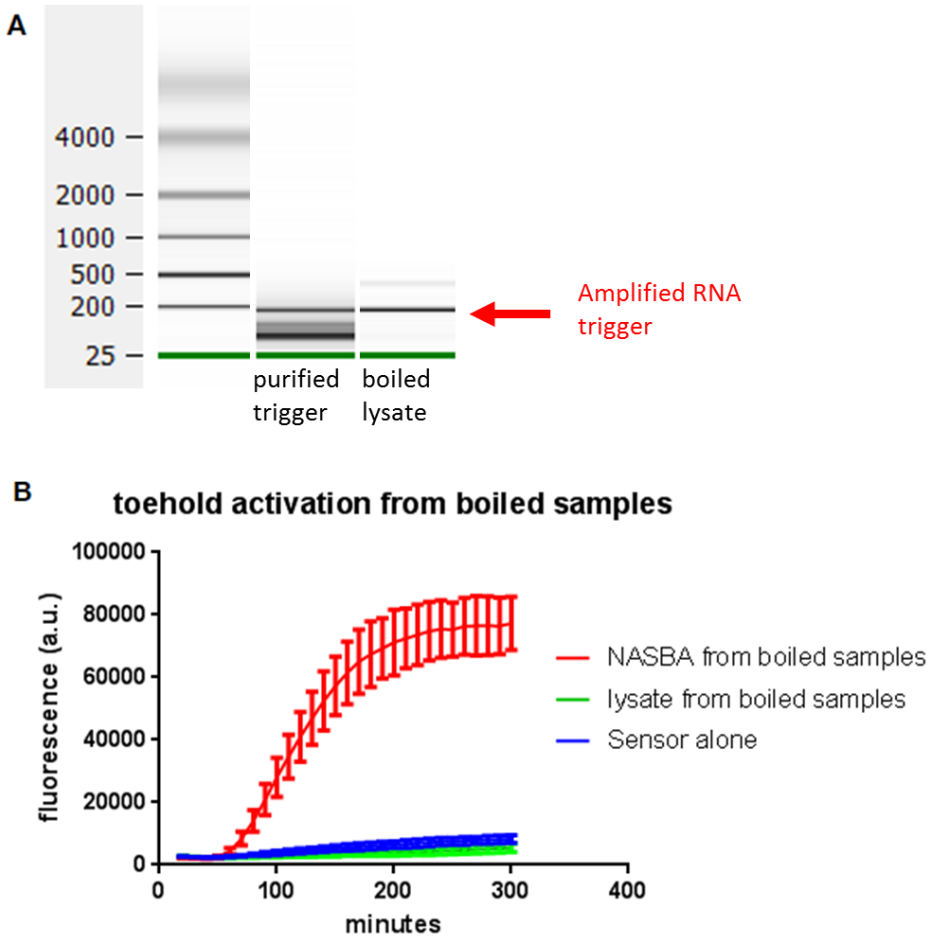

Figure 13. Boiling procedure for extracting plasmid-expressed RNA in *E. coli*.
(A) NASBA was performed on lysate collected from *E. coli* boiled at 95°C for four minutes to extract RNA. NASBA outputs were run on an Agilent Bioanalyzer for analysis, which confirmed that NASBA amplification was able to proceed from boiled lysate samples. (B) Samples from (A) were used as inputs for a paper-based toehold reaction. Only NASBA reactions from boiled *E. coli* lysate were able to activate the toehold.

3.4 Diagnostic workflow validation with active Zika virus

We next sought to validate our sensor platform with live Zika virus. First, we verified that our amplification and detection scheme could successfully detect full-length genomic RNA purified from Zika virus (Uganda strain MR 766) (Figure 14A). We designed new NASBA primers to accommodate sequence differences between the

Uganda Zika strain (Genbank accession number: AY632535) and the American Zika strain (Genbank accession number: KU312312) that our sensors and primers had originally been designed to detect. Computational analysis suggested that Uganda-lineage Zika RNA would activate sensor 32B despite two base mismatches in the toehold region, and this was confirmed experimentally (Figure 14A). We also demonstrated sensor orthogonality to full-length genomic Dengue RNA isolated from three different Dengue serotypes using these methods (Figure 14A).

Once we confirmed that the sensors behaved as expected on full-length genomic RNA, we sought to validate the sample preparation scheme and diagnostic workflow from start to finish. Active Zika virus was cultured in the laboratory and spiked into human serum (7%) at a final concentration of 12 fM, to mimic a clinical sample. The viral sample was then heated to 95°C for two minutes, and the resulting lysate was subjected to NASBA amplification for three hours. Sensor activation from the NASBA-amplified viral sample was monitored on the portable electronic reader. We successfully detected activation of sensor 32B from a diagnostic workflow initiated with live Zika virus (Figure 14B).

For the final validation of our system, we acquired and tested plasma samples from a viremic macaque infected with Zika virus (Genbank accession number: KJ776791) (Zika experimental science team). The macaque was found to have a plasma viral load of 1.7×10^6 copies/ml (2.8 fM), by a standard qRT-PCR protocol, which was within the detection limits of our platform as tested on synthetic RNA amplicons. The viremic plasma was diluted 1:10 in water to reduce known inhibitory effects of plasma on

downstream reactions. The diluted plasma was then taken through our sample processing and diagnostic workflow. The sample was heated to 95°C for two minutes and then amplified via NASBA for three hours. Paper-based reactions were monitored on the portable electronic reader, and showed strong activation with both sensors 27B and 32B in less than 30 minutes (Figure 14C and 14D).

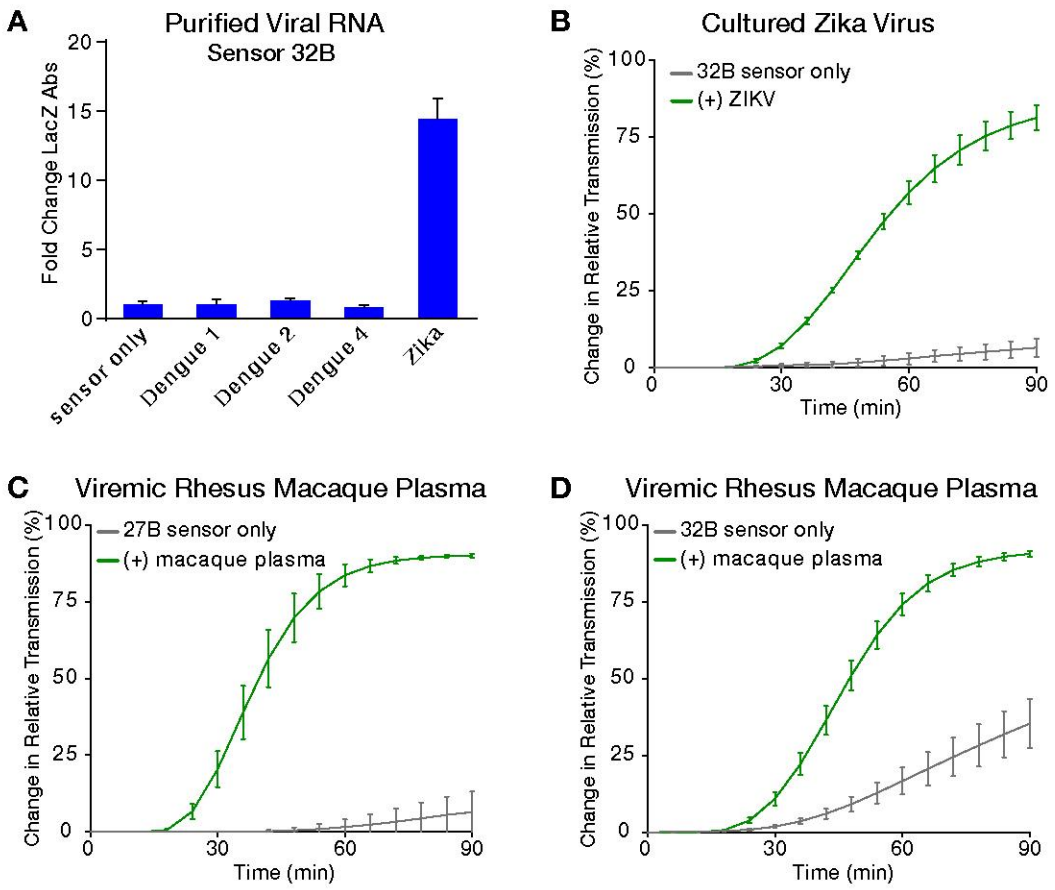

Figure 14. Validation of diagnostic workflow on live Zika virus samples.
(A) Specificity of sensor 32B against purified genomic RNA. Sensor 32B was tested for specificity using NASBA reaction products performed on 30fM RNA purified from Zika virus and three different Dengue virus serotypes. Fold change is calculated from absorbance (570 nm) at 60 min after rehydration and incubation of freeze-dried paper-based reactions at 37^0C. Error bars represent SD from three replicates. (B) Detection of live Zika virus. Ten femtomolar of laboratory-cultured Zika virus was spiked into human serum (7%), heated to 95^0C for 2 min, and used to initiate NASBA-mediated RNA amplification. A 1:7 dilution of the 3 hr NASBA reaction in water was then used to rehydrate freeze-dried paper-based reactions. Time-course data were collected on the portable electronic reader. Graph plots the relative absorbance of 570 nm wavelength light compared to background. Error bars present SD from three replicates. (C and D) Detection of Zika virus in viremic rhesus macaque plasma using sensors 27B and 32B. Plasma containing 2.8 fM of Zika virus was diluted 1:10 in nuclease free water, heated to 95^0C for 2 min, and used to initiate NASBA-mediated RNA amplification. 3 hour NASBA reactions were monitored on the portable electronic reader as in (B). Figure taken from (Pardee, Green et al. 2016).

3.5 Discussion

In this work, we implemented a simple procedure to extract viral RNA that does not require specialized laboratory equipment. By simply boiling (95°C) virus samples for two minutes, we were able to extract sufficient quantities of RNA for amplification and detection in our diagnostic platform (Figures 12A and 14B, 14C, and 14D). We note that we worked quickly to transfer boiled viral samples to NASBA reactions that contained RNase inhibitors to protect the integrity of the viral RNA. In practice, other commercially available reagents could be added to the sample to protect RNA from degradation upon collection. Of note, we were able to reliably extract RNA from three different sample types using our methodology: engineered lentivirus (Figure 12A), cultured Zika virus (Figure 14B) and plasma from an infected rhesus macaque (Figure 14C and 14D), highlighting the robustness of our sample preparation scheme.

Additionally, we demonstrated that simply boiling an RNA virus liberates sufficient material for downstream amplification and detection processes (Figures 12 and 14). Finally, our methods were validated on viremic plasma samples (Figure 14C and 14D), demonstrating a level of sensitivity that would be required for use of this diagnostic scheme in the field.

Our platform provides multiple levels of molecular programmability that greatly improve diagnostic specificity. Both the toehold switches and NASBA primers can be designed to target regions specific to a given genome, while excluding regions with significant homology to other organisms. We demonstrated the effectiveness of this design algorithm with sensor 32B, which was able to distinguish genomic Zika RNA

from the genomic RNA of three different Dengue serotypes (Figure 14A). Given the high sensor success rate and low barriers to development, we envision that sensors could be easily multiplexed to ensure high confidence diagnosis (reducing both false negative and false positive results) while keeping costs low. Furthermore, the diagnostic platform could be deployed as panels that include sensors for strain-specific identification and related infections to help monitor the spread of illness.

However, in some cases, it is beneficial for a diagnostic platform to be able to tolerate genetic mutations within a particular nucleic acid sequence. Evolutionary drift, for example, is an unavoidable feature of our ongoing arms race with pathogens that all molecular diagnostics must confront. Our assay in particular has the capacity to tolerate the expected genetic variation found in nature. We analyzed the binding between the toehold switch 32B and RNA sequences from homologous regions in Zika strains isolated from Africa and Asia (Supplemental Information: Extended Experimental Procedures from (Pardee, Green et al. 2016)). Both of these strains are predicted to fully activate the toehold sensors, even with up to 4-nt (11%) mismatches. In fact, we were able to demonstrate this using RNA triggers from the American strain, two different African strains and an Asian lineage of the virus (Figure 14 and 17D). Additionally, a critical feature of our technology is the ability to rapidly and inexpensively prototype new genetic sensors, thus allowing for a rapid response to genetic variations and mutations as they arise.

CHAPTER FOUR: ONE-POT NASBA

4.1 Introduction

We are also actively working towards combining the NASBA and toehold switch sensor reactions in a one-pot assay that will further streamline the diagnostic protocol and shorten the timeframe for readout. In this chapter, I discuss the optimization experiments we have performed towards this goal.

4.2 Results

4.2.1 Experimental design

NASBA and cell-free TXTL are two very different reactions that occur at different temperatures under very different buffer conditions (Figure 15). Our goal is to combine these two reactions into a single one-pot paper-based reaction that allows for RNA amplification and toehold sensor detection to occur simultaneously. This would significantly reduce the readout time of our system and simplify the diagnostic protocol, allowing this platform to be more readily used in low-resource areas.

For simplicity, we began by comparing the reagents and reaction conditions for the NEB PURExpress *In Vitro* Protein Synthesis Kit (catalog number E6800L) and the NASBA kit available from LifeSci (catalog numbers: NEC-1-24, NECB-24, and NECN-24). Our approach is two-fold: first, we tested the sensitivity of each reaction to temperature variations (4.2.2); then, we began titrating buffer components to find a "middle-ground" that allows both reactions to proceed simultaneously with relatively strong efficiency (4.2.3).

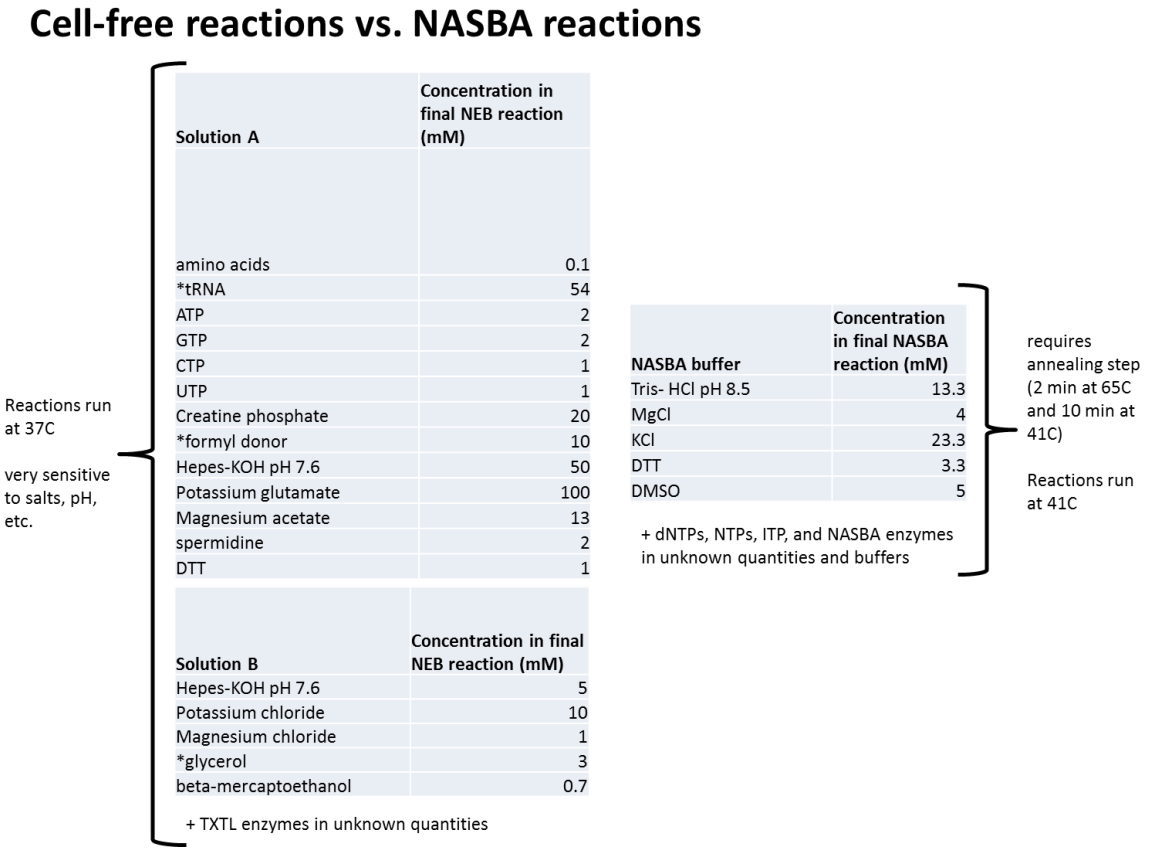

Figure 15. Comparison of NEB Cell-Free TXTL vs. NASBA reaction components
A comparison of the reaction conditions and buffer components required for NEB PURExpress TXTL reactions and NASBA reactions. The differing buffer conditions and temperature requirements of each of these reactions renders their combination into a single one-pot reaction nontrivial.

4.2.2 Temperature effects on NASBA and TXTL reactions

The first set of experiments was designed to test the tolerance of the NASBA and NEB reactions to different temperature conditions (Figure 16). These tests were conducted on a several different toehold sensors to ensure that results were robust across different toehold and NASBA primer sets. Note that Sensor 3B is the same sensor as Zika Sensor 27B and Sensor 8B is the same sensor as Zika Sensor 32B.We found that NASBA performed robustly at temperatures ranging from 41°C to 38°C, with a slight drop in

reaction efficiency at 37°C for two of the sensors (Figure 16A and 16C). We also found that the NEB reactions performed well from 37°C to 39°C, but dropped sharply in performance at temperatures above 39°C (data not shown).

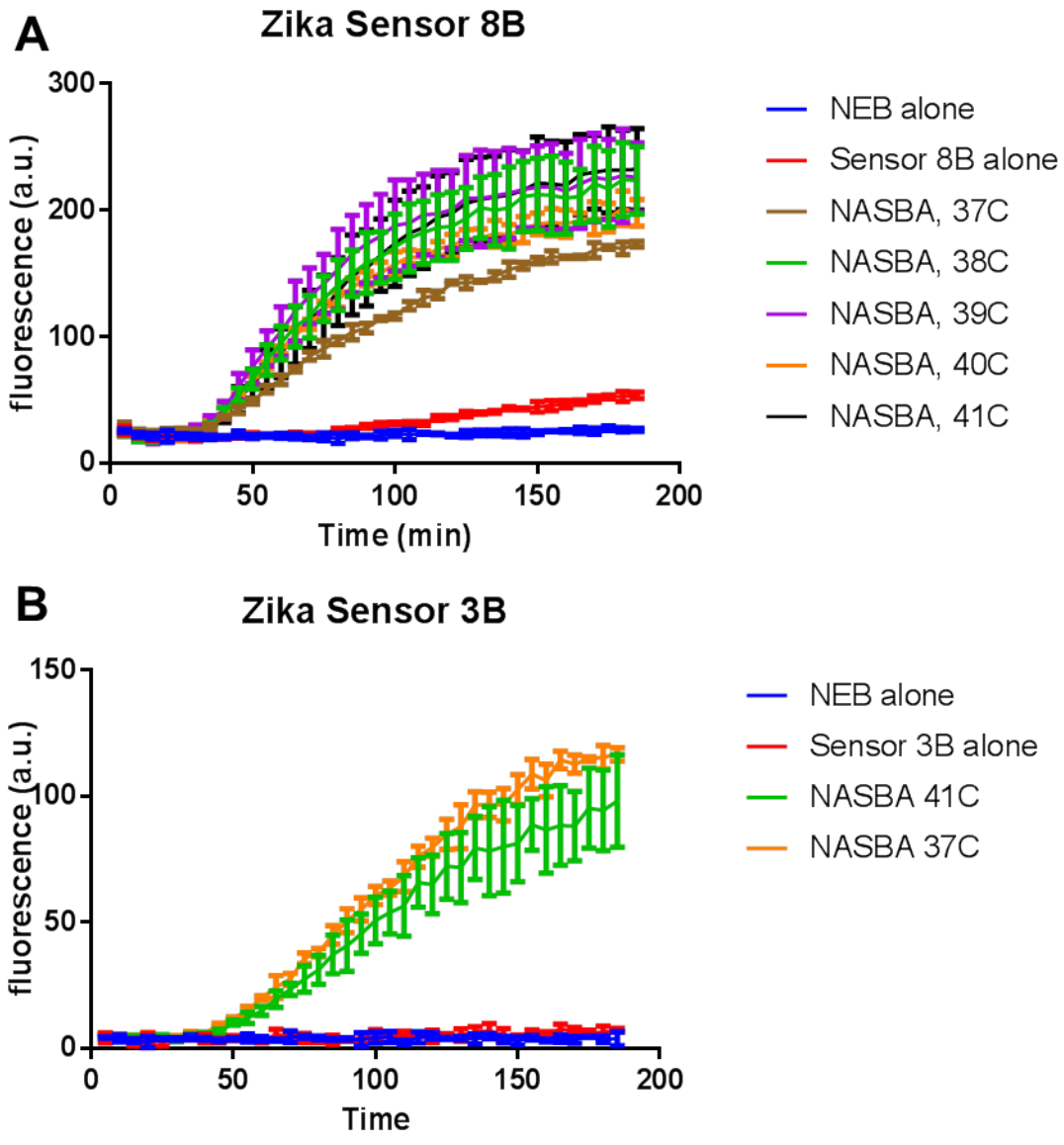

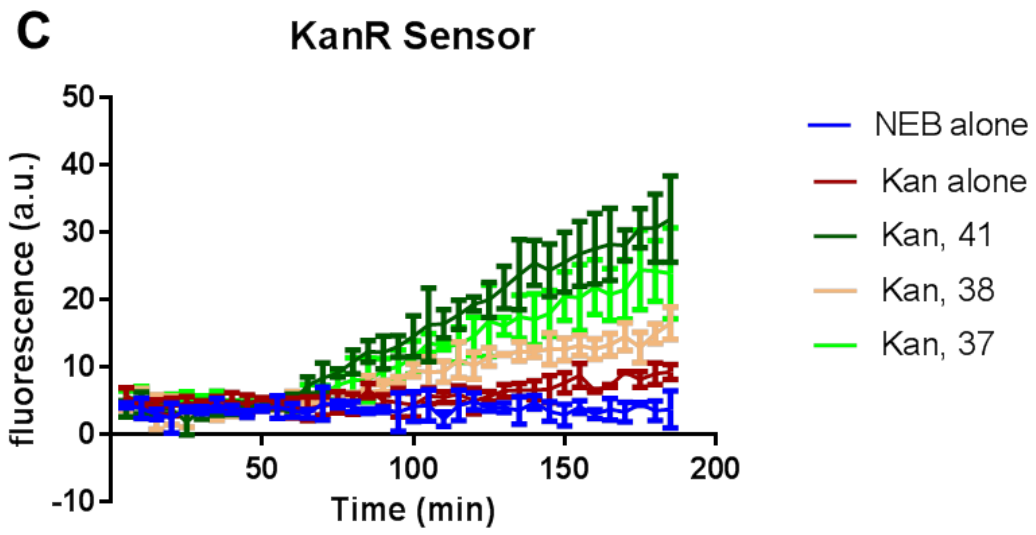

Figure 16. Temperature titration for NASBA reaction.
A comparison of NASBA efficiency at temperatures ranging from 37°C to 41°C for three different toehold sensors: Zika sensor 8B (A), Zika sensor 3B (B), and the KanR sensor (C). NASBA reactions are comparable in efficiency for this range of reaction temperature, with a slight drop off at 37°C for some toehold sensors.

The next set of experiments was designed to test the tolerance of the NASBA reaction to different annealing conditions. In the standard NASBA protocol, the NASBA buffer components, NASBA primers, and RNA trigger are all heated to 65°C for two minutes and then left to anneal for ten minutes at 41°C, prior to addition of the NASBA enzymes. We ran tests to compare this standard protocol to taking only the RNA trigger, and only the RNA trigger and NASBA primers through these heating steps (Figure 17). We also compared the effects of switching the 65°C step for a 95°C step, and switching the 41°C step for ten minutes at either 37°C or room temperature. These experimental conditions were chosen in the hopes of simplifying the NASBA reaction conditions for easy sample processing in low-resource settings. We found that the temperature

variations did not significantly affect the efficiency of the NASBA reactions, and that, instead, the components of the reactions that were taken through the heating and annealing steps had a greater effect on noise in the downstream toehold reactions (Figure 17).

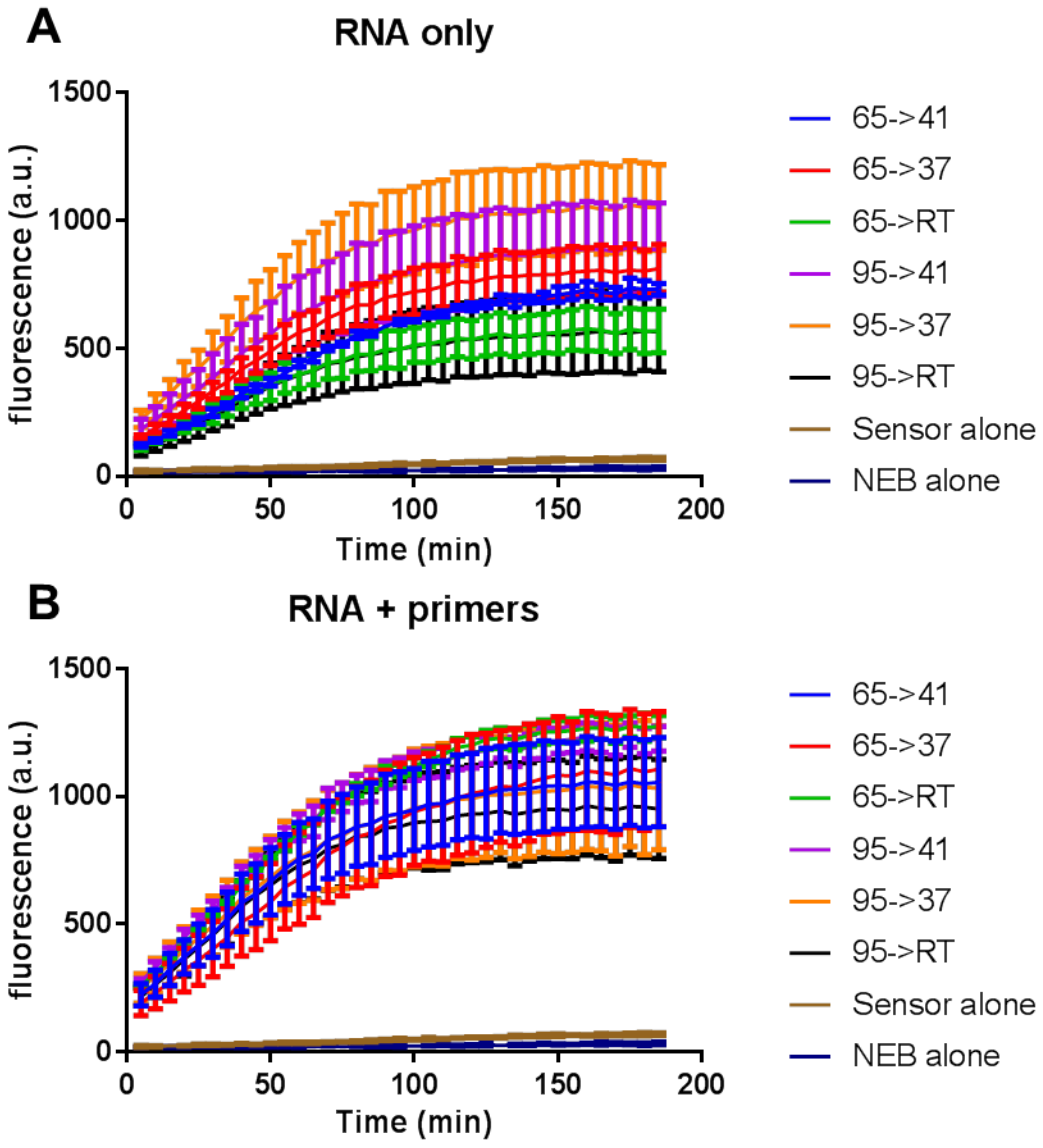

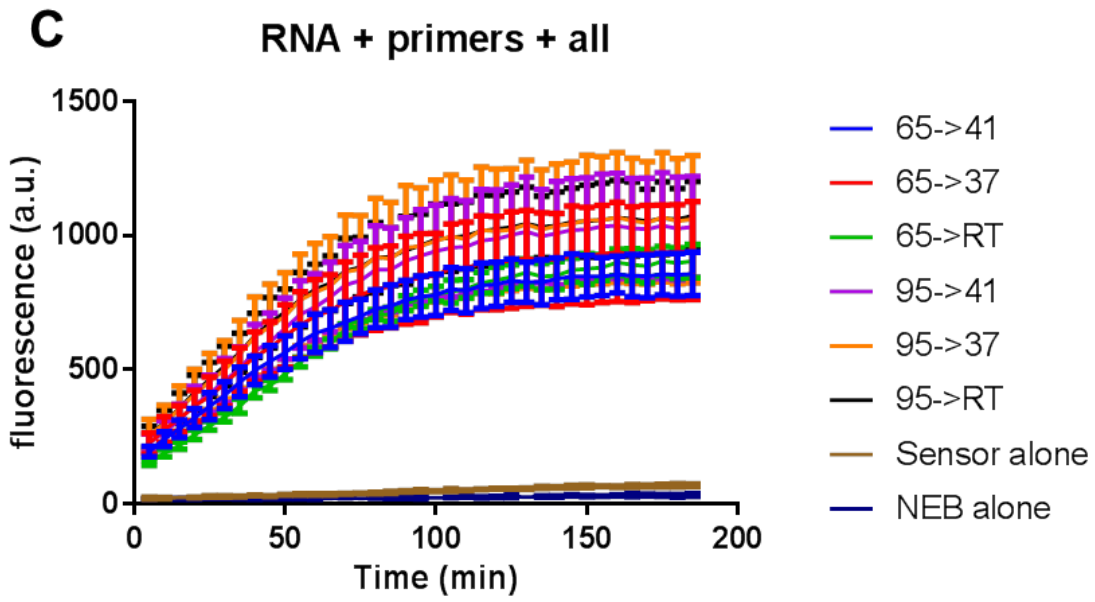

Figure 17. Annealing conditions parameter space search for NASBA reaction.
A comparison of NASBA efficiency for reactions initialized with different annealing conditions. (A) Only trigger RNA was taken through the annealing procedures, with all other components added after the annealing step. (B) Trigger RNA and NASBA primers were taken through the annealing procedures. (C) All NASBA components except NASBA enzymes (as per the original NASBA protocol) were taken through the annealing procedures. All reactions were performed using Zika Sensor 8B. Annealing conditions include: 2 min initial heating step at either 65°C or 95°C, followed by 10 minute incubation at 41°C, 37°C, or room temperature. The isothermal component of the NASBA reactions was performed at 41°C for two hours.

Finally, we looked at a dose response of the RNA input into NASBA at different reaction temperatures (Figure 18). We found that NASBA rapidly loses sensitivity as the reaction temperature decreases from 41°C. These results suggest that finding an optimal reaction temperature is a critical component of successfully optimizing a one-pot NASBA/TXTL reaction.

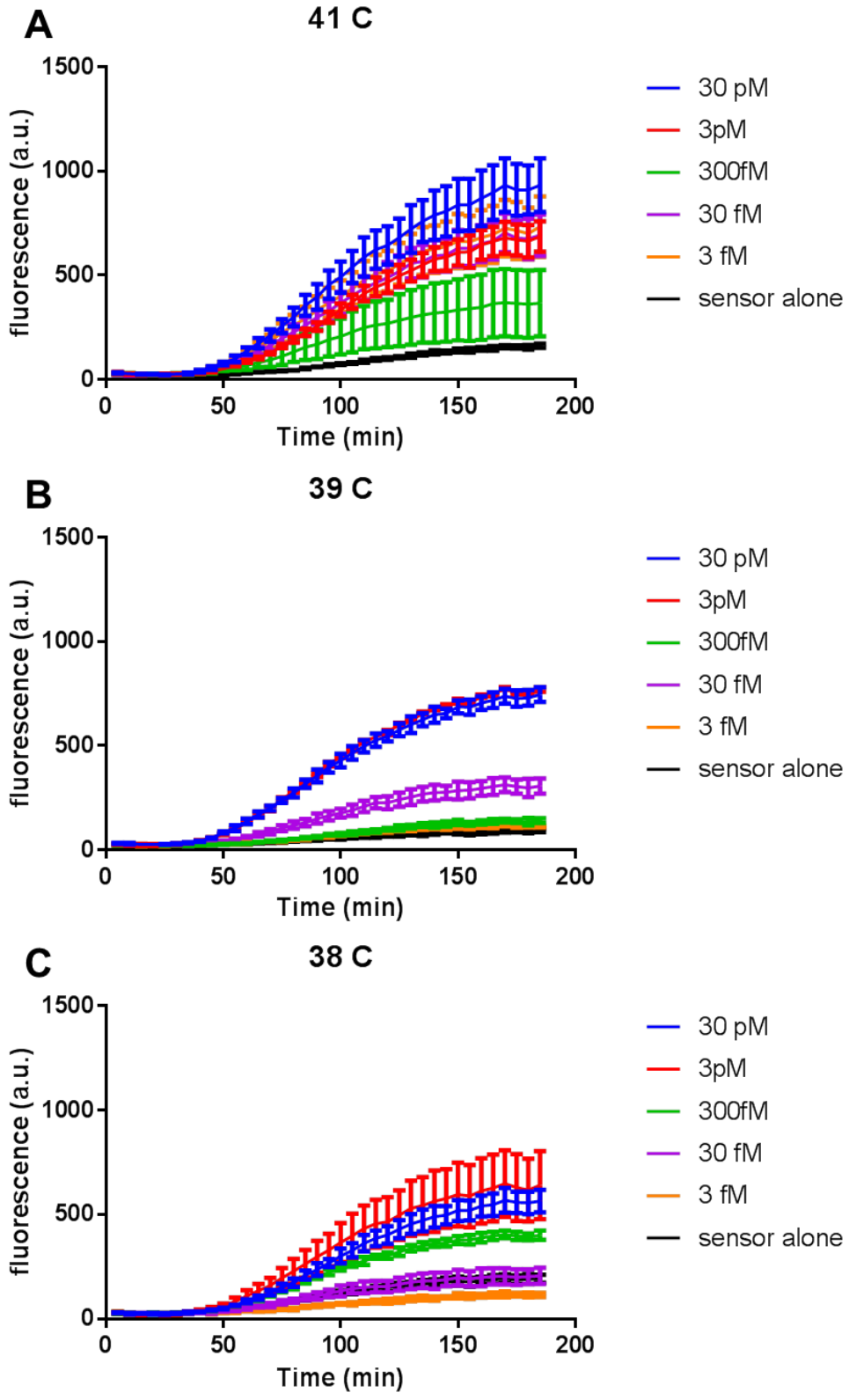
A
41 C
fluorescence (a.u.)
1500
1000
500
0
0
50
100
150
200
Time (min)
30 pM
3pM
300fM
30 fM
3 fM
sensor alone
B
39 C
fluorescence (a.u.)
1500
1000
500
0
0
50
100
150
200
Time (min)
30 pM
3pM
300fM
30 fM
3 fM
sensor alone
C
38 C
fluorescence (a.u.)
1500
1000
500
0
0
50
100
150
200
Time (min)
30 pM
3pM
300fM
30 fM
3 fM
sensor alone

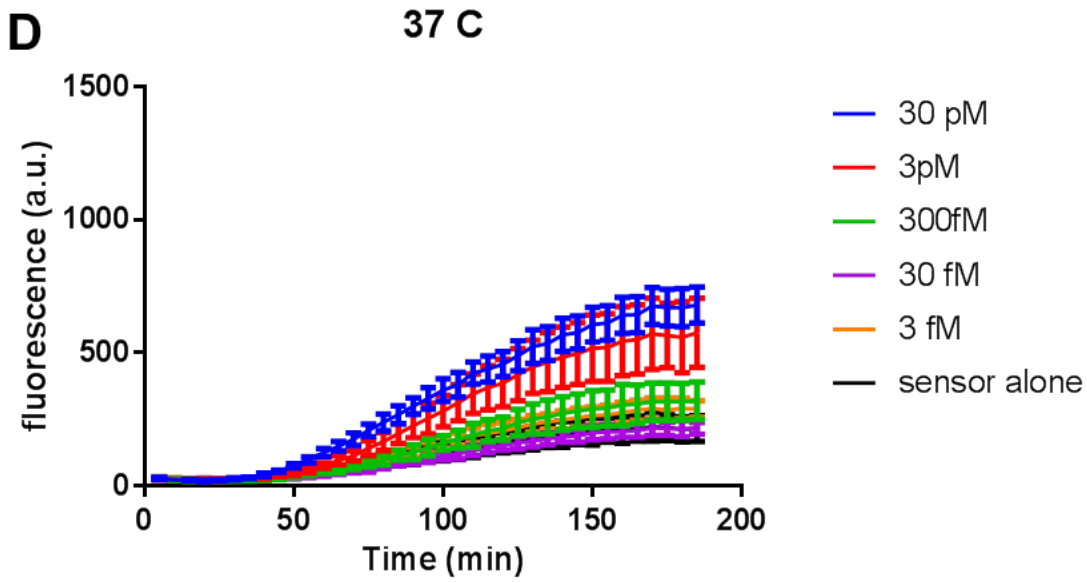

Figure 18. NASBA reaction dose response under different reaction temperature conditions. A comparison of NASBA efficiency for reactions initialized with different concentrations of trigger RNA. NASBA was run for two hours at 41°C (A), 39°C (B), 38°C (C), and 37°C (D). All reactions were performed using Zika Sensor 8B. These results indicate that NASBA loses sensitivity and dynamic range as reaction temperature decreases, suggesting that finding an optimal "middle ground" temperature may be necessary for successfully combining NASBA and TXTL reactions into a one-pot assay.

4.2.3 Buffer titrations

We then began titrating buffer conditions for a one-pot NASBA reaction. This work was initiated with Melina Fan during her sabbatical with the Collins lab. Here, I present work begun after her tenure. All of the experiments described in this section were performed on the freeze-dried paper-based system. Notably, because of the number of components going into the one-pot reactions, freeze-drying was a necessary step to properly concentrate the reagents for the final paper-based reaction.

We began by comparing buffer concentrations of each reaction and creating a "NASBA buffer supplement" and "NASBA nucleotide supplement". The starting concentrations of each reagent are described in the table below (Table 1); these concentrations were determined during Melina's tenure by comparing reagent concentrations in each reaction (NEB PURExpress and NASBA) and performing rough titrations of several key reagents. Our initial sets of one-pot experiments failed, with none yielding any toehold signal above the sensor alone condition (data not shown). We approached solving this problem in two ways: one was to confirm that NASBA components were not inhibiting the toehold reaction; the other was to confirm that NASBA components could be freeze-dried on paper and function upon rehydration, like the NEB toehold reactions.

NASBA Buffer Supplement 1.0				
	stock concentration (M)	final concentration (mM)	25X solution	uL of stock in 100 uL final volume
Tris HCl pH 8.5	1	20	500	50
MgCl	1	3	75	7.5
KCl	1	15	375	37.5
DTT	1	2	50	5
			final volume	100

NASBA Nucleotide Supplement 1.0				
	stock concentration (mM)	final concentration (mM)	16X solution	uL of stock in 100 uL final volume
CTP	100	0.5	8	8
ATP	100	0.5	8	8
GTP	100	0.5	8	8
UTP	100	0.5	8	8
dATP	100	1	16	16
dTTP	100	1	16	16
dGTP	100	1	16	16
dCTP	100	1	16	16
			final volume	96
			uL water to add	4

Table 1. Initialization of one-pot NASBA reaction buffer supplements.

From experiments performed during Melina's tenure, we knew that the ITP component of the NASBA nucleotide mix was inhibitory to the toehold reactions (data not shown). We thus decided to test the effect of each NASBA supplement component on the toehold reaction, to confirm whether there were other reagents inhibitory to the toehold reactions. These tests were performed with Zika sensor 3B because of the low

background and high activity of this sensor (Figure 19). We discovered that dNTPs were inhibitory to the toehold reactions. Because dNTPs are an obligatory component of the NASBA reactions, we could not eliminate them from the one-pot reaction. We thus performed a titration of dNTPs, including dNTPs sourced from different stock solutions, and found that a concentration of .1 mM dNTPs is permissive to toehold activity (Figure 20).

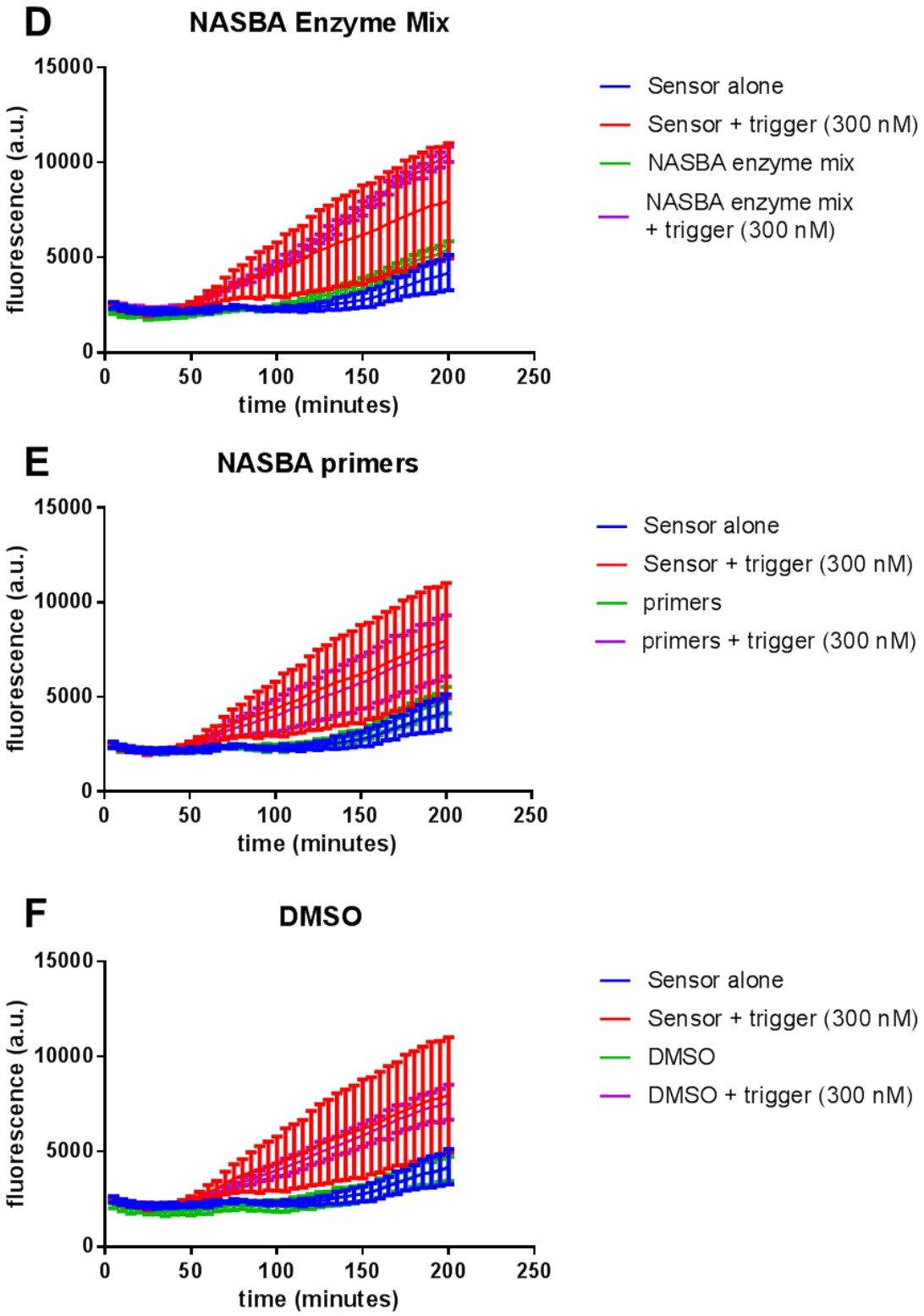

Figure 19. Effects of NASBA reaction components on TXTL toehold reaction.

A comparison of NEB reaction efficiency in the presence of different NASBA reaction components; the reactions were performed using the Zika 3B toehold sensor. (A) The control reactions, not supplemented with any NASBA components. (B) The NASBA nucleotide supplement, consisting of dNTPs and NTPs, contained at least one component inhibitory to the toehold reaction. The NASBA buffer supplement (C), NASBA enzyme mix (D), NASBA primers (E), and DMSO (F), were all permissive to the toehold reaction.

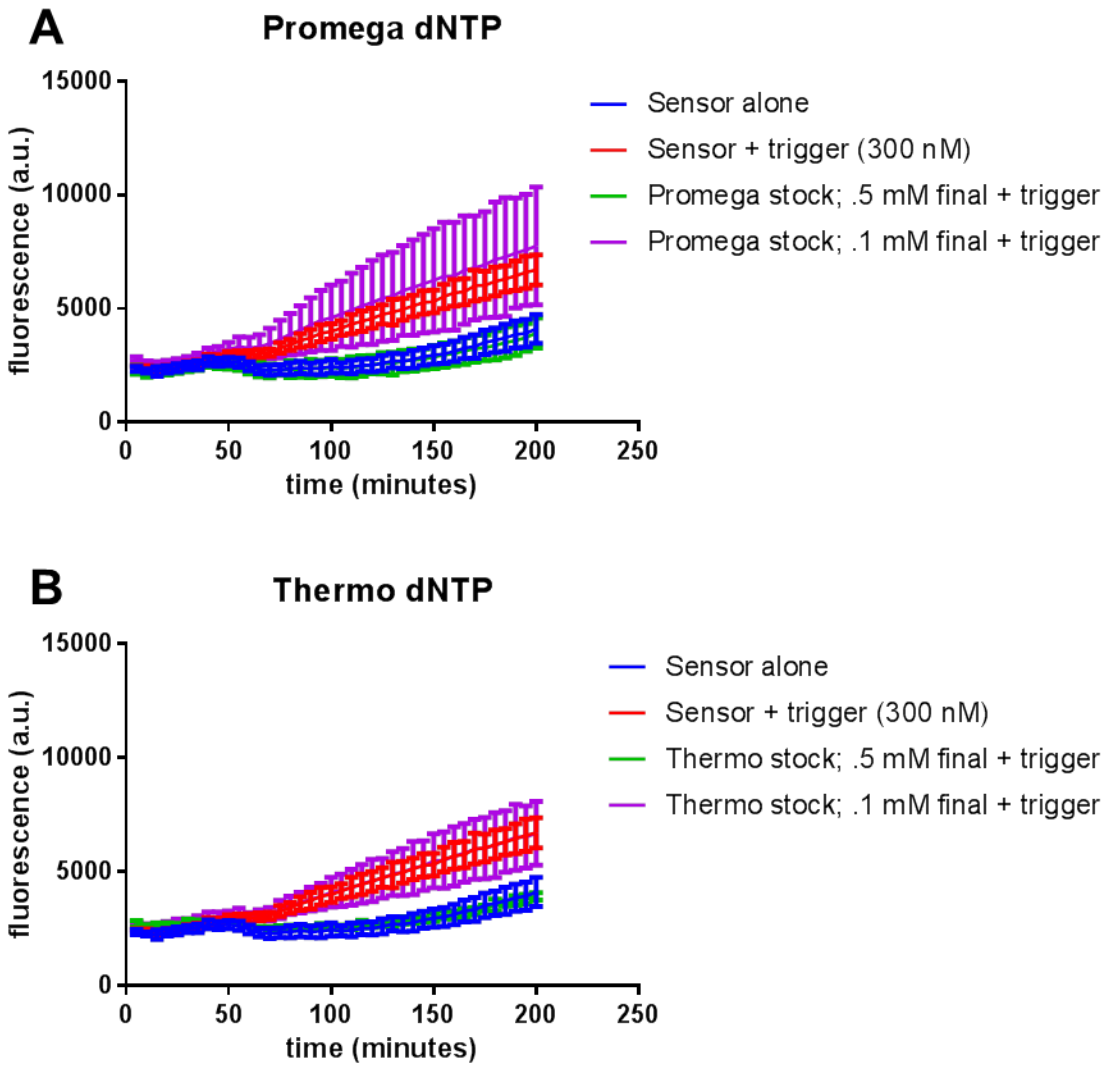

Figure 20. dNTPs are inhibitory to the toehold reactions at high concentrations.
A comparison of NEB reaction efficiency in the presence of .5 mM and .1 mM final concentrations of dNTPs, from two different sources (Promega and Thermo); the reactions were performed using the Zika 3B toehold sensor. Both Promega (A) and Thermo (B) dNTPs were inhibitory at .5mM and permissive at .1mM to the toehold reactions.

We then wanted to test whether NASBA would be permissive to freeze-drying on paper. We knew that the toehold reaction could function post-freeze-drying, but had no evidence that NASBA enzymes and buffers would be able to function upon rehydration. We freeze-dried the one-pot reaction with an updated dNTP concentration (.1mM of each dNTP), without the sensor. We then rehydrated the reaction with trigger only and incubated the paper-based reactions at 37°C for two hours to allow the NASBA reaction to run without interference or competition for resources from the toehold reaction. After the two hour incubation, we added in the toehold sensor and monitored reaction output.

The results indicated that NASBA reactions were able to run successfully (Figure 21). We also noted that the 300nM RNA input activated toeholds in the NASBA background but not in the normal NEB background, as would be expected for such a high RNA input. This suggests that the RNA trigger was likely degraded during the two hour incubation, and that the NASBA reaction was able to sufficiently compensate for this via RNA amplification in the one-pot reaction. This result may indicate that the RNase inhibitor does not function after freeze-drying, and that in the future it may be worth to explore this more thoroughly, in particular if diagnostic sensitivity becomes an issue.

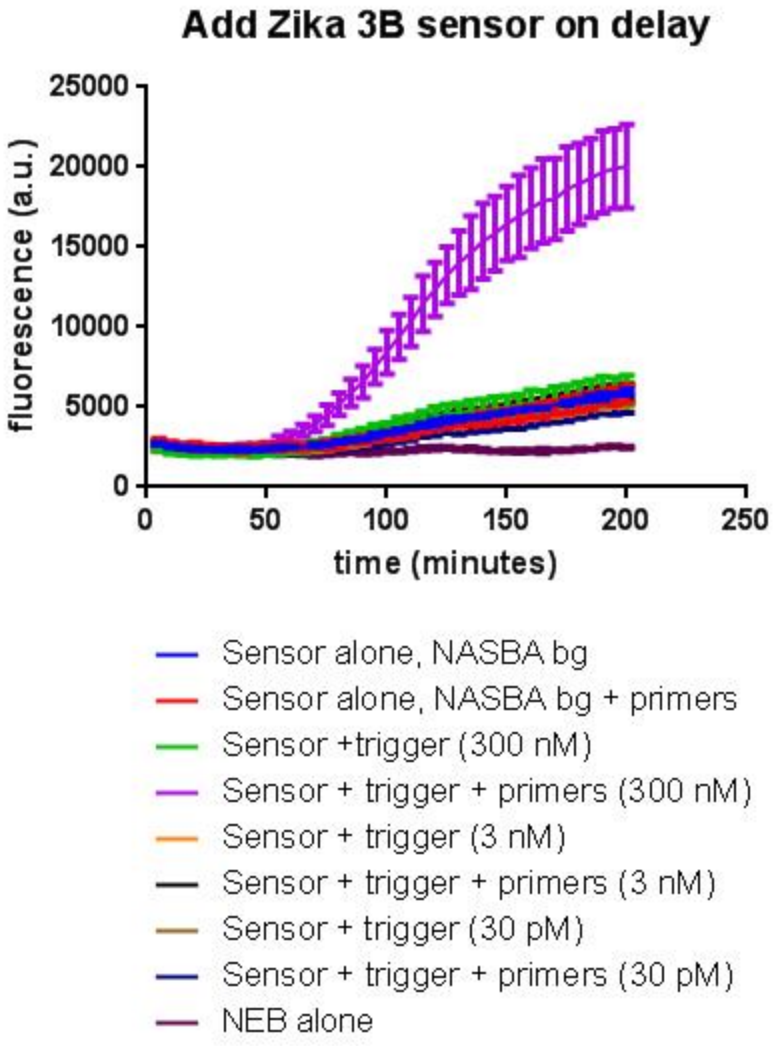

Figure 21. NASBA can be freeze-dried on paper.
One-pot NASBA/NEB reactions were freeze-dried on paper, without the toehold sensor. Reactions were rehydrated and incubated at 37°C for two hours to allow the NASBA reactions to run without interference from the toehold sensor. After two hours, toehold sensors were applied to the paper-based reaction and the reactions were monitored for toehold activity. Reactions were run for 300 nM, 3 nM, and 3pM of trigger RNA input. Only the 300 nM input with the full NASBA background (+ primers) was able to activate the toehold switch. Under normal conditions, 300nM should activate the toehold, even without NASBA-mediated signal amplification. Because this was not the case, these data suggest that the RNase inhibitor does not function post freeze-drying: in the no-primer control reaction with a 300 nM input, the input RNA may have been degraded during the two hour incubation period prior to toehold addition, resulting in no toehold activation; in the "+ primer" reaction condition, NASBA was able to run to completion and compensate for RNA degradation, resulting in successful activation of the toehold switch.

After confirming that NASBA can be freeze dried, we continued with the titration of individual reaction components. We first looked into the NTP concentration of the NASBA nucleotide supplement. We found that high concentrations of NTPs were inhibitory to the NEB toehold reaction (Figure 22A), but allowed for signal amplification in the one-pot reaction (Figure 22B and 22C). These results suggest that the reaction components interact with one another in a non-predictable fashion, and that the reaction parameter space must be thoroughly searched in order to find the optimal one-pot reaction conditions.

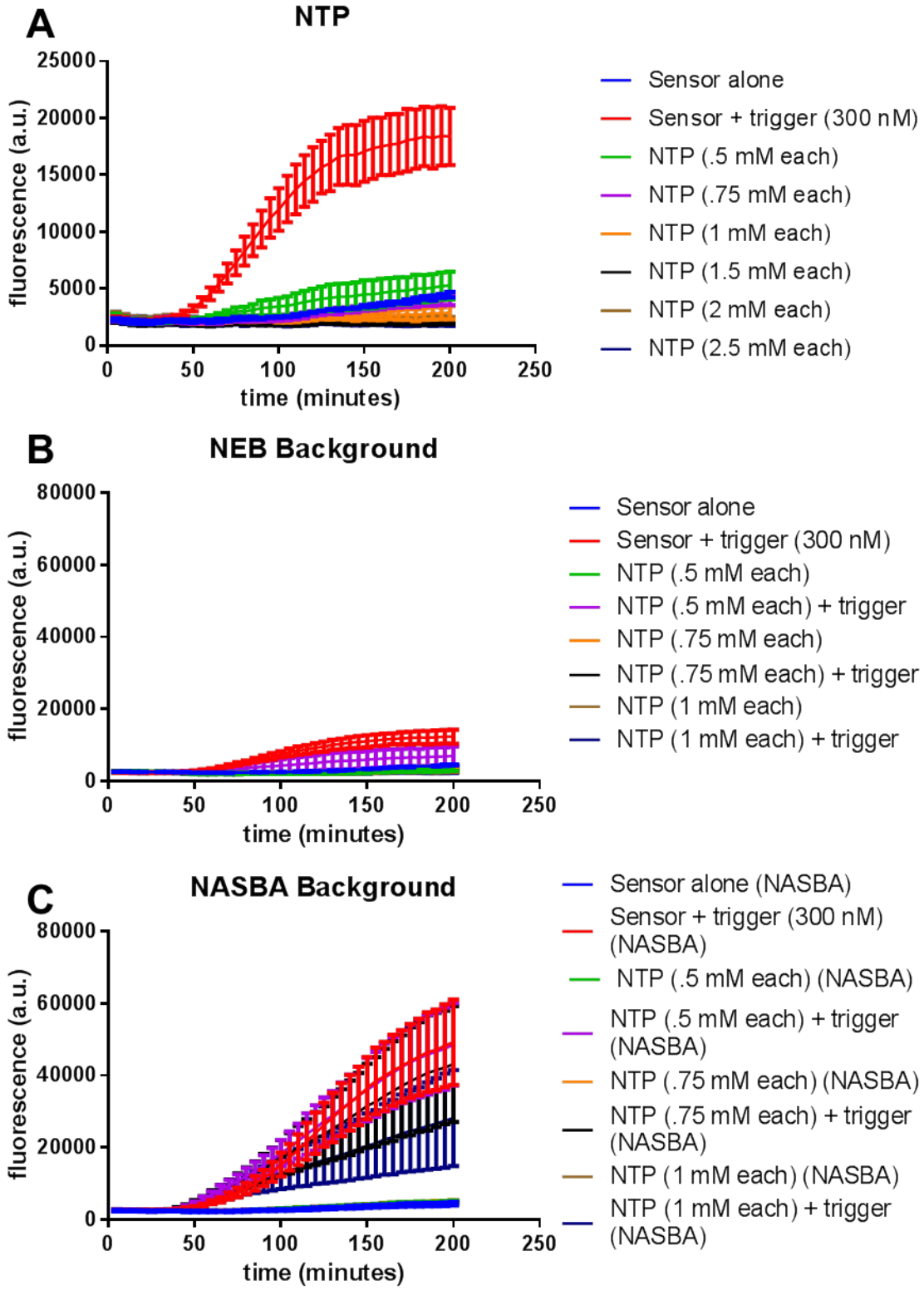
A
NTP
fluorescence (a.u.)
time (minutes)
Sensor alone
Sensor + trigger (300 nM)
NTP (.5 mM each)
NTP (.75 mM each)
NTP (1 mM each)
NTP (1.5 mM each)
NTP (2 mM each)
NTP (2.5 mM each)
B
NEB Background
fluorescence (a.u.)
time (minutes)
Sensor alone
Sensor + trigger (300 nM)
NTP (.5 mM each)
NTP (.5 mM each) + trigger
NTP (.75 mM each)
NTP (.75 mM each) + trigger
NTP (1 mM each)
NTP (1 mM each) + trigger
C
NASBA Background
fluorescence (a.u.)
time (minutes)
Sensor alone (NASBA)
Sensor + trigger (300 nM) (NASBA)
NTP (.5 mM each) (NASBA)
NTP (.5 mM each) + trigger (NASBA)
NTP (.75 mM each) (NASBA)
NTP (.75 mM each) + trigger (NASBA)
NTP (1 mM each) (NASBA)
NTP (1 mM each) + trigger (NASBA)

Figure 22. NTPs are inhibitory to the NEB reaction, but amplify signal in the one-pot NASBA reaction.
All reactions were run with the Zika 3B toehold switch. (A) NTPs were titrated in a regular toehold NEB reaction, demonstrating that concentrations down to .5 mM NTPs are inhibitory to the NEB reactions. (B) A replicate experiment of (A) yielded similar results; graph is scaled for easy comparison with (C). (C) One-pot NASBA (NASBA background) reactions were able to tolerate up to 1 mM NTPs, and yielded significant signal amplification over the traditional NEB toehold reaction.

We proceeded to investigate which component of NASBA helps alleviate the NTP inhibition. To do this, we ran NEB reactions supplemented with an inhibitory concentration of NTPs and various NASBA components (NASBA buffer supplement, NASBA enzyme mix, dNTPs, DMSO, and primers). We discovered that the NASBA buffer supplement and the DMSO both help alleviate NTP inhibition (Figure 23C and D); we did not test which specific component of the NASBA buffer supplement is responsible for this phenotype. Notably, we were not able to amplify signal in any of the reactions other than the reaction complete with all of the necessary NASBA components, indicating that proper NASBA functioning is likely responsible for the signal amplification in the one-pot reaction (Figure 23A and B).

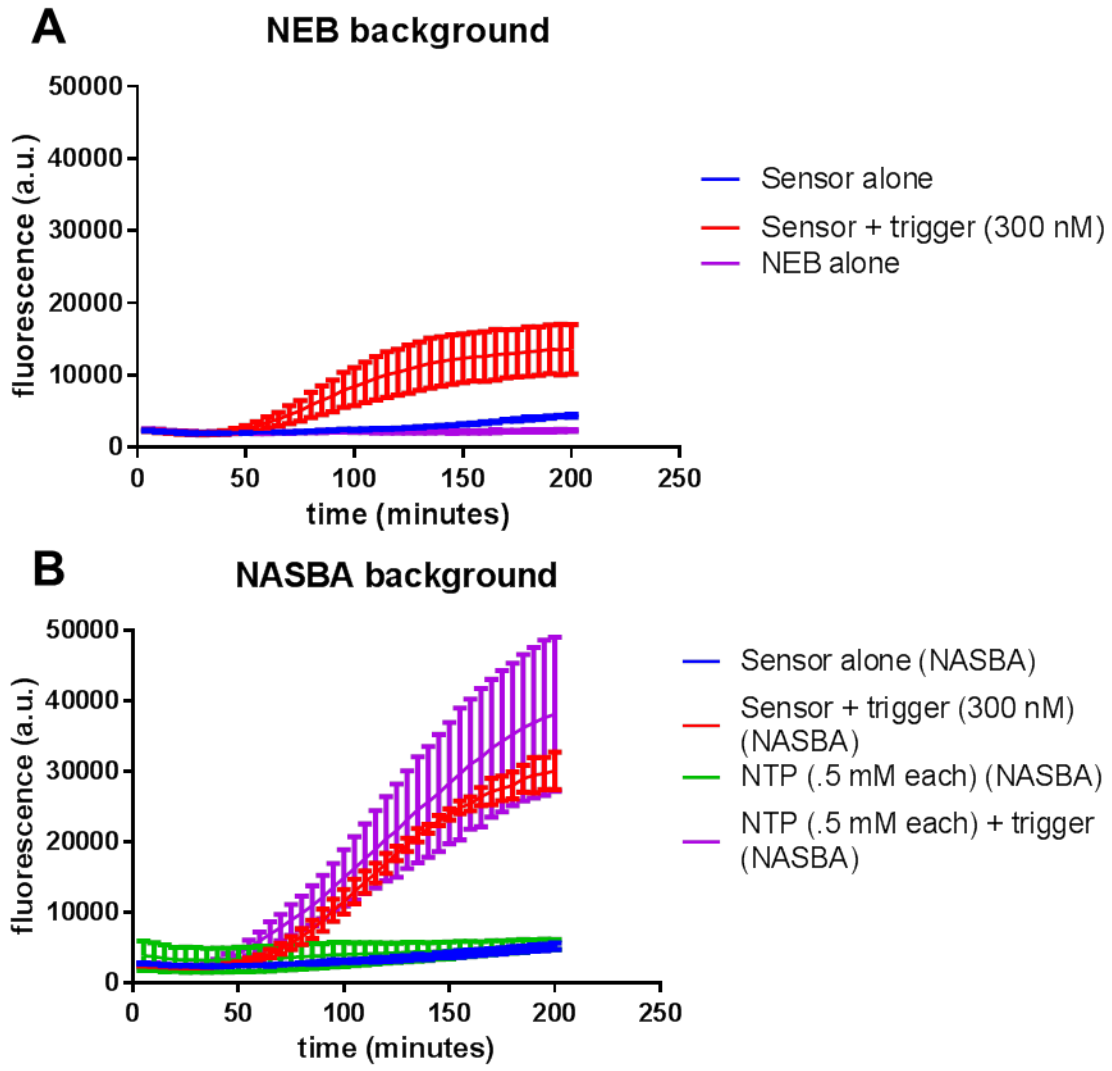
A
NEB background
fluorescence (a.u.)
50000
40000
30000
20000
10000
0
0
50
100
150
200
250
time (minutes)
Sensor alone
Sensor + trigger (300 nM)
NEB alone
B
NASBA background
fluorescence (a.u.)
50000
40000
30000
20000
10000
0
0
50
100
150
200
250
time (minutes)
Sensor alone (NASBA)
Sensor + trigger (300 nM) (NASBA)
NTP (.5 mM each) (NASBA)
NTP (.5 mM each) + trigger (NASBA)

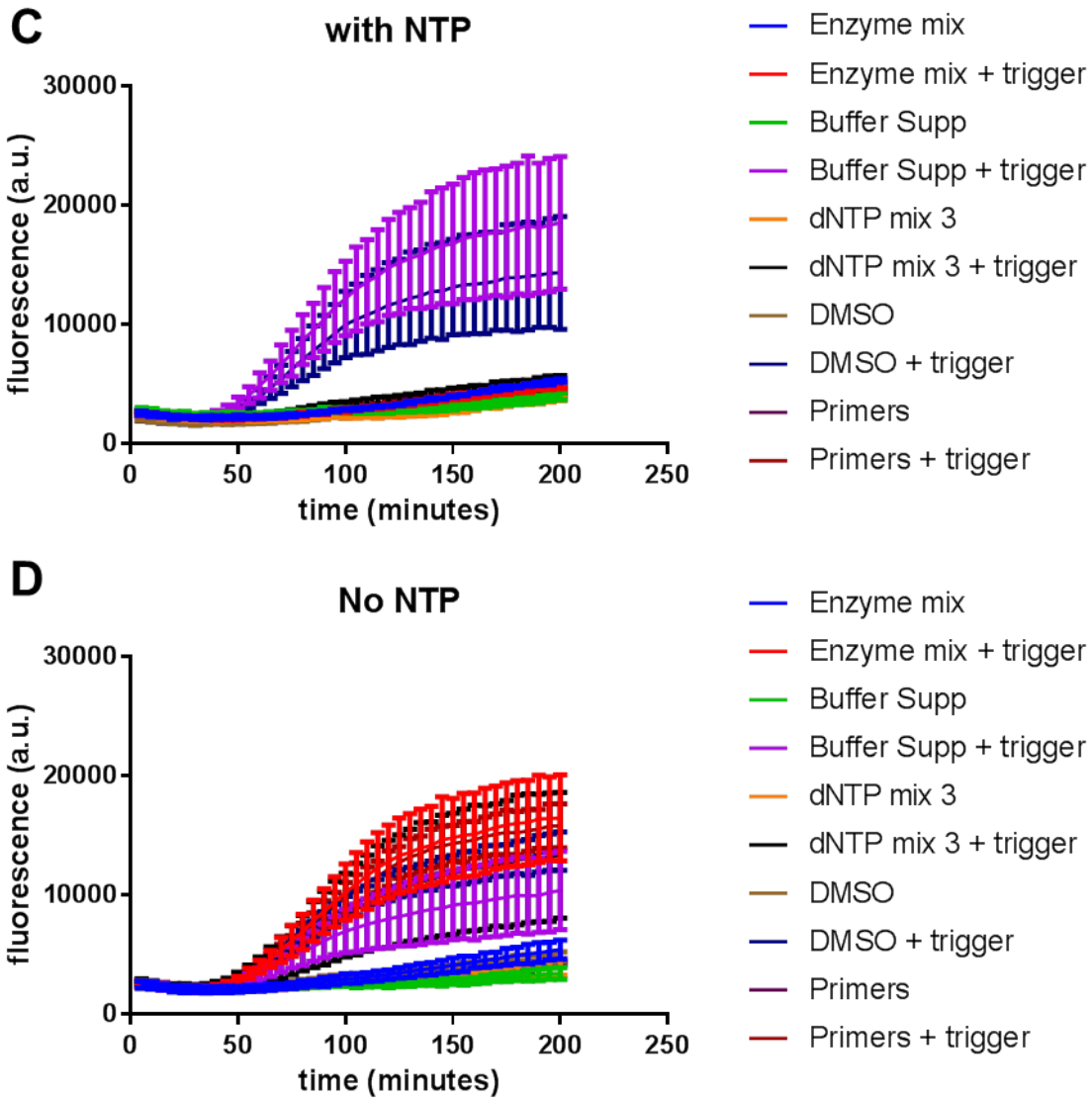

Figure 23. NASBA buffer supplement and DMSO both contribute to alleviation of NTP inhibition on NEB toehold reaction.
All reactions were run with the Zika 3B toehold switch. (A) A standard NEB toehold reaction serves as a point of comparison for (B) through (D). (B) One-pot NASBA (NASBA background) yielded significant signal amplification over the traditional NEB toehold reaction. (C) A standard NEB toehold reaction with an inhibitory concentration of NTPs (.5 mM each) was able to run to completion only when supplemented with either DMSO or NASBA buffer supplement. However, this reaction did not yield signal amplification, suggesting that these reagents alone are not responsible for the signal amplification observed in (B). (D) A standard NEB toehold reaction (without NTPs) supplemented with the components tested in (C) serves as a point of comparison the reactions in (C).

We then wanted to confirm that the signal amplification was due to NASBA functioning properly, and not due to any individual component of NASBA amplifying sensor activity on its own. We found that, indeed, every single component of NASBA must be present in order for signal amplification, indicating that NASBA is likely working properly on paper in the one-pot reaction to amplify the trigger RNA (Figure 24). We also tested a titration of inputs into the functioning one-pot reaction, to test the dynamic range and sensitivity of the one-pot reaction (Figure 25).

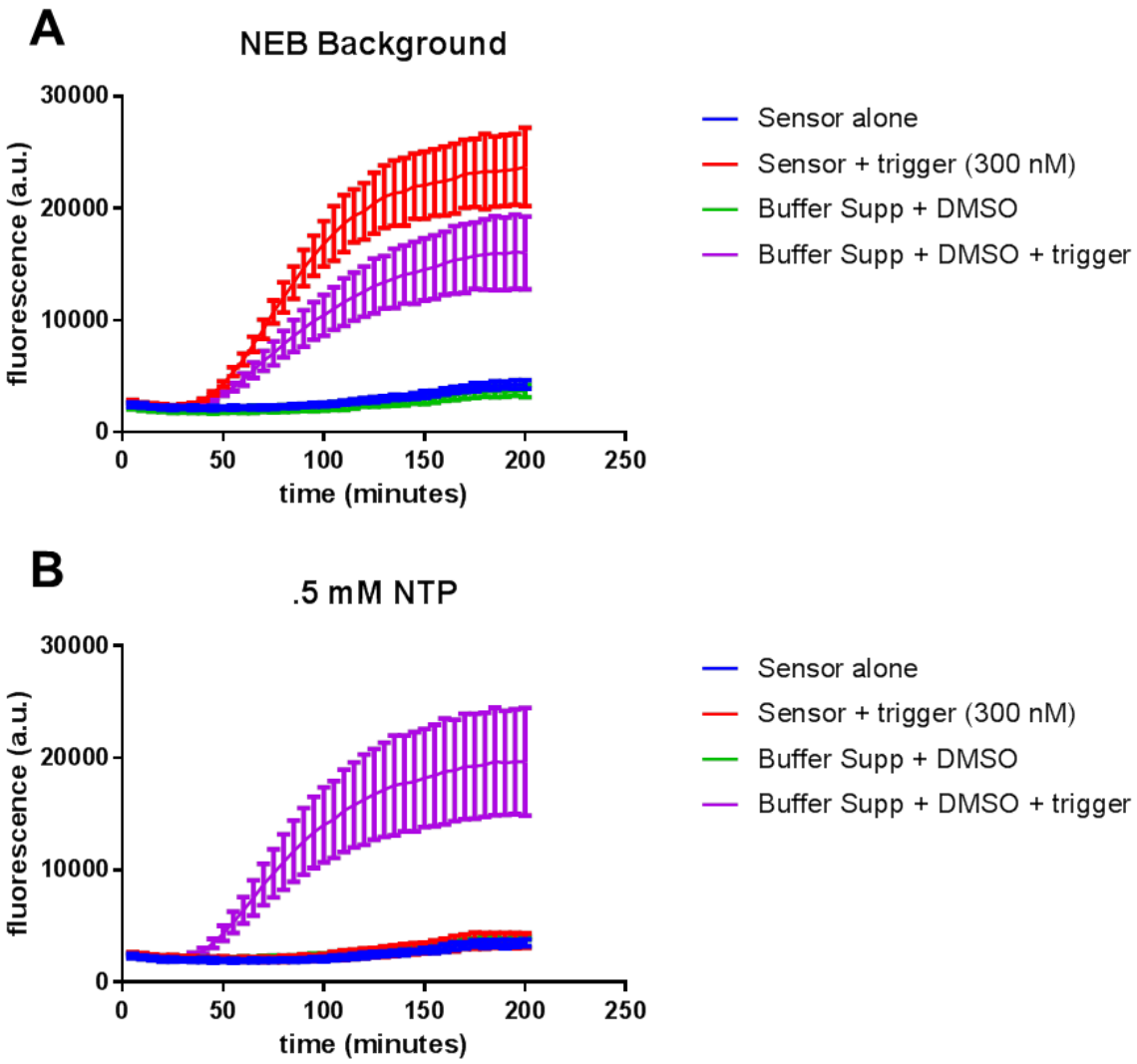

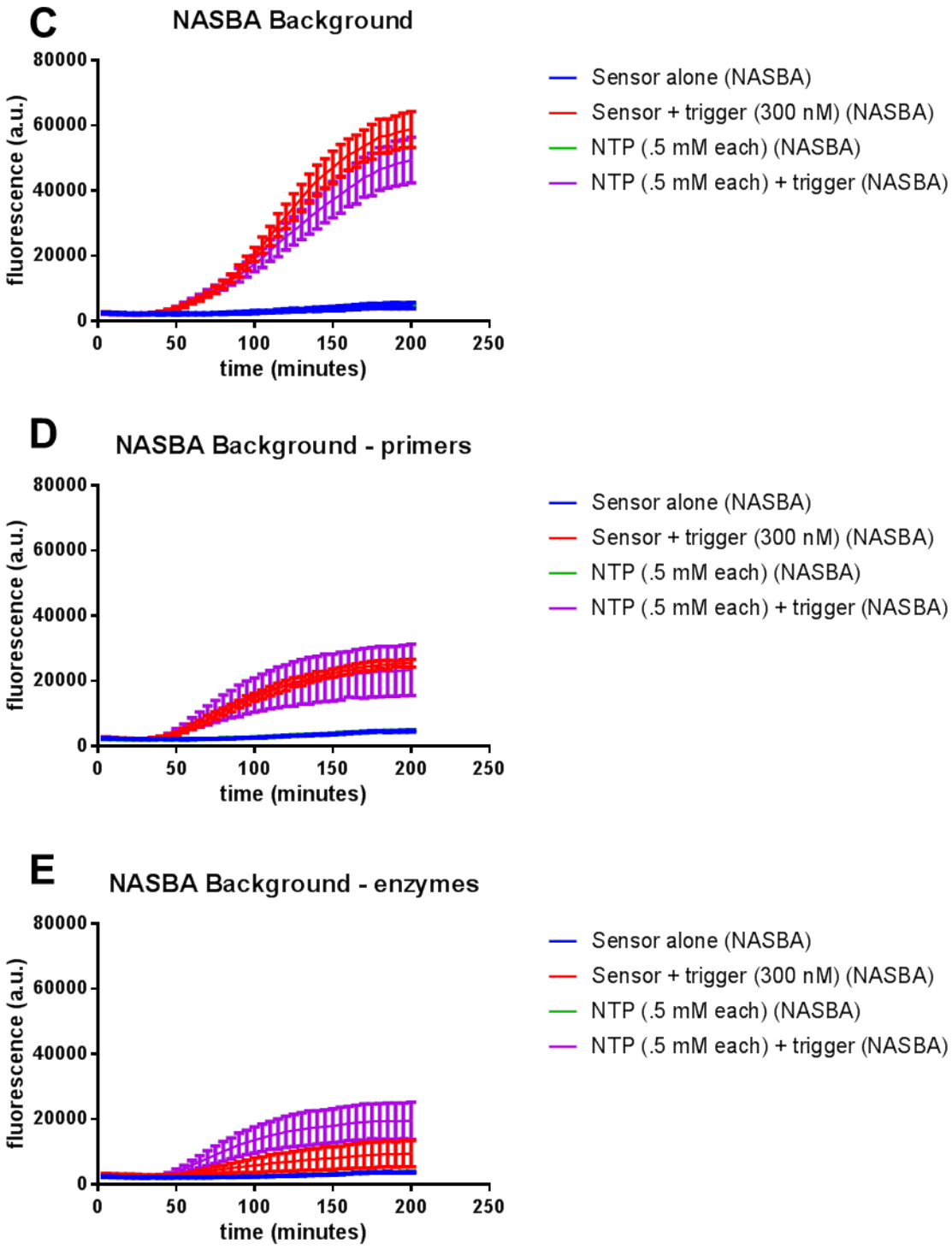

Figure 24. NASBA buffer supplement and DMSO alone are sufficient for inhibition alleviation, but not for signal amplification in the standard NEB toehold reaction.
All reactions were run with the Zika 3B toehold switch. (A) A standard NEB toehold reaction serves as a point of comparison. The addition of the NASBA buffer supplement and DMSO is not

sufficient for signal amplification in this reaction (B) A standard NEB toehold reaction is inhibited by the addition of .5 mM NTPs. This inhibition can be alleviated by the addition of the NASBA buffer supplement and DMSO, but signal amplification cannot be achieved in these reaction conditions. (C) One-pot NASBA (NASBA background) yielded significant signal amplification over the traditional NEB toehold reaction. The addition of .5 mM NTPs is not necessary for amplification to occur, suggesting that the quantity of NTPs found in the NEB reaction may be sufficient for the one-pot reaction. (D) The one-pot NASBA reaction cannot amplify toehold signal in the absence of the NASBA primers. (E) The one-pot NASBA reaction cannot amplify toehold signal in the absence of the NASBA enzymes.

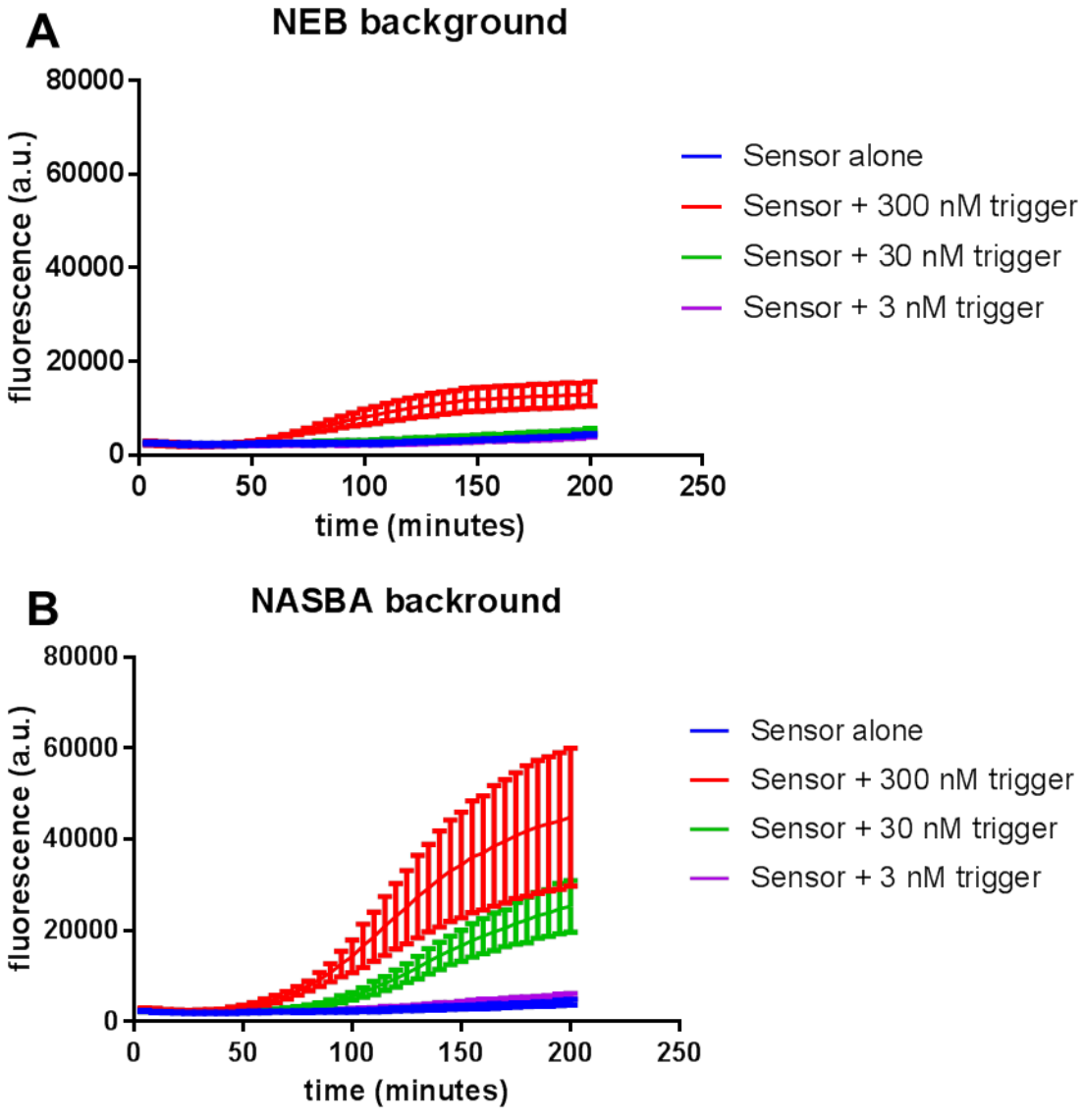

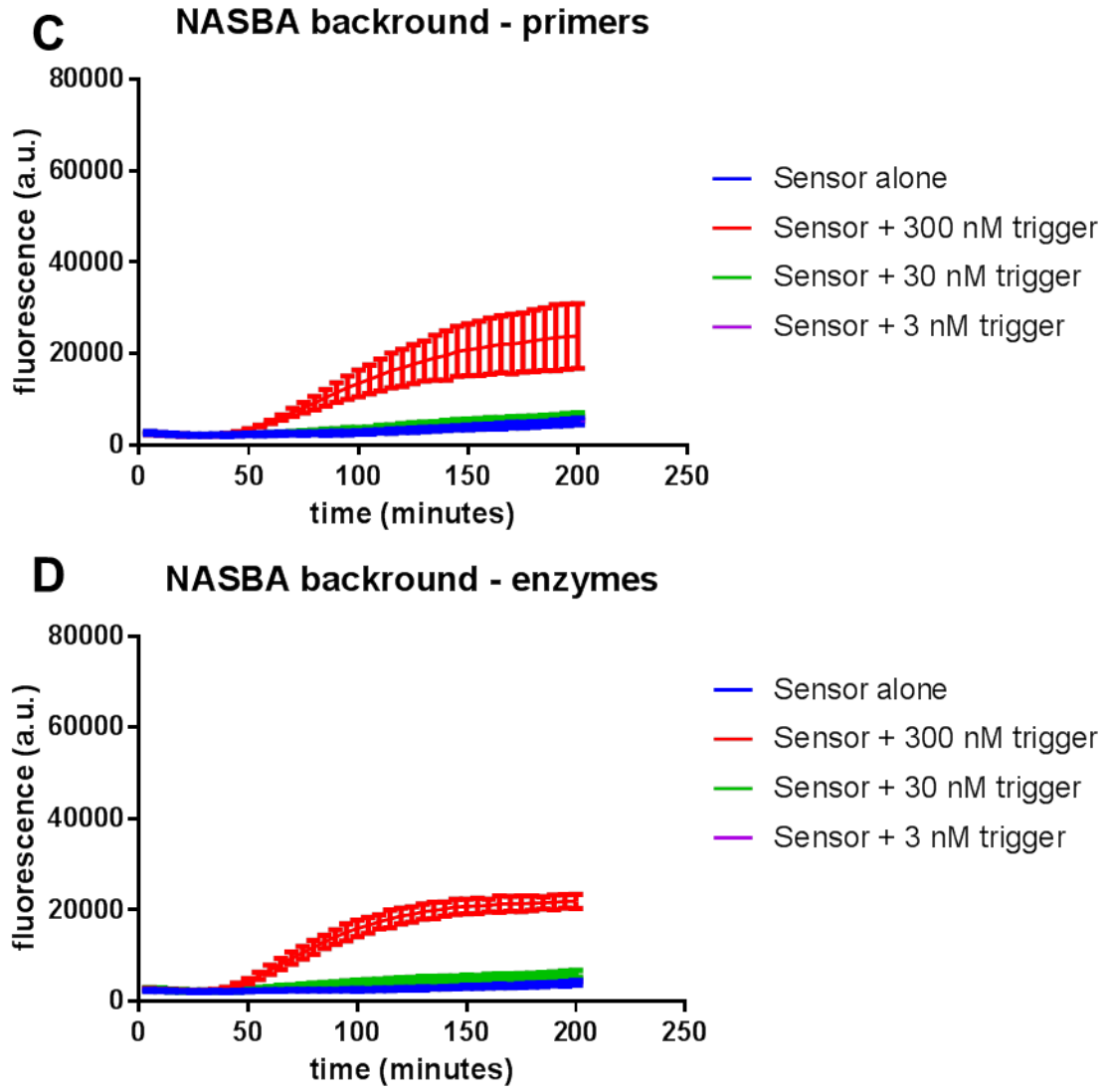

Figure 25. Titration of trigger input into one-pot NASBA reaction.
All reactions were run with the Zika 3B toehold switch. (A) A standard NEB toehold reaction serves as a point of comparison. (B) One-pot NASBA (NASBA background) yielded significant signal amplification over the traditional NEB toehold reaction for both 300 nM trigger input and 30 nM trigger input. (C) The one-pot NASBA reaction cannot amplify toehold signal in the absence of the NASBA primers. (D) The one-pot NASBA reaction cannot amplify toehold signal in the absence of the NASBA enzymes.

With a functioning one-pot reaction, we moved towards optimization of the reaction conditions. We approached this by titrating buffer components one by one and

updating the NASBA supplements appropriately before moving on to the next component. Each reaction condition was tested against an NEB background reaction (with no amplification), as well as a defective NASBA background that was missing a key component of the NASBA reaction, such as primers or enzymes, and which serves as a negative control.

Our baseline conditions are shown in Figure 26, for comparison. We found that the optimal reaction conditions include: running the reaction at 39°C (Figure 27), rehydration with 4% DMSO (Figure 28) (note that DMSO is an organic compound that cannot be freeze-dried), no additional NTPs beyond what is included in the standard NEB reaction (Figure 29), and .5 mM dNTP (Figure 30).

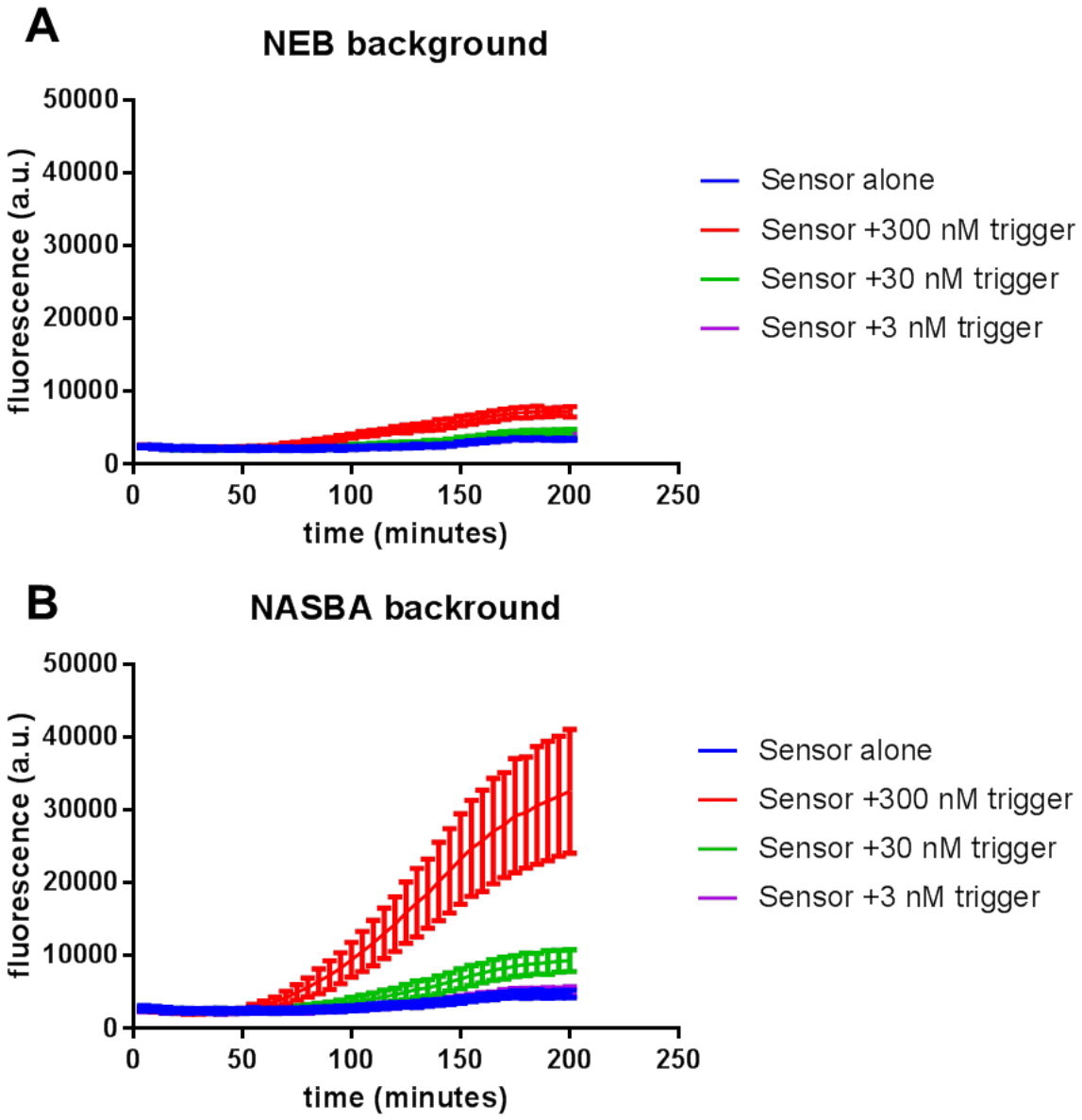
A
NEB background
fluorescence (a.u.)
50000
40000
30000
20000
10000
0
0
50
100
150
200
250
time (minutes)
Sensor alone
Sensor +300 nM trigger
Sensor +30 nM trigger
Sensor +3 nM trigger
B
NASBA backround
fluorescence (a.u.)
50000
40000
30000
20000
10000
0
0
50
100
150
200
250
time (minutes)
Sensor alone
Sensor +300 nM trigger
Sensor +30 nM trigger
Sensor +3 nM trigger

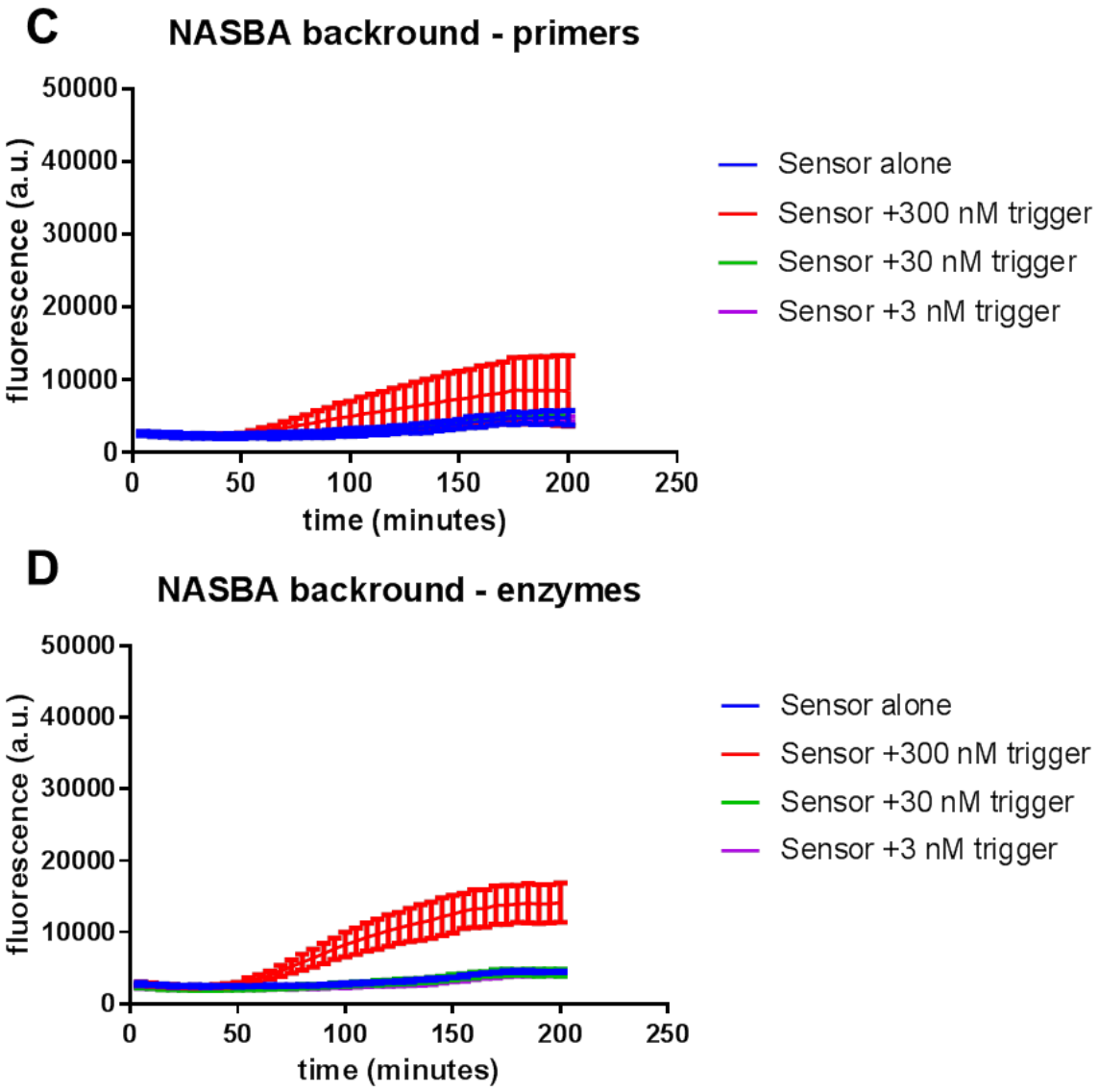

Figure 26. Baseline one-pot NASBA reaction.
All reactions were run with the Zika 3B toehold switch; this reaction is with a new batch of sensor, which yields slightly maximum output than the batch used in Figure 25. (A) A standard NEB toehold reaction serves as a point of comparison. (B) One-pot NASBA (NASBA background) yielded significant signal amplification over the traditional NEB toehold reaction for both 300 nM trigger input and 30 nM trigger input. (C) The one-pot NASBA reaction cannot amplify toehold signal in the absence of the NASBA primers. (D) The one-pot NASBA reaction cannot amplify toehold signal in the absence of the NASBA enzymes.

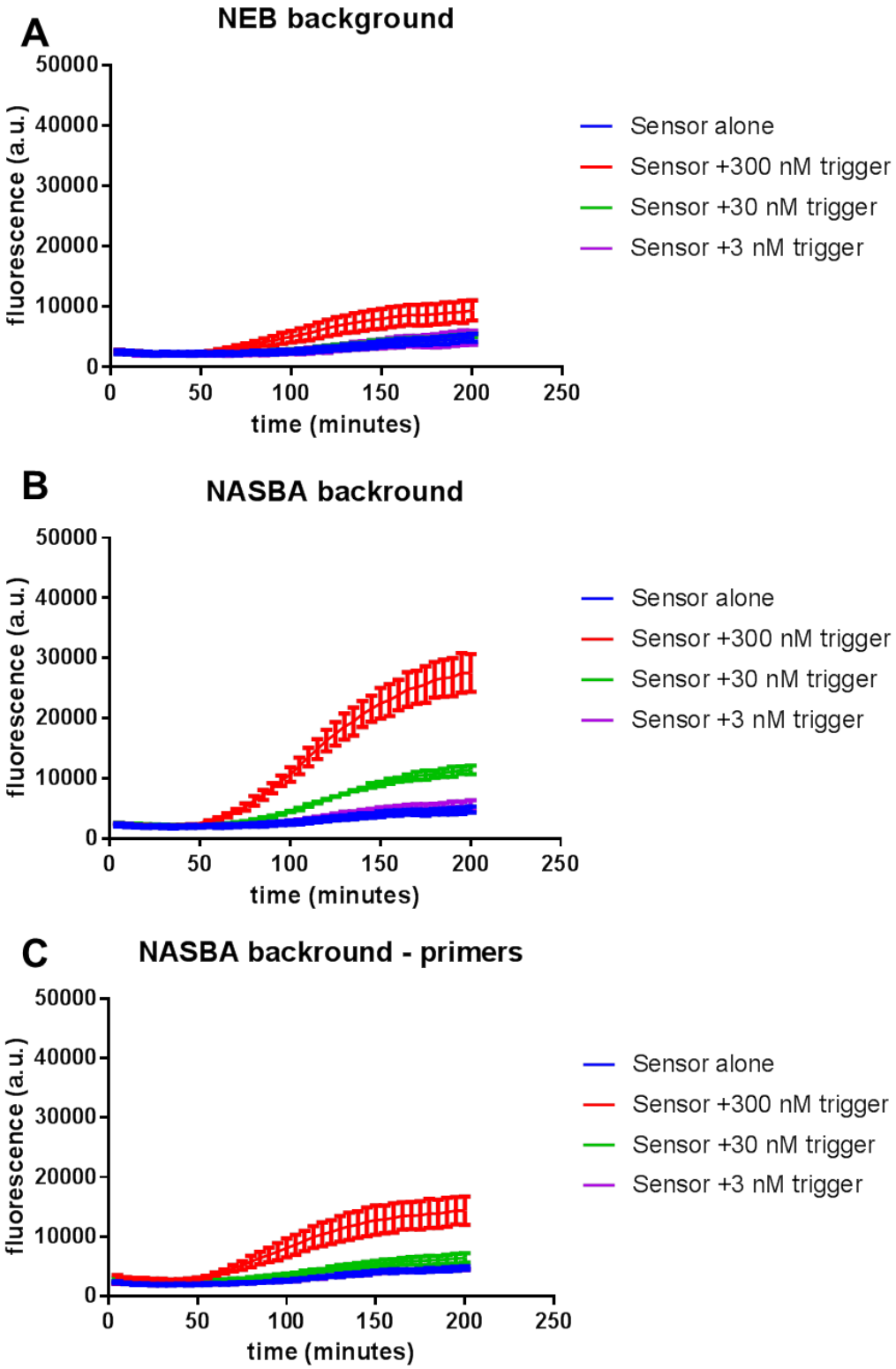

Figure 27. One-pot NASBA reaction at 39°C yields better amplification than at 37°C.
All reactions were run with the Zika 3B toehold switch. Reactions were run at 39°C, yielding

better amplification and less noise in reaction output. (A) A standard NEB toehold reaction serves as a point of comparison. (B) One-pot NASBA (NASBA background) yielded significant signal amplification over the traditional NEB toehold reaction for both 300 nM trigger input and 30 nM trigger input. (C) The one-pot NASBA reaction cannot amplify toehold signal in the absence of the NASBA primers. (D) The one-pot NASBA reaction cannot amplify toehold signal in the absence of the NASBA enzymes.

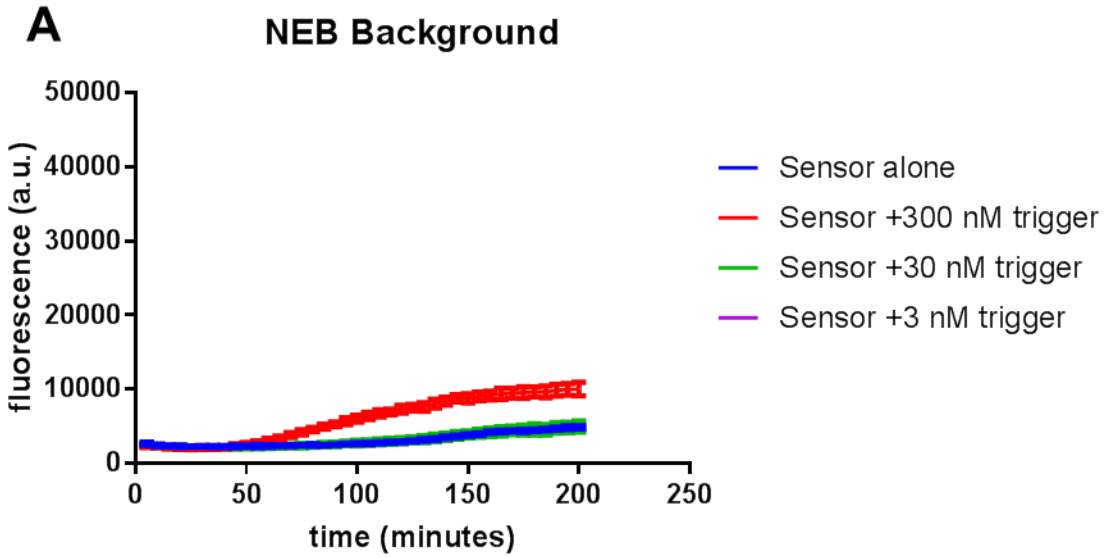

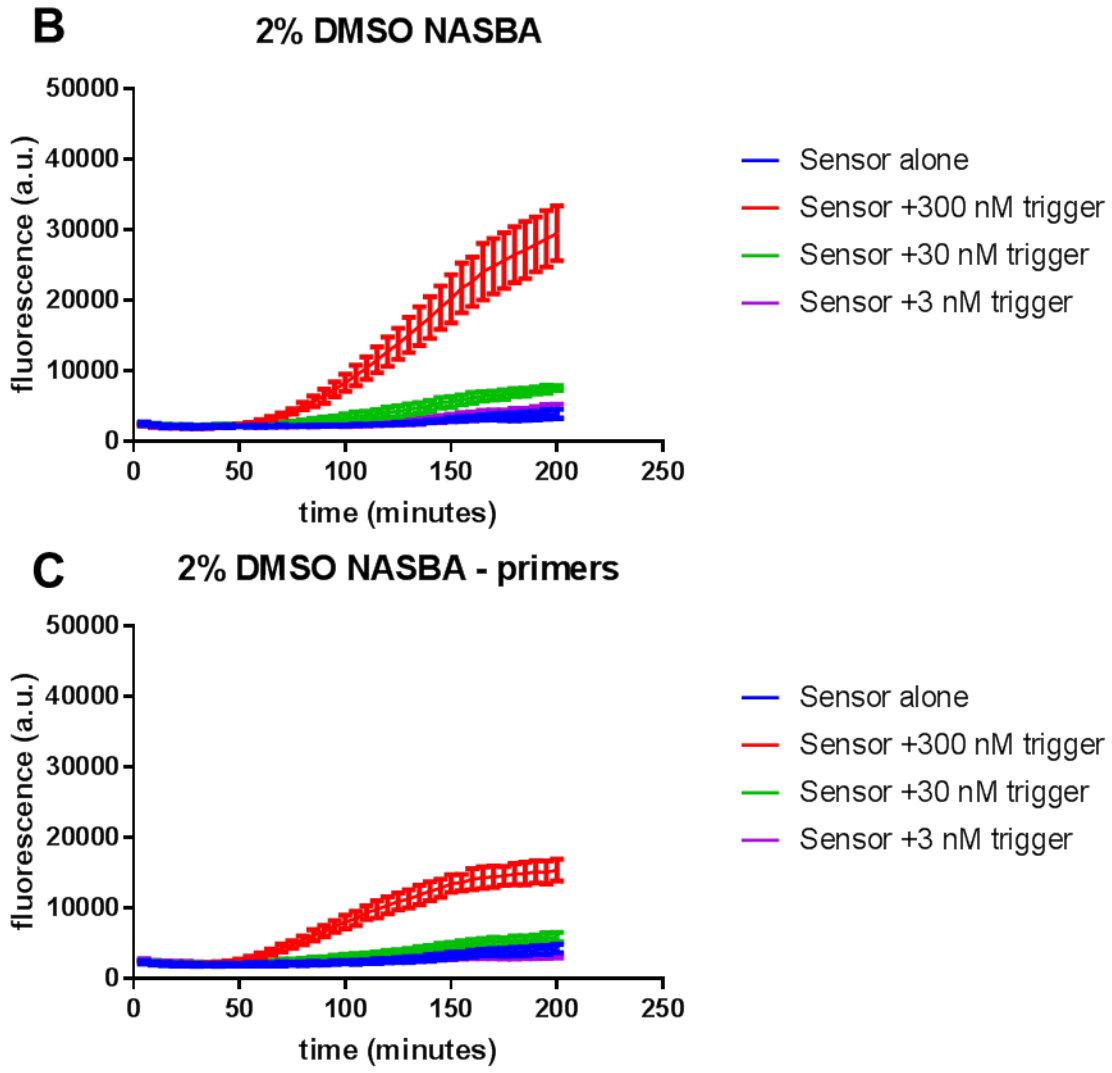
B
2% DMSO NASBA
fluorescence (a.u.)
50000
40000
30000
20000
10000
0
0
50
100
150
200
250
time (minutes)
Sensor alone
Sensor +300 nM trigger
Sensor +30 nM trigger
Sensor +3 nM trigger
C
2% DMSO NASBA - primers
fluorescence (a.u.)
50000
40000
30000
20000
10000
0
0
50
100
150
200
250
time (minutes)
Sensor alone
Sensor +300 nM trigger
Sensor +30 nM trigger
Sensor +3 nM trigger

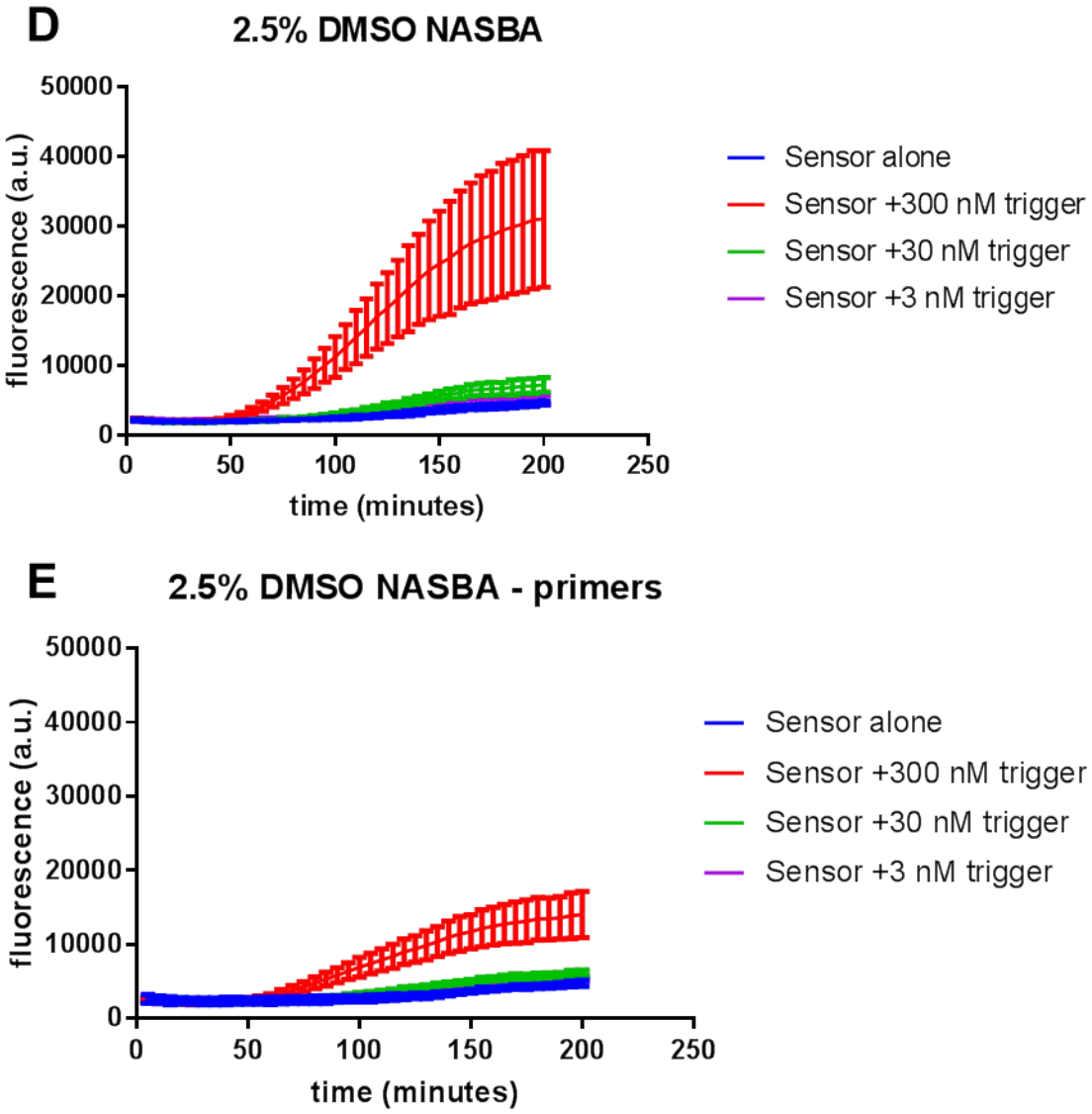
D
2.5% DMSO NASBA
fluorescence (a.u.)
50000
40000
30000
20000
10000
0
0
50
100
150
200
250
time (minutes)
Sensor alone
Sensor +300 nM trigger
Sensor +30 nM trigger
Sensor +3 nM trigger
E
2.5% DMSO NASBA - primers
fluorescence (a.u.)
50000
40000
30000
20000
10000
0
0
50
100
150
200
250
time (minutes)
Sensor alone
Sensor +300 nM trigger
Sensor +30 nM trigger
Sensor +3 nM trigger

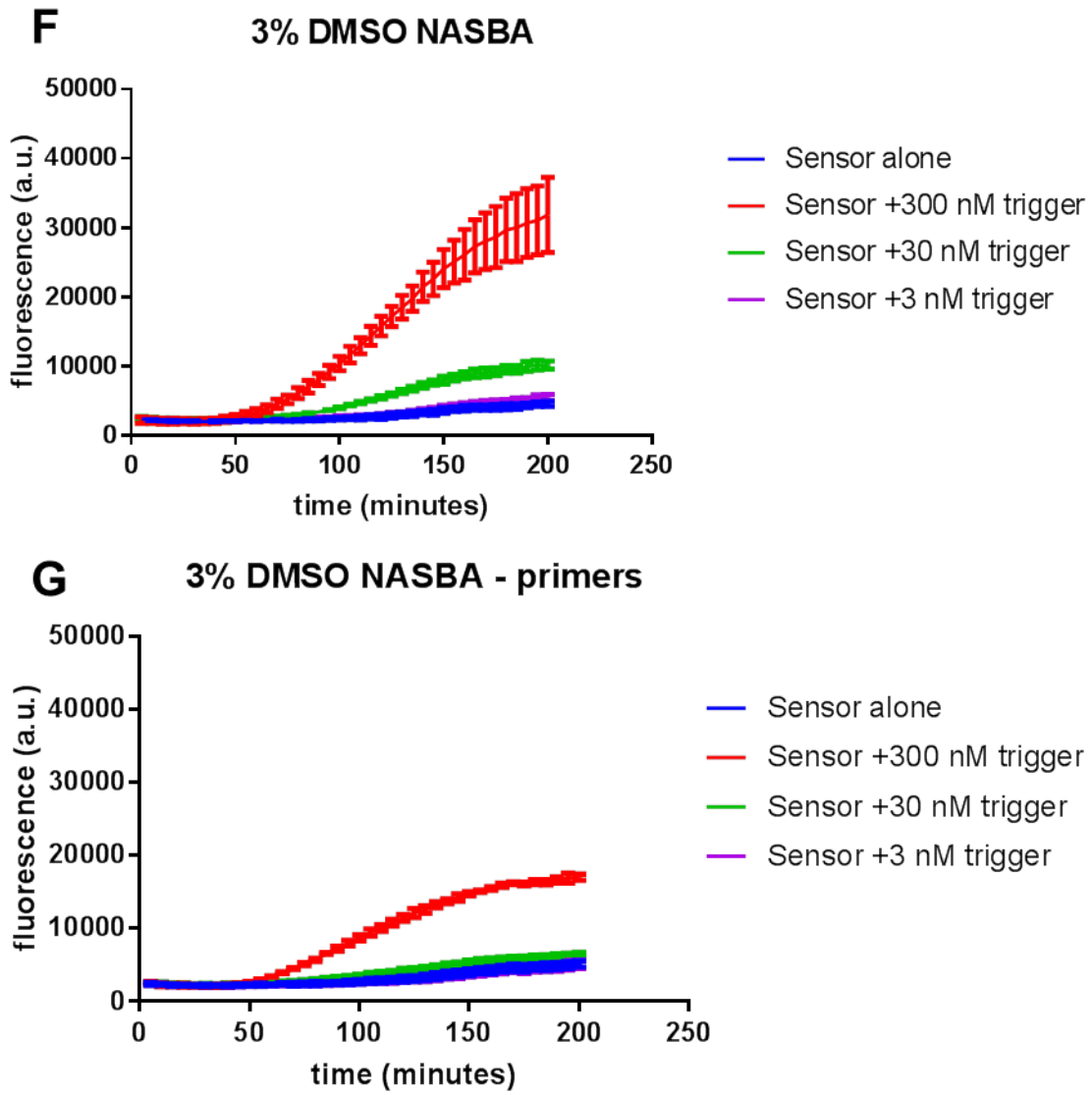
F
3% DMSO NASBA
fluorescence (a.u.)
50000
40000
30000
20000
10000
0
0
50
100
150
200
250
time (minutes)
Sensor alone
Sensor +300 nM trigger
Sensor +30 nM trigger
Sensor +3 nM trigger
G
3% DMSO NASBA - primers
fluorescence (a.u.)
50000
40000
30000
20000
10000
0
0
50
100
150
200
250
time (minutes)
Sensor alone
Sensor +300 nM trigger
Sensor +30 nM trigger
Sensor +3 nM trigger

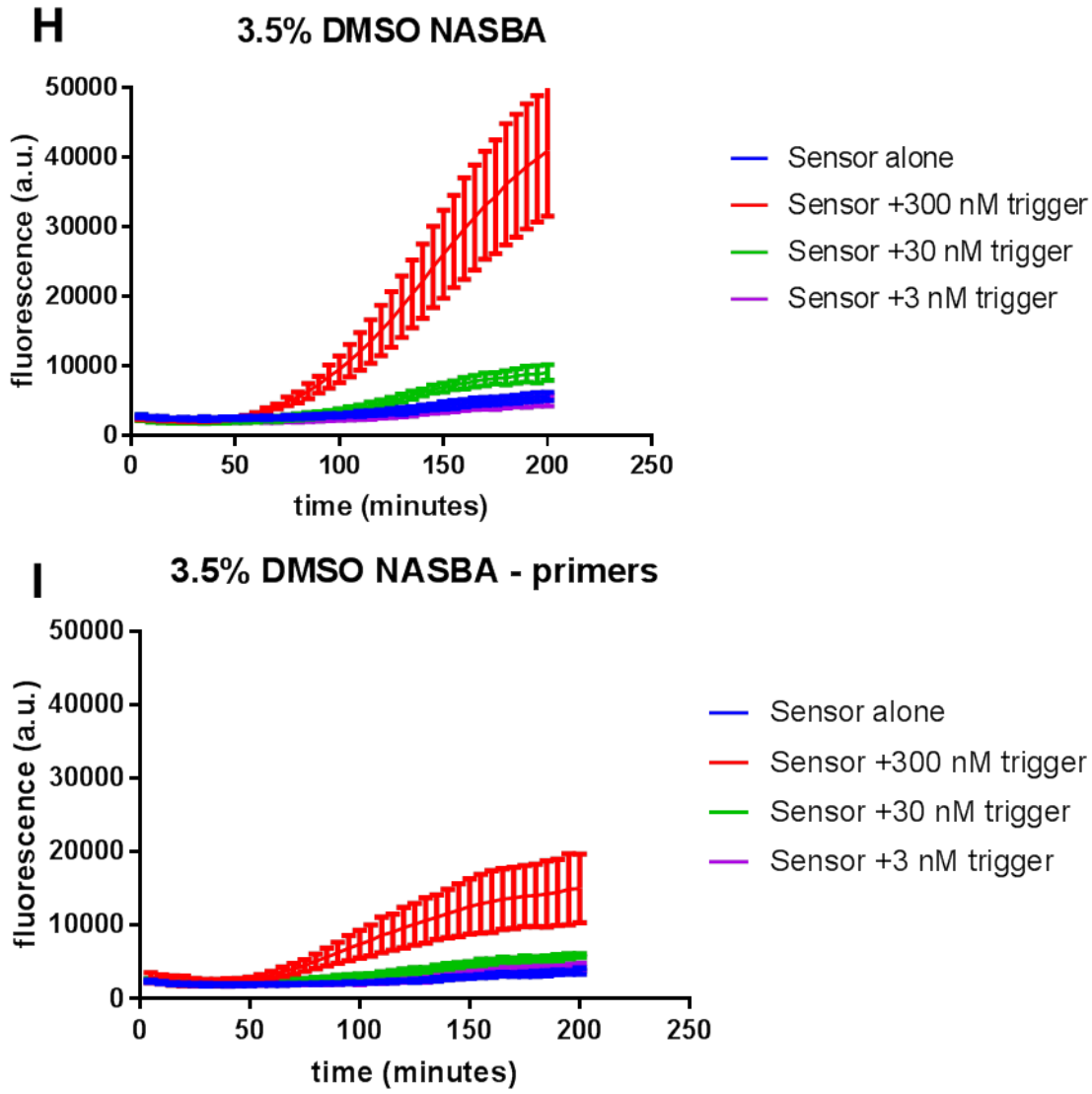
H
3.5% DMSO NASBA
fluorescence (a.u.)
50000
40000
30000
20000
10000
0
0
50
100
150
200
250
time (minutes)
Sensor alone
Sensor +300 nM trigger
Sensor +30 nM trigger
Sensor +3 nM trigger
I
3.5% DMSO NASBA - primers
fluorescence (a.u.)
50000
40000
30000
20000
10000
0
0
50
100
150
200
250
time (minutes)
Sensor alone
Sensor +300 nM trigger
Sensor +30 nM trigger
Sensor +3 nM trigger

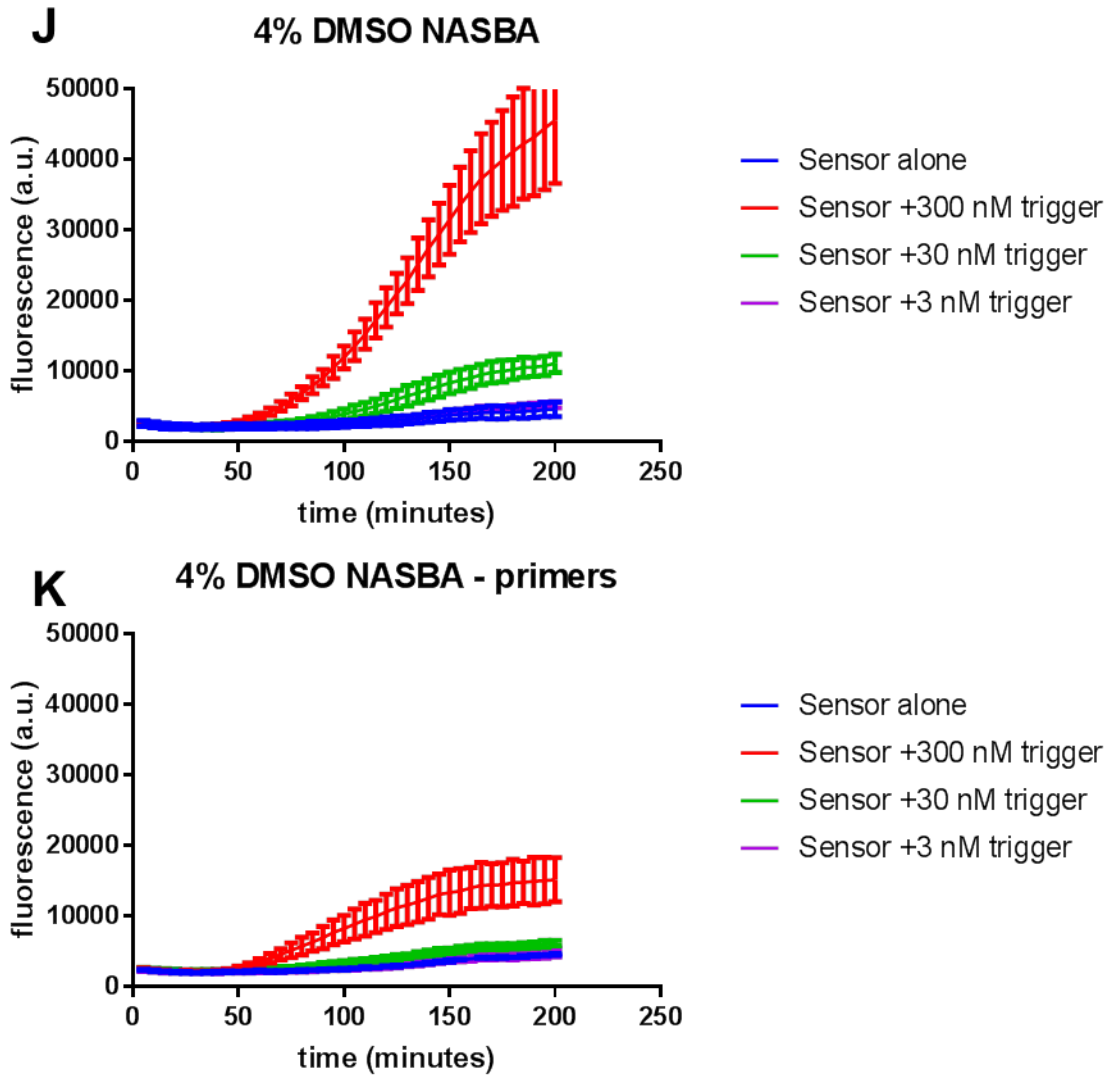

Figure 28. One-pot NASBA reaction rehydrated with 4% DMSO is optimal.
All reactions were run with the Zika 3B toehold switch at 39°C. Freeze-dried reactions were rehydrated with 2% (B, C), 2.5% (D, E), 3% (F, G), 3.5% (H, I), and 4% (J, K) DMSO. Subsequent experiments rehydrated with high concentrations of DMSO did not yield improved amplification (data not shown). (A) A standard NEB toehold reaction serves as a point of comparison. (B) through (K) DMSO titration on NASBA background, with and without primers. The one-pot NASBA reaction cannot amplify toehold signal in the absence of the NASBA primers, serving as a negative control for each condition.

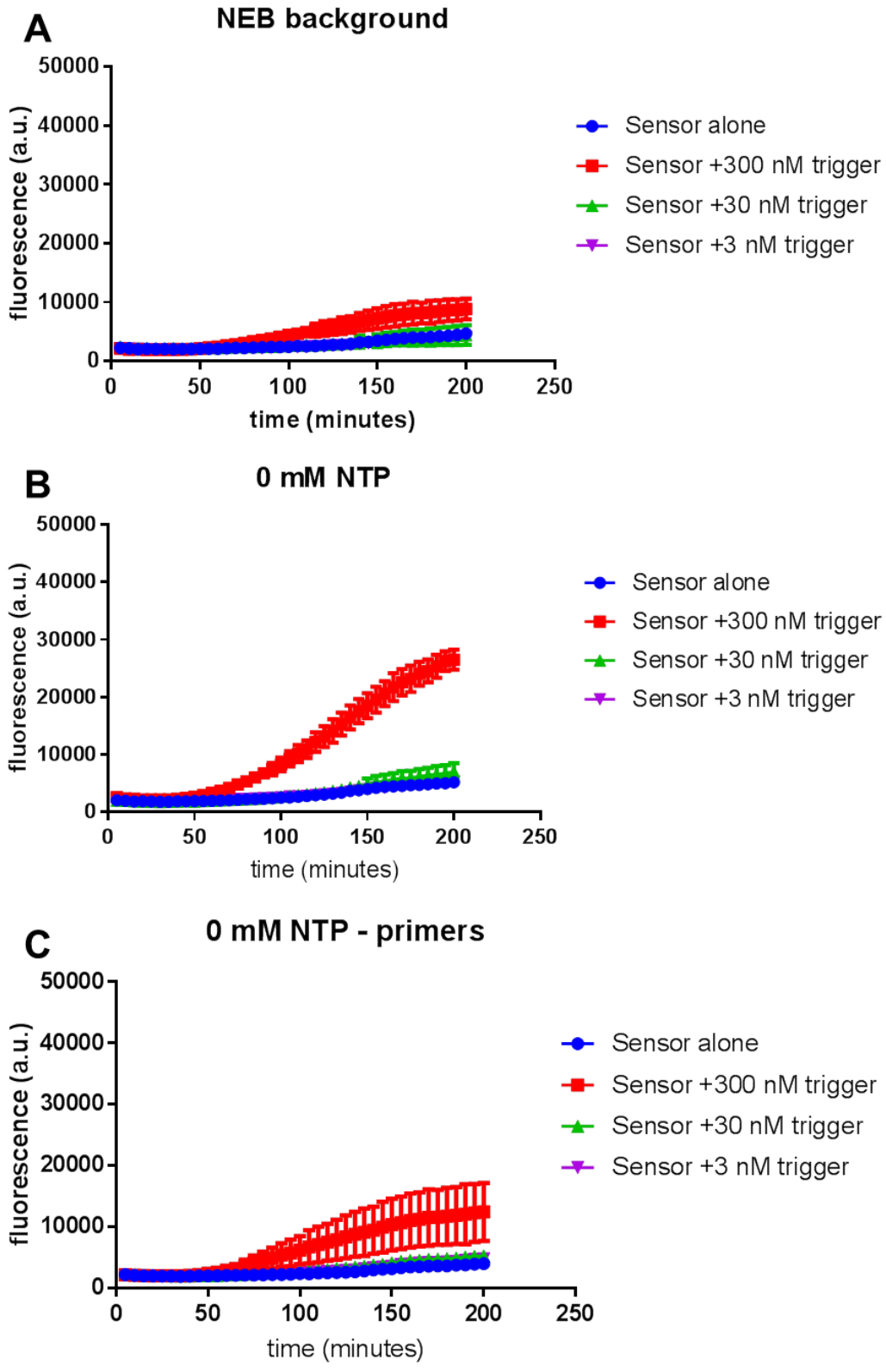
A
NEB background
fluorescence (a.u.)
50000
40000
30000
20000
10000
0
0
50
100
150
200
250
time (minutes)
Sensor alone
Sensor +300 nM trigger
Sensor +30 nM trigger
Sensor +3 nM trigger
B
0 mM NTP
fluorescence (a.u.)
50000
40000
30000
20000
10000
0
0
50
100
150
200
250
time (minutes)
Sensor alone
Sensor +300 nM trigger
Sensor +30 nM trigger
Sensor +3 nM trigger
C
0 mM NTP - primers
fluorescence (a.u.)
50000
40000
30000
20000
10000
0
0
50
100
150
200
250
time (minutes)
Sensor alone
Sensor +300 nM trigger
Sensor +30 nM trigger
Sensor +3 nM trigger

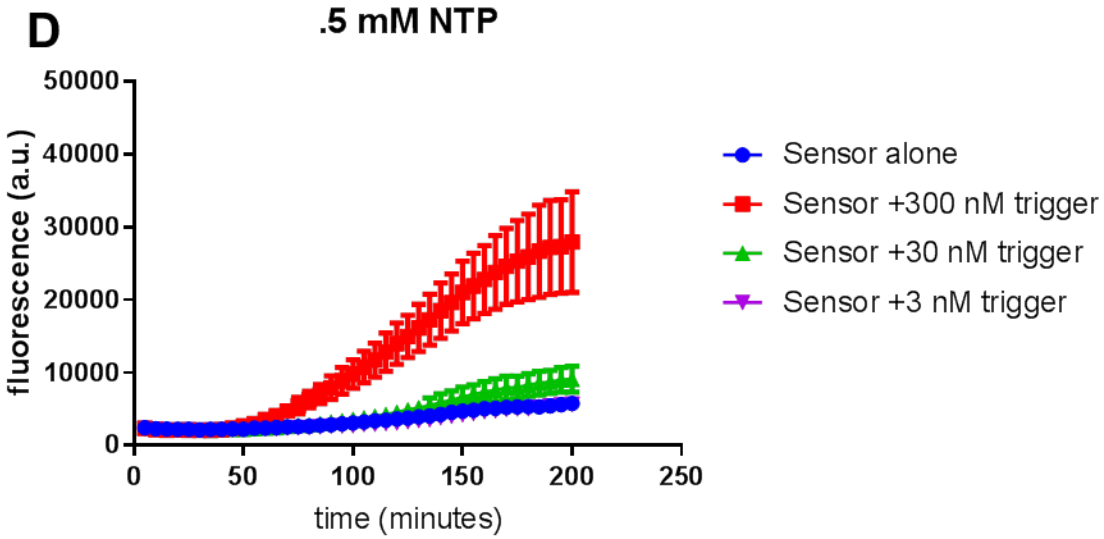
D
.5 mM NTP
fluorescence (a.u.)
50000
40000
30000
20000
10000
0
0
50
100
150
200
250
time (minutes)
Sensor alone
Sensor +300 nM trigger
Sensor +30 nM trigger
Sensor +3 nM trigger

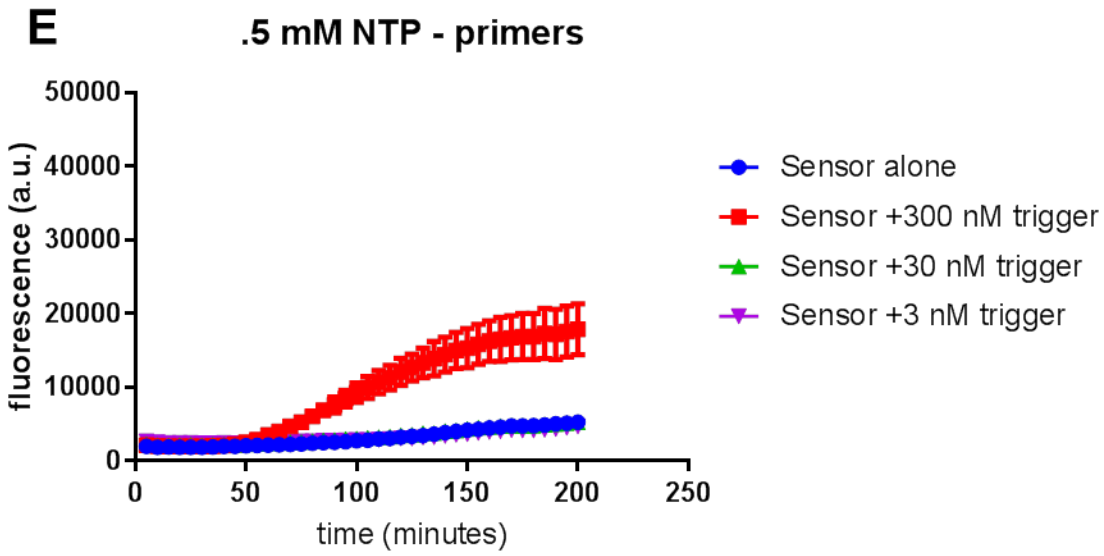
E
.5 mM NTP - primers
fluorescence (a.u.)
50000
40000
30000
20000
10000
0
0
50
100
150
200
250
time (minutes)
Sensor alone
Sensor +300 nM trigger
Sensor +30 nM trigger
Sensor +3 nM trigger

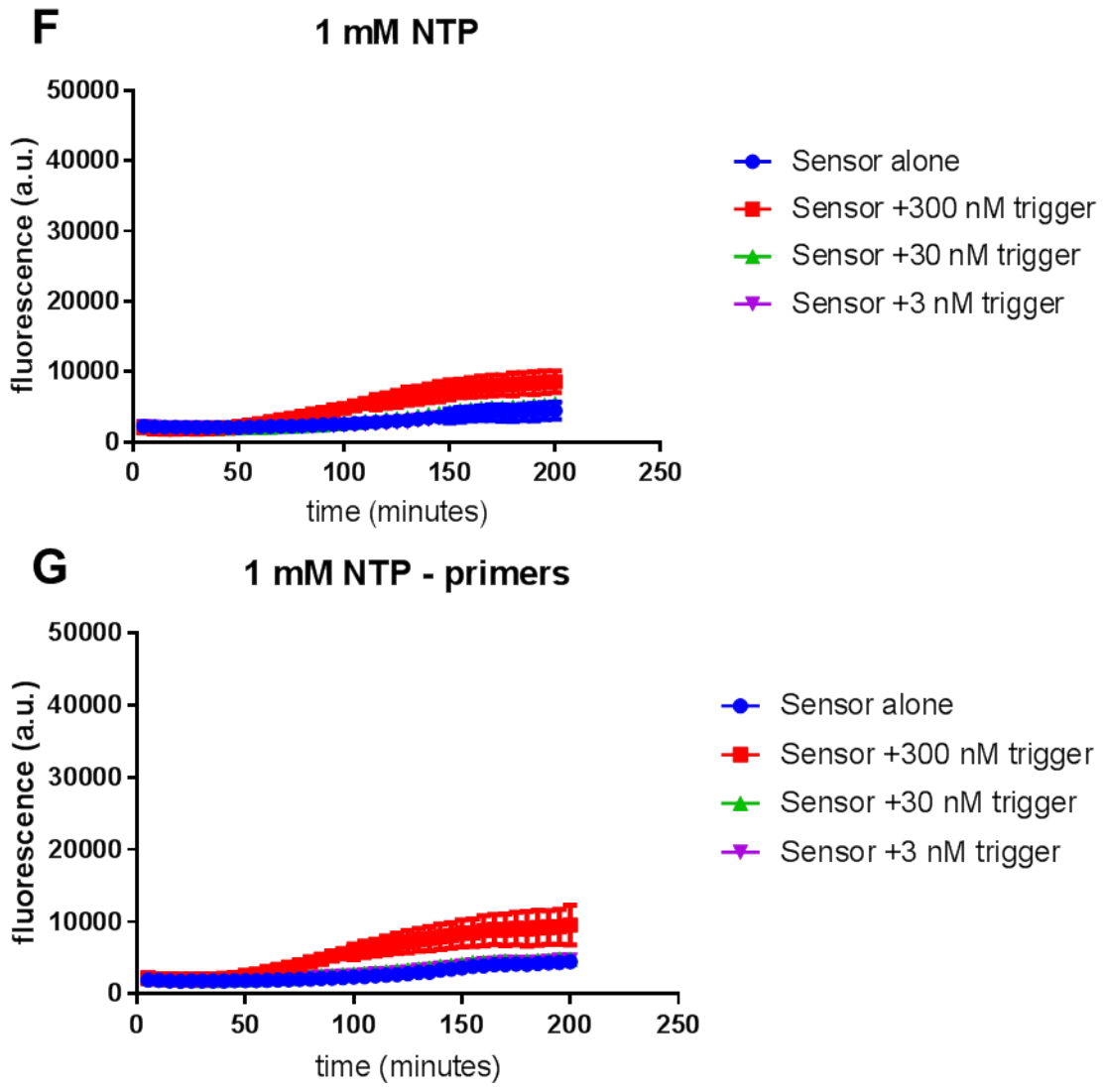
F
1 mM NTP
fluorescence (a.u.)
50000
40000
30000
20000
10000
0
0
50
100
150
200
250
time (minutes)
Sensor alone
Sensor +300 nM trigger
Sensor +30 nM trigger
Sensor +3 nM trigger
G
1 mM NTP - primers
fluorescence (a.u.)
50000
40000
30000
20000
10000
0
0
50
100
150
200
250
time (minutes)
Sensor alone
Sensor +300 nM trigger
Sensor +30 nM trigger
Sensor +3 nM trigger

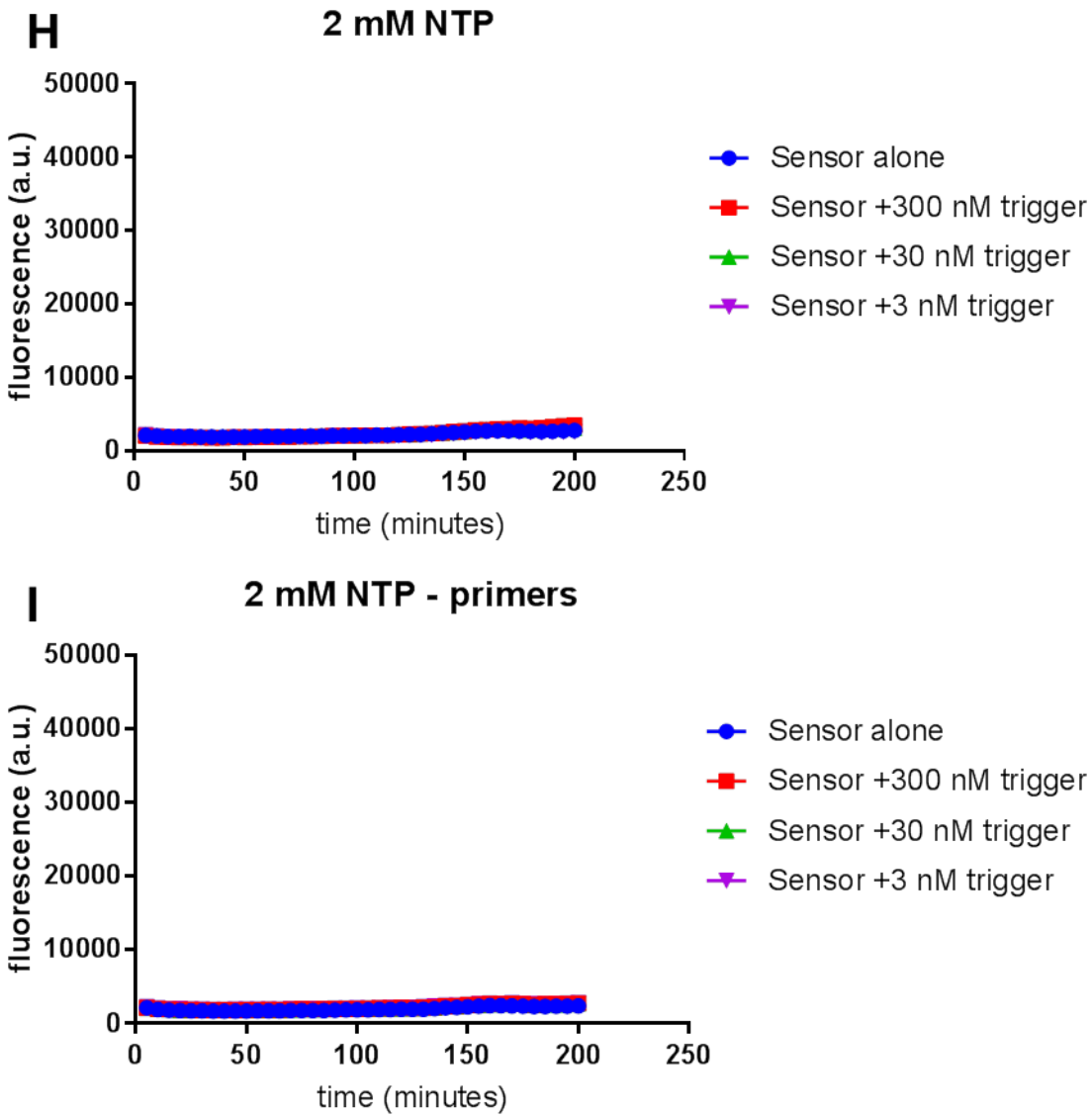
H
2 mM NTP
fluorescence (a.u.)
50000
40000
30000
20000
10000
0
0
50
100
150
200
250
time (minutes)
Sensor alone
Sensor +300 nM trigger
Sensor +30 nM trigger
Sensor +3 nM trigger
I
2 mM NTP - primers
fluorescence (a.u.)
50000
40000
30000
20000
10000
0
0
50
100
150
200
250
time (minutes)
Sensor alone
Sensor +300 nM trigger
Sensor +30 nM trigger
Sensor +3 nM trigger

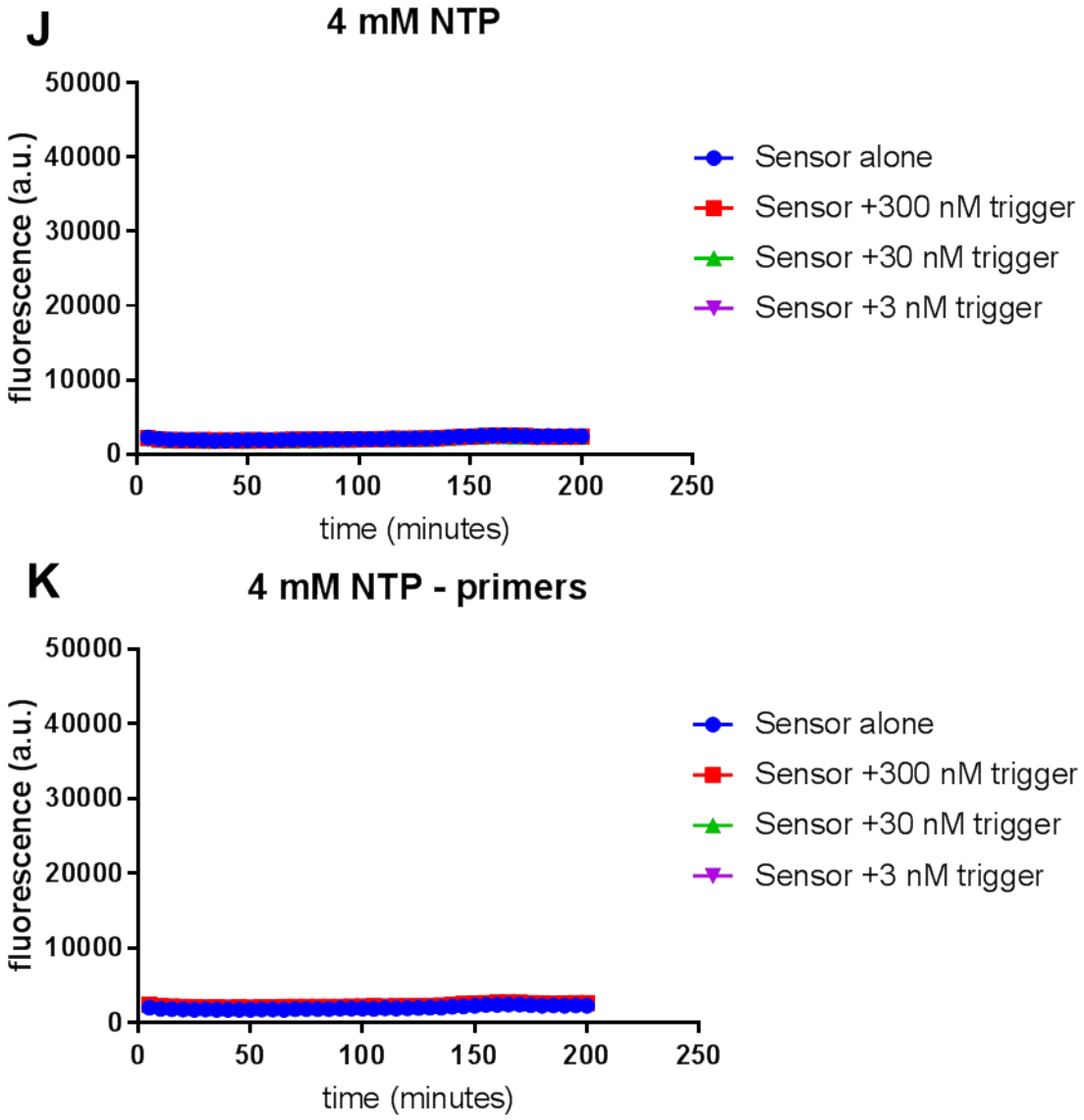

Figure 29. One-pot NASBA reaction with NTP titration.
All reactions were run with the Zika 3B toehold switch at 39°C and rehydrated with 4% DMSO. Reactions were freeze-dried with 0mM (B, C), .5 mM (D, E), 1 mM (F, G), 2 mM (H, I), and 4 mM (J, K) NTPs. NTPs at high concentrations were found to be inhibitory to the one-pot reaction. (A) A standard NEB toehold reaction serves as a point of comparison. (B) through (K) NTP titration on NASBA background, with and without primers. The one-pot NASBA reaction cannot amplify toehold signal in the absence of the NASBA primers, serving as a negative control for each condition.

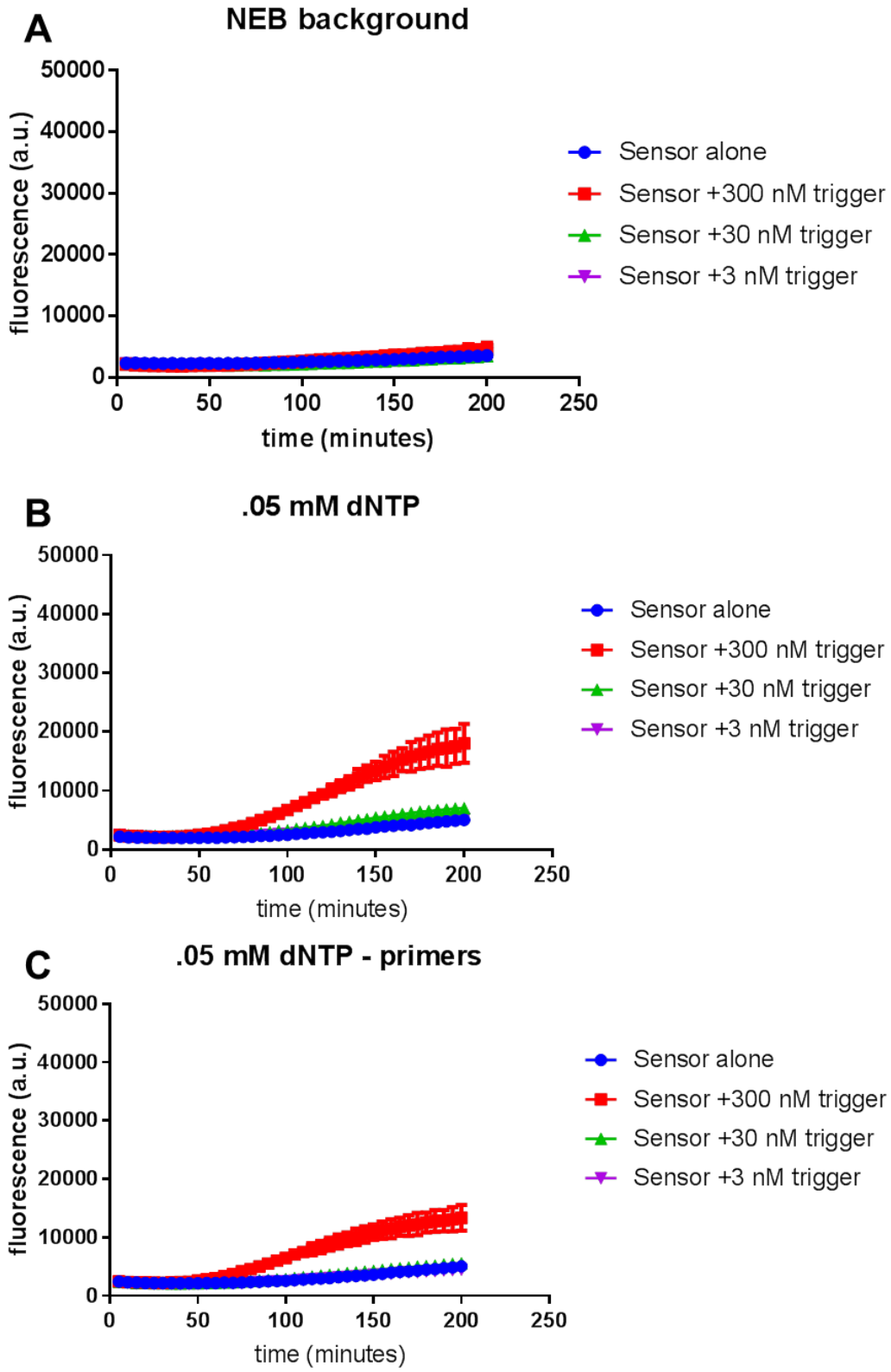
A
NEB background
fluorescence (a.u.)
50000
40000
30000
20000
10000
0
0
50
100
150
200
250
time (minutes)
Sensor alone
Sensor +300 nM trigger
Sensor +30 nM trigger
Sensor +3 nM trigger
B
.05 mM dNTP
fluorescence (a.u.)
50000
40000
30000
20000
10000
0
0
50
100
150
200
250
time (minutes)
Sensor alone
Sensor +300 nM trigger
Sensor +30 nM trigger
Sensor +3 nM trigger
C
.05 mM dNTP - primers
fluorescence (a.u.)
50000
40000
30000
20000
10000
0
0
50
100
150
200
250
time (minutes)
Sensor alone
Sensor +300 nM trigger
Sensor +30 nM trigger
Sensor +3 nM trigger

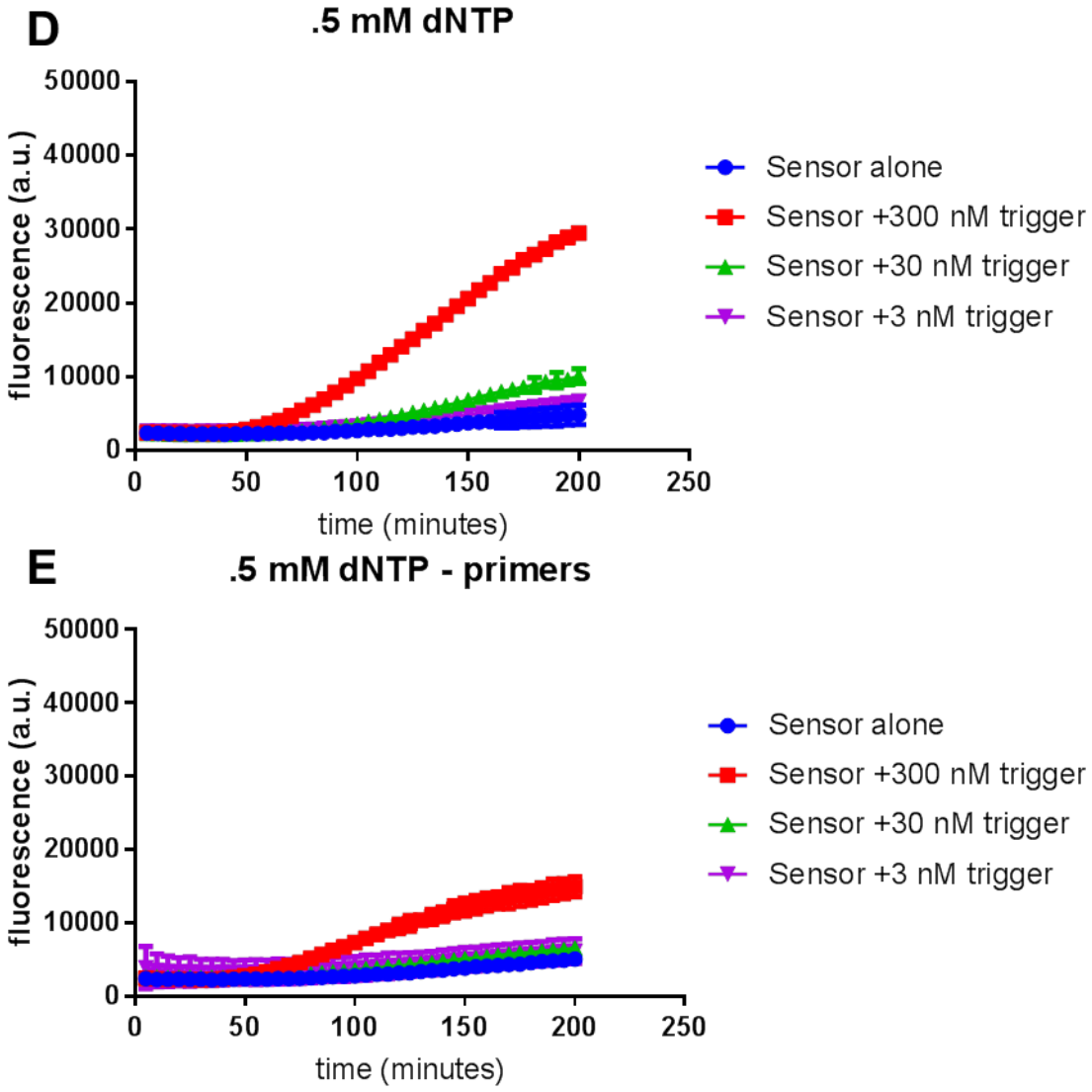
D
.5 mM dNTP
fluorescence (a.u.)
50000
40000
30000
20000
10000
0
0
50
100
150
200
250
time (minutes)
Sensor alone
Sensor +300 nM trigger
Sensor +30 nM trigger
Sensor +3 nM trigger
E
.5 mM dNTP - primers
fluorescence (a.u.)
50000
40000
30000
20000
10000
0
0
50
100
150
200
250
time (minutes)
Sensor alone
Sensor +300 nM trigger
Sensor +30 nM trigger
Sensor +3 nM trigger

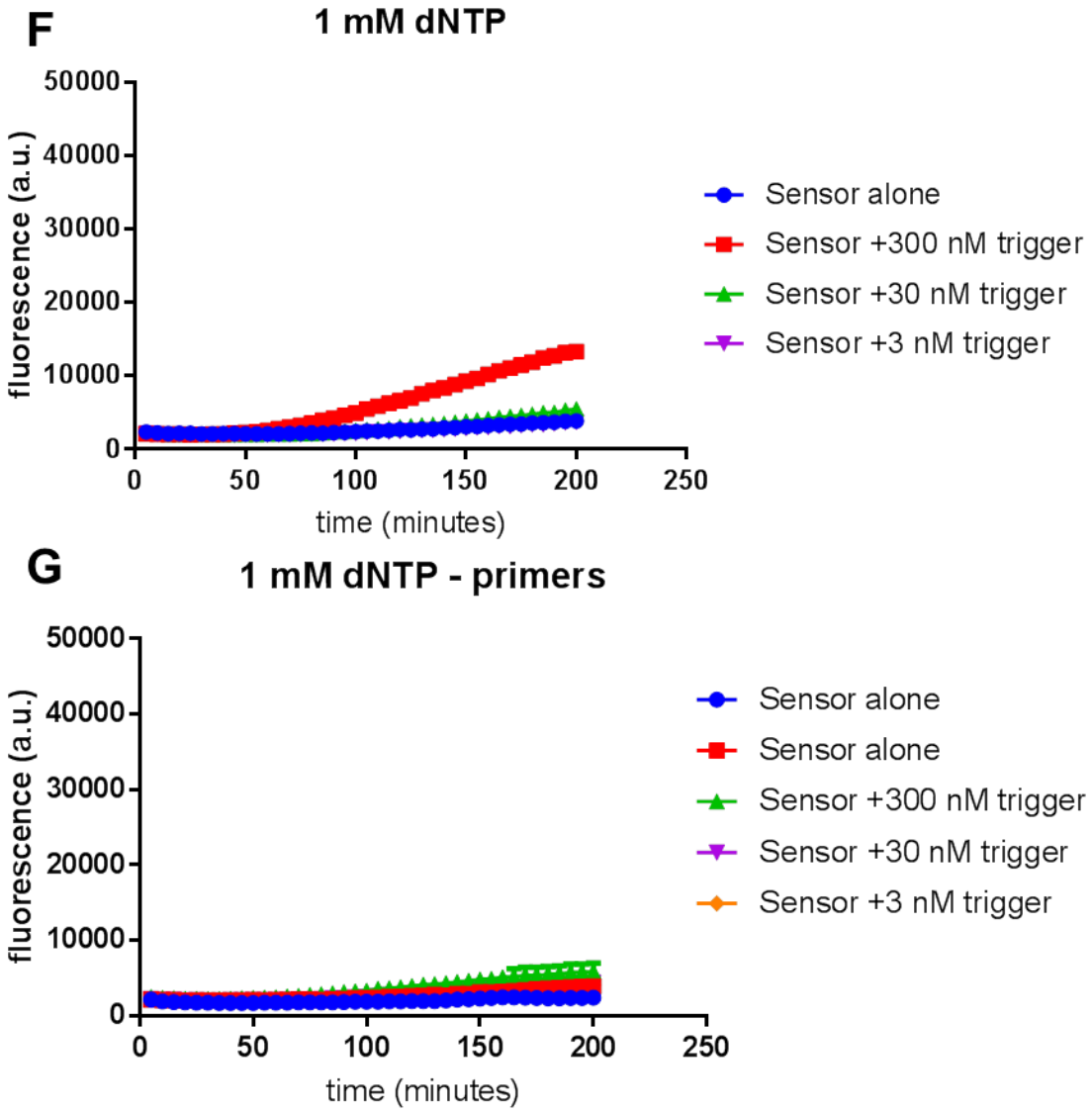
F
1 mM dNTP
fluorescence (a.u.)
50000
40000
30000
20000
10000
0
0
50
100
150
200
250
time (minutes)
Sensor alone
Sensor +300 nM trigger
Sensor +30 nM trigger
Sensor +3 nM trigger
G
1 mM dNTP - primers
fluorescence (a.u.)
50000
40000
30000
20000
10000
0
0
50
100
150
200
250
time (minutes)
Sensor alone
Sensor alone
Sensor +300 nM trigger
Sensor +30 nM trigger
Sensor +3 nM trigger

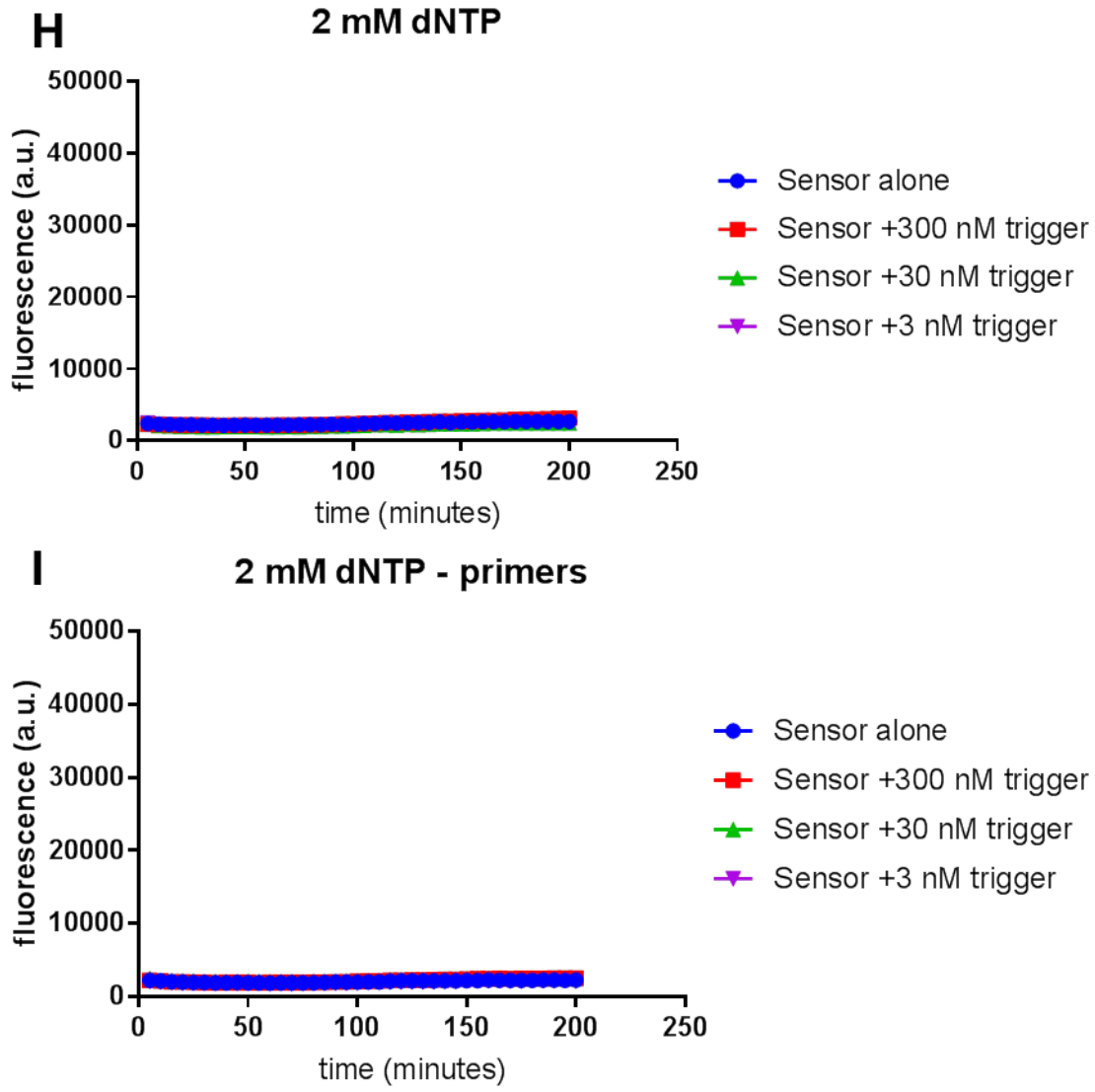

Figure 30. One-pot NASBA reaction with dNTP titration.
All reactions were run with the Zika 3B toehold switch at 39°C, rehydrated with 4% DMSO, and no additional NTPs beyond those already present in the NEB reaction. Reactions were freeze-dried with .05mM (B, C), .5 mM (D, E), 1 mM (F, G), and 2 mM (H, I) dNTPs. dNTPs at high concentrations were found to be inhibitory to the one-pot reaction. (A) A standard NEB toehold reaction serves as a point of comparison. (B) through (I) dNTP titration on NASBA background, with and without primers. The one-pot NASBA reaction cannot amplify toehold signal in the absence of the NASBA primers, serving as a negative control for each condition.

4.2.4 Alternative approaches

We looked into switching the NASBA reverse transcriptase enzyme (AMV reverse transcriptase), which runs most efficiently at 42°C, with a different reverse transcriptase that works better at 37°C. Sensiscript and Omniscript (Qiagen catalog numbers 205213 and 205113, respectively) are both reverse transcriptases that have been shown to work well at 37°C. These two enzymes additionally exhibit RNase H and DNA-dependent DNA polymerase activity, potentially allowing for minimizing enzymatic additions to the one-pot NASBA reaction. We ran several tests using these enzymes (data not shown). However, the results of these tests indicate that the NASBA primers would likely need to be redesigned to work well with these enzymes, as the primers we designed for NASBA do not appear to be compatible. It may be worth trying this approach in the future, especially to minimize costs and maximize reaction efficiency.

Another alternative approach to synthesizing the one-pot NASBA system would be to build a bacterial strain that expresses NASBA enzymes and make a "home-brew" TXTL system out of this strain. The engineered strain would need to express a subset of the following enzymes: reverse transcriptase, Rnase H, DNA polymerase, and T7 RNA polymerase. Presumably the bacterial strain's native DNA polymerase could be used for NASBA, thus eliminating the need to express this enzyme synthetically. As mentioned previously, the AMV reverse transcriptase used in the standard NASBA protocol is the limiting enzyme that functions best at higher temperatures (above 37°C). As such, it may be worth searching for a bacteriophage species that expresses a reverse transcriptase naturally upon infection. A reverse transcriptase from this source would be more likely to

work efficiently at 37°C in conjunction with other enzymes present in the cell lysate. Synthesizing a cell-free TXTL system from an engineered strain is tractable using the Jewett lab's comprehensive protocol for making TXTL systems in-house (Kwon and Jewett 2015). Notably, we have been able to robustly replicate this protocol in the lab with several engineered *E. coli* strains. Additionally, if necessary, these NASBA enzymes could be added in synthetically to the one-pot reaction, though this would add to the cost of each reaction.

To move these options forward, we ran preliminary experiments to test for inhibition of TXTL reactions by various relevant enzymes and buffers. All enzymes and buffers, except Omniscript and Sensiscript, were purchased from NEB, and the toehold reactions were performed using Zika Sensor 3B (Figure 31). We found that AMV reverse transcriptase, the Omniscript/Sensiscript buffer, NEB Buffer 2, and the RNase H buffer, all inhibit the TXTL toehold reaction at the concentrations we tested. However, some components, such as the AMV reverse transcriptase buffer and the Klenow DNA Polymerase allow the toehold reaction to function properly and yet other components including the Omniscript, Sensiscript, and RNase H enzymes are permissive for the toehold reaction and additionally display some amount of signal amplification.

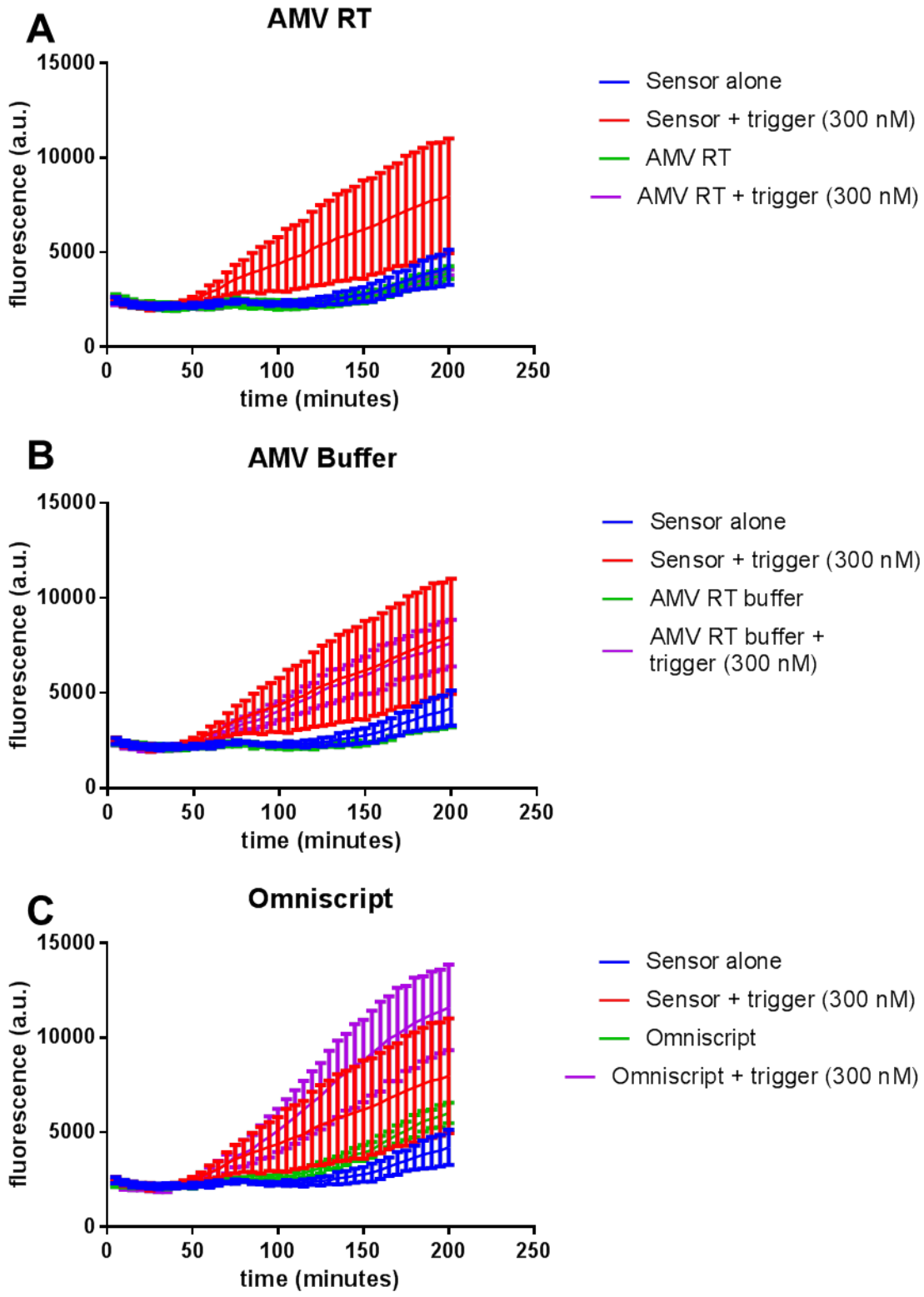
A
AMV RT
15000
10000
5000
0
fluorescence (a.u.)
0
50
100
150
200
250
time (minutes)
Sensor alone
Sensor + trigger (300 nM)
AMV RT
AMV RT + trigger (300 nM)
B
AMV Buffer
15000
10000
5000
0
fluorescence (a.u.)
0
50
100
150
200
250
time (minutes)
Sensor alone
Sensor + trigger (300 nM)
AMV RT buffer
AMV RT buffer +
trigger (300 nM)
C
Omniscript
15000
10000
5000
0
fluorescence (a.u.)
0
50
100
150
200
250
time (minutes)
Sensor alone
Sensor + trigger (300 nM)
Omniscript
Omniscript + trigger (300 nM)

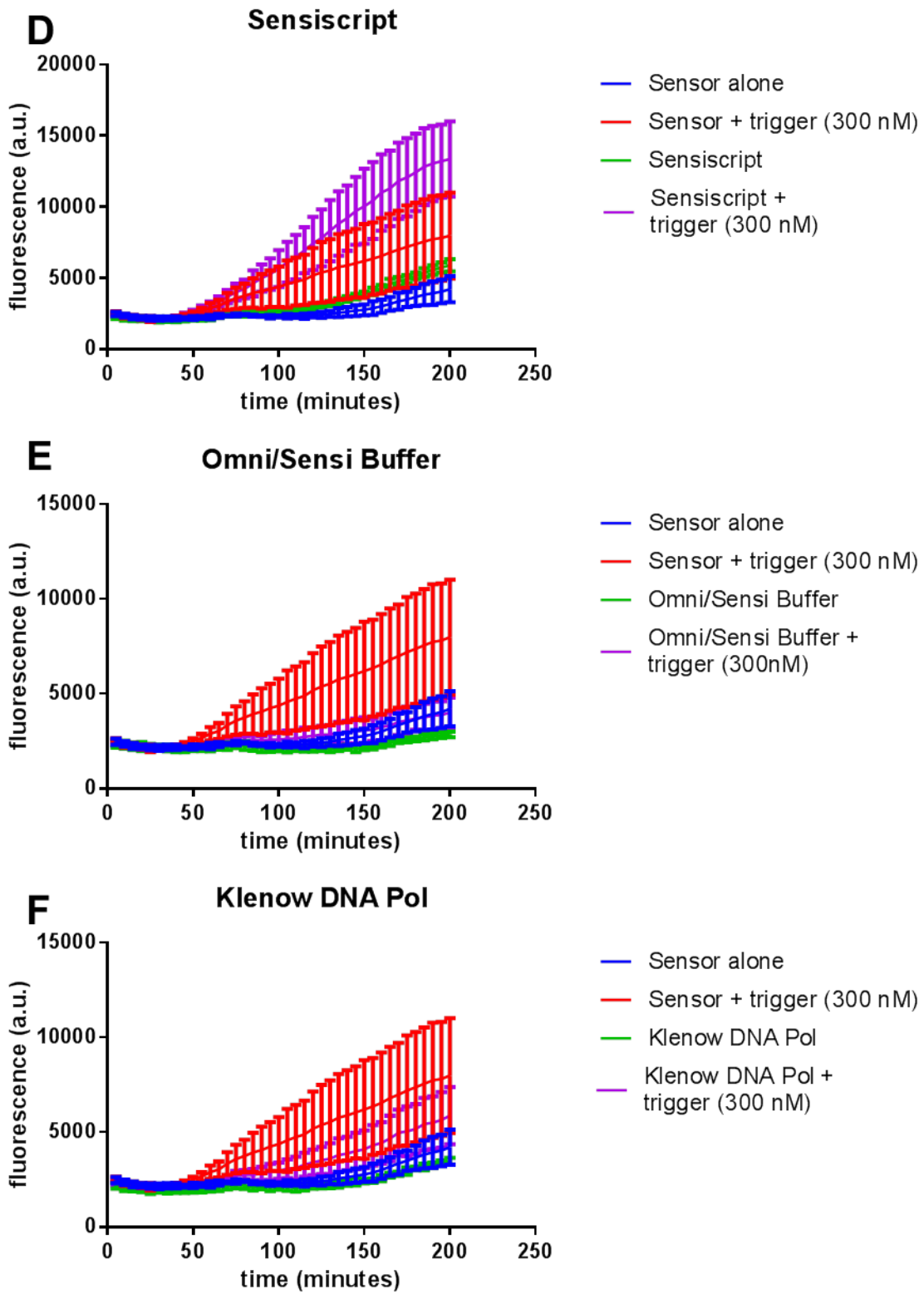
D
Sensiscript
fluorescence (a.u.)
time (minutes)
Sensor alone
Sensor + trigger (300 nM)
Sensiscript
Sensiscript + trigger (300 nM)
E
Omni/Sensi Buffer
fluorescence (a.u.)
time (minutes)
Sensor alone
Sensor + trigger (300 nM)
Omni/Sensi Buffer
Omni/Sensi Buffer + trigger (300nM)
F
Klenow DNA Pol
fluorescence (a.u.)
time (minutes)
Sensor alone
Sensor + trigger (300 nM)
Klenow DNA Pol
Klenow DNA Pol + trigger (300 nM)

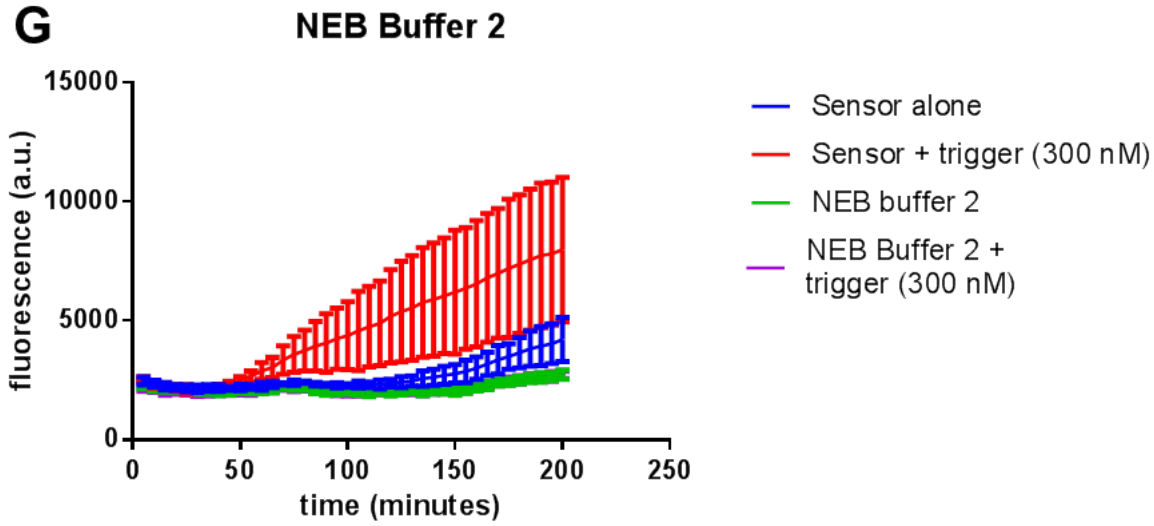

Figure 31. Effects of various enzymes and buffers on NEB toehold reaction.
(A) The addition of AMV reverse transcriptase enzyme inhibits the toehold reaction. (B) The AMV reverse transcriptase buffer is permissive to the toehold reaction. (C) The addition of Omniscript slightly enhances toehold activity. (D) The addition of Sensiscript slightly enhances toehold activity. (E) The Omniscript/Sensiscript buffer inhibits the toehold reaction. (F) Addition of Klenow DNA polymerase does not affect the toehold reaction. (G) NEB Buffer 2 is inhibitory to the toehold reaction. All reactions were run with the Zika 3B toehold switch.

4.3 Conclusion and future directions

We have promising results that indicate that it is possible to combine NASBA and the toehold reactions into a single paper-based one-pot reaction. However, more work is needed to continue the optimization process and search the parameter space for the optimal reaction conditions. One approach towards this optimization process is to continue with the one-by-one titrations of each buffer component. Keeping in mind that each component may affect the other in a nonlinear fashion, it would be necessary to titrate and test each component multiple times, varying the concentrations of the other buffer components. Alternative approaches such as doping in individual enzymes rather than the singular NASBA Enzyme mix and synthesizing a TXTL system in-house from a

bacterial strain that expresses NASBA enzymes should also be considered, especially to improve reaction sensitivity and lower reagent costs.

CHAPTER FIVE: FUTURE DIRECTIONS

5.1 Introduction

The following chapter introduces future directions for the paper-based platform. The first two sections (Sections 5.2 and 5.3) describe a proposal for the development of an antibiotic susceptibility testing (AST) platform using the paper-based diagnostic. The next section (Section 5.4) describes other technological advancements and approaches for building on the paper-based platform's diagnostic capabilities.

5.2 Background and motivation for paper-based AST

5.2.1 The antibiotic resistance problem

The Centers for Disease Control and Prevention (CDC) reports that the rise of antibiotic resistance has become a public health crisis, leading to over 2 million infections and 23,000 deaths per year in the United States alone (2013). Limited diagnostic capabilities leave health-care providers unable to precisely diagnose clinical infections and administer effective treatments in a timely manner. Furthermore, the use of broad-spectrum antibiotics clears out microbial niches and enables microbiome colonization by opportunistic pathogens (Kessel 2015). This threat has motivated efforts to reinvigorate antibiotic research and streamline funding and approval processes for new therapies (Hwang, Powers et al. 2015). However, the rapid transmission of antibiotic resistance challenges our present ability to develop additional small-molecule therapeutics, broad spectrum or otherwise (Ng, Ferreyra et al. 2013). Furthermore, lack of effective diagnostic measures leads to widespread misuse of antibiotic treatments, promoting

further development and spread of antibiotic resistance. The societal and monetary costs associated with the lack of effective diagnostic measures calls for improved antimicrobial testing capabilities (Hwang, Powers et al. 2015; Kessel 2015).

5.2.2 Antibiotic susceptibility testing (AST)

The growing prevalence of antibiotic resistance calls for new approaches in the development of antimicrobial diagnostics. Such diagnostics are essential in guiding the application of targeted therapies and preventing the evolution and spread of antibiotic resistance. Current antibiotic susceptibility testing (AST) methods are slow, leading to the empiric use of non-specific broad-spectrum antibiotics that cause iatrogenic infections and contribute to the increasing prevalence of antibiotic-resistant microbes. Clinically tractable diagnostics must be low-cost, rapid, sensitive, easy to use, and quickly adaptable to new targets.

Current ‘gold standard’ AST measures are based on minimum inhibitory concentration assays that evaluate long-term growth of clinical isolates in the presence of antibiotics (Andrews 2001). However, these assays are slow, taking at minimum 48 to 72 hours to produce accurate results. Other resistance-determination schemes rely on nucleic-acid based detection of genetic resistance measures. Though rapid and minimally labor intensive, these tests are costly and must be developed anew for each resistance gene, limiting their widespread use and applicability as the rapid emergence of new resistance mechanisms continues.

The lack of direct point-of-care (POC) antibiotic susceptibility determination leads to empiric use of non-specific broad-spectrum antibiotics. However, such

treatments often result in the elimination of both pathogenic and commensal microorganisms, clearing out native microbial niches which leads to iatrogenic infections such as *Clostridium difficile* and contributes to the increasing prevalence of antibiotic-resistant microbes (Kalghatgi, Spina et al. 2013; Modi, Collins et al. 2014).

5.2.3 Transcriptional signatures are indicative of antibiotic susceptibility

Antibiotic exposure has been shown to rapidly induce stereotypical transcriptional responses in microbes susceptible to antibiotics (Barczak, Gomez et al. 2012). These mRNA-based signatures have been used to identify microbial species in clinical samples and have also been shown to allow for rapid characterization of antibiotic susceptibility. They indicate robust changes to the transcriptome in response to antibiotic treatment, and have been shown to correlate with antibiotic susceptibility but not with antibiotic resistance. While transcript-based AST has demonstrated success in the laboratory, the methodology utilized is not clinically tractable due to time-and labor-intensive sample processing and the expensive and highly specialized instrumentation required for reliable diagnosis.

5.3 Paper-based AST proposal outline

I propose the development of a diagnostic tool to addresses the need for POC AST. The proposed approach takes advantage of the cell-free paper-based platform to deploy RNA sensors that can identify transcriptional signatures associated with antibiotic susceptibility. Because this approach takes advantage of phenotypic susceptibility markers rather than genetic markers of resistance, this testing method is agnostic to mechanism of resistance and is thus widely applicable and adaptable to new

organism/drug combinations. Furthermore, this diagnostic will provide a colorimetric output that can be read in a rapid, easy-to-use, and cost-effective manner via the electronic optical reader.

I propose to detect these native transcriptional signatures using RNA toehold switches, which have been shown to sense clinically relevant mRNA transcripts on the cell-free paper-based platform (Pardee, Green et al. 2014; Pardee, Green et al. 2016). The proposed platform scheme accepts an input of patient bacterial samples that have been treated with antibiotics for 15 to 30 minutes (Figure 32). The samples will then be processed and loaded onto a paper-based toehold sensor array for analysis.

The following sections delineate an approach for engineering this system. Section 5.3.1 proposes to develop and characterize RNA toehold switches for detection of antibiotic susceptibility markers. The next section (Section 5.3.2) focuses on advancing practical diagnostic applications and detection limits of this platform by incorporating an optimized one-pot NASBA protocol (described in Chapter 4). Lastly, section 5.3.3 proposes employment of the synthetic biology molecular toolbox to engineer logic-based circuits that integrate information from multiple toehold switch sensors into a single output measure of antibiotic susceptibility.

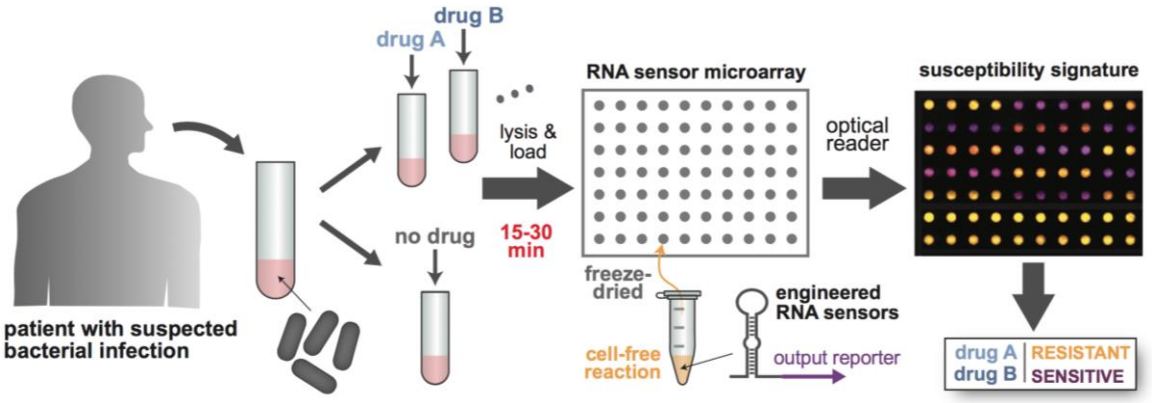

Figure 32. Paper-based antibiotic susceptibility testing platform.
The proposed clinical scheme involves sample collection and amplification from a patient with a suspected bacterial infection. The bacterial sample will then be briefly treated with antibiotics and prepared for loading on to the paper-based RNA sensor platform. mRNA susceptibility signatures will be reported on colorimetrically using engineered toehold switches. Figure from A. Khalil.

5.3.1 Design and characterize RNA toehold switch sensors for detection of native mRNA transcripts that are indicative of antibiotic susceptibility

The first challenge is to develop toehold switch sensors for a subset of transcripts that are highly indicative of antibiotic susceptibility. I propose to develop sensors for *E. coli* in response to three clinically relevant antibiotics: ciprofloxacin, ampicillin, and gentamicin. The transcripts most indicative of antibiotic susceptibility for these drug/microbe combinations have been previously identified, and include a family of three to five transcripts per drug (Figure 33) (Barczak, Gomez et al. 2012).

I propose to design several toehold switch sensors to diagnose the presence of each of these relevant transcripts. The toehold switches will then be screened for activity, sensitivity, and detection limits on the freeze-dried paper-based system. Initial experiments will be performed on total RNA purified from antibiotic-treated bacterial cultures; later tests will focus on optimizing transcript detection directly from cell lysate

material using the boiling protocol (Chapter 3), and ultimately from samples mimicking clinical isolation methods (such as urine-obtained isolates spiked into urine samples). Experiments will be carried out to determine the minimal sample processing that is necessary for robust transcript detection on paper.

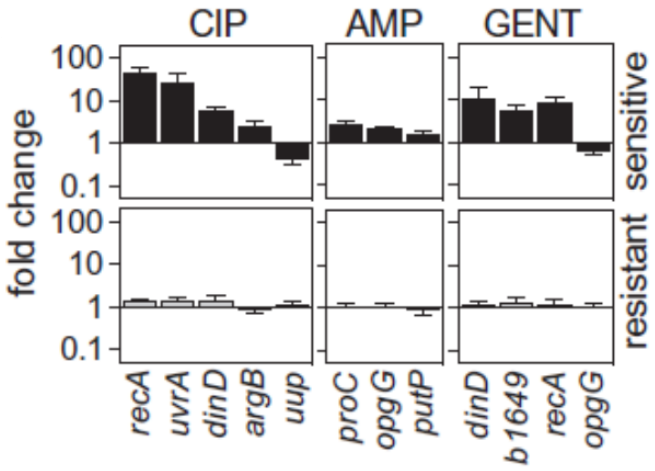

Figure 33. Transcriptional signatures correlate with antibiotic sensitivity.
mRNA susceptibility signatures for *E. coli* have been reported for ciprofloxacin, ampicillin, and gentamicin. These transcriptional signatures are able to differentiate sensitive and resistant bacterial populations in less than 30 minutes. Image from (Barczak, Gomez et al. 2012).

5.3.2 Optimize isothermal on-paper RNA amplification to increase diagnostic sensitivity

The next challenge is to optimize the one-pot NASBA amplification technique described in Chapter 4 and to incorporate the toehold switch sensors from section 5.3.1 into this streamlined amplification-detection protocol. I propose to develop a NASBA protocol that can be used to amplify and detect native mRNA transcripts that naturally occur at levels below the limit of detection of the toehold switch alone. This will allow

for easy expansion of the RNA amplification protocol to other toehold switch sensor targets, furthering the general diagnostic applications of the toehold switch technology. Fulfillment of this goal will occur in three optimization steps: optimizing the isothermal NASBA reaction at 37^0C to ease clinical tractability; freeze-drying the NASBA reaction on paper; and optimizing an on-paper one-pot reaction that allows the NASBA protocol and toehold switch reporters to work together simultaneously to increase diagnostic detection limits.

5.3.3 Design synthetic circuity that allows for integration of inputs from multiple mRNA transcripts into a single output indicative of antibiotic susceptibility.

Lastly, I propose to develop synthetic biology-based genetic circuitry that allows for multiplexed detection of stereotypical transcriptional changes in a one-pot reaction. Multiplexed detection of different transcript species will allow for integration of signal from the three to five transcripts that comprise one antibiotic-dependent transcriptional signature. This integration will allow for a simple yes/no output read in regards to antibiotic susceptibility and will significantly reduce the cost associated with the proposed AST by reducing the number of reactions needed to obtain a reliable diagnosis. To achieve this, I propose to utilize basic synthetic biology tools to build biomolecular circuitry that is sensitive and robust. Toehold switches have been shown to be highly orthogonal, and can easily be used to evaluate multi-input AND logic (Pardee, Green et al. 2014). Other methods such as CRISPR-based or intein-based circuits may also be used to integrate multiple inputs into a single output on paper (Chavez, Scheiman et al. 2015).

I propose to first design a simple, two-input AND gate that can integrate signal from two RNA toehold switch sensors, and to then expand to three-, four-, and five-input AND gates that integrate signal from the toehold switch sensors designed and optimized in Section 5.3.1.

5.4 Other technological advancements

5.4.1 NASBA-CRISPR cleavage assay to provide single base-pair discrimination

This section describes an innovation developed for Zika virus strain discrimination that can be paired with the paper-based toehold diagnostic platform (Pardee, Green et al. 2016). During epidemic outbreaks, it is often valuable to monitor pathogen lineage and geographic spread. In some cases, genetic variants may be responsible for different clinical manifestations of infection. For example, the Zika strain found in Brazil has been uniquely connected with higher incidences of fetal microcephaly and Guillain-Barre syndrome (Calvet et al., 2016; Mlakar et al., 2016). To allow for strain-specific detection and tracking, we developed an assay that provides single-base discrimination in a manner that is compatible with our freeze-dried sensor platform. Our assay, which we term NASBA-CRISPR Cleavage (NASBACC), leverages the sequence-specific nuclease activity of CRISPR/Cas9 to discriminate between viral lineages (Figure 34A). To do this, NASBACC exploits the ability of Cas9 to selectively cleave DNA only in the presence of an NGG protospacer adjacent motif (PAM). Since any non-biased mutation has a 48% probability of either creating a new PAM site or destroying an existing one (Table S1 from (Pardee, Green et al. 2016)), there many strain-specific PAM

sites that can be used for lineage discrimination (Figure 34B and 34C). In the NASBACC detection scheme, RNA sequences undergo NASBA amplification utilizing a reverse primer designed to append the trigger sequence of a synthetic toehold switch (sensor H, Figure 34A) (Pardee et al., 2014). In the presence of the appropriate PAM sequence and guide RNA target site, the double-stranded DNA that is synthesized as part of the NASBA reaction undergoes Cas9-mediated cleavage, resulting in a truncated RNA product that is unable to activate the sensor H toehold switch. In the absence of the PAM sequence, the full-length RNA product containing the sensor H trigger sequence is generated, allowing for sensor H activation. Trigger RNA is only amplified from DNA that is not cut by Cas9, thereby allowing for strain-specific detection using toehold sensor H.

Using the paper-based system, sensor 32B was able to distinguish between Zika and Dengue RNA sequences. However, this sensor could not discriminate between the African (Genbank accession number: KF268950) and American (Genbank accession number: KU312312) Zika variants (Figure 34D), a feature which may be useful in certain diagnostic applications. To address this, we applied our NASBACC detection scheme to discriminate between the African and American Zika strains. Due to a single base difference in the trigger regions of these two strains, a PAM site only exists in the American-lineage Zika virus sequence (Figure 34C). Thus, only the American strain sequence was cleaved by Cas9, which led to amplification of truncated RNA that did not activate the sensor H toehold switch (Figure 34E). Conversely, the African strain sequence does not contain the PAM site and was not cleaved by Cas9, which resulted in

amplification of full-length RNA that activated the sensor H toehold switch. Incorporating NASBACC into our diagnostic workflow can provide precise genotypic information within a few hours. As with the other biomolecular elements of this workflow, Cas9 is compatible with lyophilization and could be used in the field (Figure S5 from (Pardee, Green et al. 2016)).

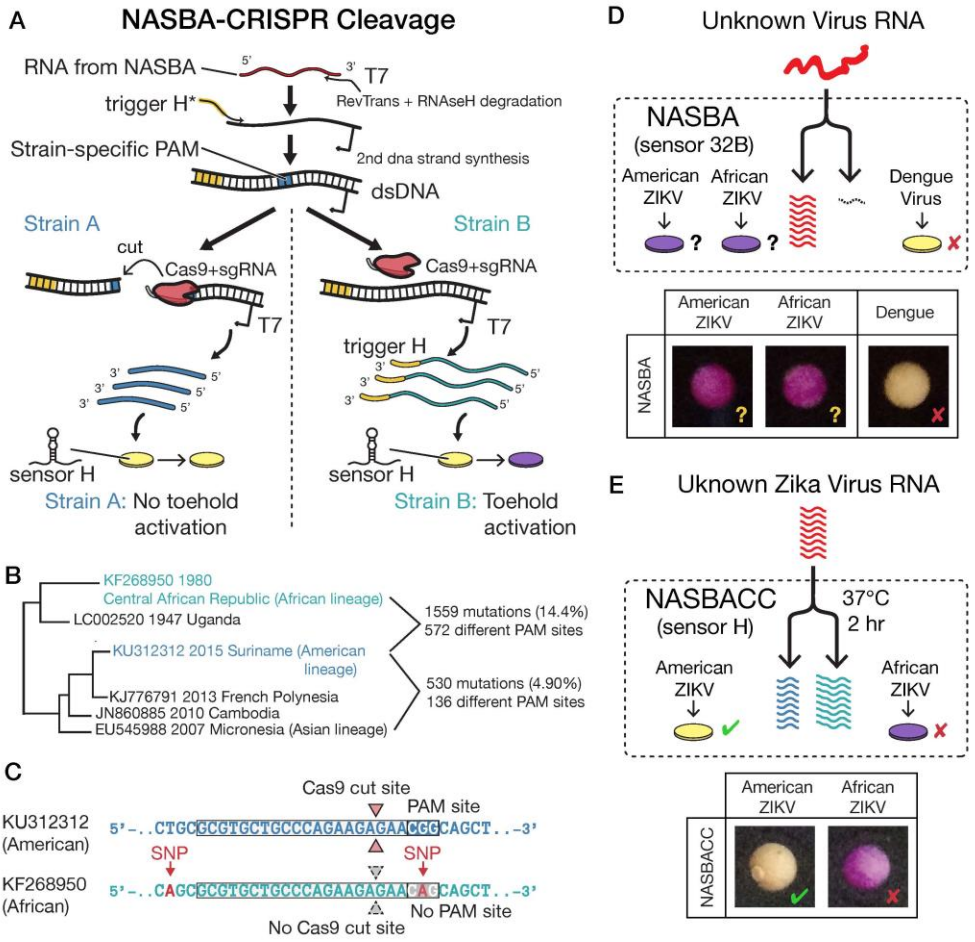

Figure 34. NASBA-CRISPR Cleavage (NASBACC) allows for strain differentiation at a single-base resolution.

(A) Schematic representation of NASBACC genotyping following a positive Zika diagnosis. A synthetic trigger sequence is appended to a NASBA-amplified RNA fragment through reverse transcription. The presence of a strain-specific PAM leads to the production of either truncated or full-length trigger RNA, which differentially activates a toehold switch (sensor H) (Pardee et al., 2014). (B) The probability that a non-biased single nucleotide polymorphism (SNP) between two strains can be discriminated by CRISPR/Cas9 is 48% (Table S4 from (Pardee, Green et al. 2016)). Hence, genetic drift between the American and African or Asian strains, while relatively small (14.4% and 4.9% sequence dissimilarity, respectively), has created hundreds of strain-specific PAM sites. (C) A SNP between African (KF268950) and American (KU312312) strains at site 7330 disrupts an existing PAM site, allowing for Cas9-mediated DNA cleavage only in the American strain. (D) Sensor 32B can distinguish between Dengue and Zika RNA sequences, but cannot discriminate between American and African Zika strains. Paper discs containing sensor 32B were rehydrated with 300 nM trigger RNA corresponding to sequences from American-Zika, African-Zika, or Dengue. Colorimetric outputs: a purple color indicates the activation of LacZ expression from the toehold switch, and a yellow color indicates the toehold switch remained inactive. (E) NASBACC can discriminate between American- and African-lineages of Zika virus. Paper discs containing sensor H were rehydrated with a 1:10 dilution of NASBACC reactions

initiated with 0.05 µl of a 300 nM RNA sample. In this case, an inactive toehold switch leads to a positive identification of the American Zika strain.

5.4.2 CRISPR-mediated improvements to diagnostic sensitivity

More recently, our group developed a new RNA/DNA sensing technique called SHERLOCK (Specific High-sensitivity Enzymatic Reporter unLOCKing) that has even greater sensitivity and specificity for target nucleic acids (Gootenberg, Abudayyeh et al. 2017). SHERLOCK utilizes the activity of the CRISPR effector C2c2, which recognizes and cleaves target RNAs with very high precision and sensitivity when programed with an appropriate guide RNA. Our group was able to use SHERLOCK to detect DNA and RNA target molecules at a concentration of 2 attomolar, equivalent to 1 copy per uL.

5.4.3 Microfluidic device for automated sample processing and diagnostic readout

Current limitations to in-field diagnostic use of our platform include the need for an automated, simple, and portable sample handling and processing scheme. In order to advance the diagnostic capabilities of the platform, it will be necessary to develop a microfluidic device to automate sample processing and minimize the hand-on time required by the diagnostic. As an example, the processing procedures used to detect Zika virus in blood plasma samples are: (1) Boiling the plasma sample (95C, 2 min) to inactivate the virus, break down the viral capsid, and release viral RNA (2) diluting the boiled sample 1:10 into water to dilute reaction inhibitors that are naturally present in blood plasma (3) loading the diluted sample into an isothermal RNA amplification reaction (41C, 30 min to 3 hrs) (4) loading the amplified sample onto a cell-free paper-

based reaction for detection via toeholds (37C, 1hr). A microfluidic device integrated into this platform would take blood plasma as an input and automate the above steps for a final output in the form of a paper-based reaction with an easy diagnostic readout. A diagnostic device could also be programmed to quantify toehold output. As such, it is also worth exploring alternative output readouts to the toehold switches including other colorimetric readouts, as well as chemiluminescence and fluorescent markers.

5.5 Conclusion

We have devised a rapid diagnostic development pipeline in response to the ongoing Zika virus outbreak. The serious but poorly understood complications of this viral infection make its timely diagnosis critical for patient health and for limiting its rapid proliferation. However, the poor performance of antibody detection methods (Lanciotti et al., 2008; de M Campos et al., 2016; Tappe et al., 2014; Zammarchi et al., 2015) and the limitations of traditional sequence-based diagnostics have left technical and economic challenges to meeting diagnostic needs.

Our paper-based platform directly addresses these needs by enabling sequence-specific detection of Zika virus in a low-cost manner that is tractable in low-resource settings. By freeze-drying cell-free transcription and translation systems with genetic sensors onto paper, we have created a sterile and abiotic platform that can be utilized outside of laboratory conditions without concern over biosafety. Furthermore, the freeze-dried biomolecular components remain stable at room temperature, allowing for easy storage and distribution in global settings. Our application is easy to use, relying on a

colorimetric output that can be read by the naked eye or with a low-cost, battery-operated companion reader, and we are actively working to improve field-readiness via development of a third-generation reader with onboard capabilities for sample preparation and incubation.

The streamlined sensor development platform we describe here provides a generalizable method for a rapid response to any emerging outbreak. Our automated design process computationally screens for sequence specificity and feeds into a high-throughput protocol for rapid sensor prototyping *in vitro*. We have augmented our diagnostic sensors with an upstream target-amplification scheme that allows for detection of target sequences in the low femtomolar range, bringing sensor sensitivity in line with in-patient virus concentrations (Gourinat et al., 2015; Lanciotti et al., 2008).

With our goal of responding to the ongoing outbreak in a timely manner, we began our work using synthetic RNA fragments spiked into human serum, followed by engineered lentiviruses to mimic clinical samples. As with many proof-of-concept diagnostic studies, synthetic samples provided us with a powerful tool for optimizing our sensor platform ahead of the regulatory demands required for use of live pathogens (Antunes et al., 2015; Crannell et al., 2014; Rohrman et al., 2012; Stefan et al., 2016; Yen et al., 2015). Through collaborative efforts with the Zika virus community, we were able to test our platform on live Zika virus, and were pleased to find similar detection thresholds with Zika virus isolated from infected Vero cells (Figure 13B) and plasma samples from an infected rhesus macaque (Figure 13C and 13D). Our rapid response to the ongoing Zika virus outbreak and our ability to achieve clinically relevant sensitivity

and specificity highlight the utility and practicality of this platform technology.

Our synthetic biology pipeline for rapid sensor design and prototyping could be applied to a broad range of public health threats, allowing for rapid development of new diagnostics when and where they are most needed. The ease of *in vitro* sensor synthesis will allow for the widespread use of validated sensor sequences, aiding rapid global responses to current and future health crises. Finally, our ability to expeditiously design and implement our biomolecular diagnostics for an emerging pathogen using the engineering principles of synthetic biology suggests that the field will play an ever-increasing role in the support and improvement of human health.

CHAPTER SIX: METHODS

Relevant methods are highlighted in this chapter; full methods can be found in (Pardee, Green et al. 2016).

6.1 *In silico* sensor design and DNA synthesis

A set of 48 different toehold switch sensors and corresponding NASBA primers were generated using an integrated *in silico* design algorithm. See the Extended Experimental Procedures section in the Supplemental Information from (Pardee, Green et al. 2016) for full details.

6.2 DNA sensor assembly

Toehold switch constructs for the 48-sensor screen were amplified from synthetic DNA templates (Integrated DNA Technologies) and ligated to the *lacZ* reporter gene using PCR. For characterization of the top six toehold switches (Figure 7A), plasmids were constructed. The synthetic DNA templates were amplified using PCR and inserted into pET system parent plasmids (EMD Millipore) using Gibson assembly (Gibson et al., 2009) with 30 bp overlap regions. Plasmids for sensors 27B and 32B are available through Addgene (Addgene plasmid numbers: 75006 – 75011).

6.3 Cell-free reactions

Details of RNA sensor validation are described in Pardee et al. (2014). Briefly, amplified sensor DNA was column purified and tested on paper discs (2 mm) containing freeze-dried, cell-free reactions (NEB, PURExpress) in the presence or absence of trigger

RNA coding for a complementary region of the Zika virus genome (128 – 178 nts). The cell-free reactions consisted of: NEB Solution A (40%) and B (30%), chlorophenol red-β-D-galactopyranoside (Sigma, 0.6 mg/ml), RNase inhibitor (Roche, 03335402001; 0.5%), and linear DNA constructs encoding the toehold sensors (0.33 nM). The paper discs (Whatman, 1442-042) were blocked in 5% BSA overnight prior to use. The trigger RNA was produced using T7 RNAP-based transcription (Epicentre ASF3257) from linear DNA templates. Paper-based reactions (1.8 μl) were incubated at 37°C using either our companion electronic reader inside a humidified chamber or a plate reader (BioTek Neo). For the in-house reader, paper discs were placed into 2 mm holes in a removable acrylic chip; for the plate reader, paper discs were placed into black, clear bottom 384-well plates (Corning 3544).

6.4 NASBA

For NASBA reactions, the trigger elements (128 – 178 nts) were extended by 100 nts on the 5’ and 3’ ends with the relevant Zika genome sequence to provide suitable template RNAs. RNA amplicons were spiked into 7% human serum (Sigma H4522) where indicated. Reaction Buffer (Life Sciences NECB-24; 33.5%), Nucleotide Mix (Life Sciences NECN-24; 16.5%), RNase inhibitor (Roche, 03335402001; 0.5%), 12.5 μM of each NASBA primer (2%), nuclease free water (2.5%), and RNA amplicon (20%) were assembled at 4°C and incubated at 65°C for 2 min, followed by a 10-min incubation at 41°C. Enzyme Mix (Life Sciences NEC-1-24; 25%) was then added to the reaction (for a final volume of 5uL), and the mixture was incubated at 41°C for 2 hours unless noted

otherwise. For output reads with paper-based toeholds, the NASBA reactions were diluted 1:7 in water. For freeze-dried NASBA experiments, Enzyme Mix was lyophilized separately from the other components. The solution containing reaction buffer, nucleotide mix, RNase inhibitor, and primers was reconstituted in 15% DMSO, while the Enzyme Mix was reconstituted in nuclease-free water. Once reconstituted, the experiments proceeded as described above.

6.5 Lentivirus preparation and sample processing

HEK293FT cells (Life Technologies, R70007) used for virus packaging were cultured in DMEM supplemented with 10% FBS, 1% penicillin-streptomycin, and 4 mM GlutaMAX^{TM} (ThermoFisher Scientific). Twelve hours prior to transfection, 6.5 x 10^6 cells were seeded in a 10 cm dish. 7.5 µg psPAX2, 2.5 µg pMD2.G, and 10 µg pSB700 modified to include a Zika or Dengue RNA fragment were transfected using the HeBS-$CaCl_2$ method. Media was changed 12 hours post-transfection. Twenty-seven hours after changing media, viral supernatant was harvested and filtered using a 0.45 µm syringe filter. Viral supernatant was then purified with ViraBind Lentivirus Purification Kit (Cell Biolabs VPK-104) and buffer exchanged into 1xPBS with Lenti-X Concentrator (Clontech, 631231). Viral RNA concentration was quantified using QuickTiter Lentivirus Quantification Kit (VPK-112). Virus samples were spiked into 7% human serum at a final volume of 25 µl. Samples were heated to 95°C for 1 and 2 min and immediately used as input to a NASBA reaction.

6.6 Zika virus preparation and sample processing

100 µl of Zika virus isolate (MR 766) was utilized for infection of 10^6 Vero cells in 4 ml of media (DMEM supplemented with 2% fetal calf serum (FCS) and penicillin-streptomycin). The supernatant was removed after 2 h of incubation at 37°C and replaced with fresh media (DMEM, 10% FCS) for 48 h of infection. Cell debris was removed by centrifugation at 1500 rcf for 10 minutes, and aliquots of the virus were stored at -80°C until use. The virus was buffer exchanged into 1xPBS with Lenti-X Concentrator (Clontech, 631231). Virus titer was determined from virus purified with the QIAamp Viral RNA Mini Kit (Qiagen 52904), and confirmed with qRT-PCR. Virus titer corresponds to a multiplicity of infection of 6.7×10^7. Virus samples were spiked into 7% human serum at a final volume of 30 µl. Samples were heated to 95°C for 2 min and immediately used as input to a NASBA reaction. NASBA primers were re-designed to accommodate the MR 766 strain sequence (see Supplemental Information from (Pardee, Green et al. 2016)).

6.7 Calculation of fold change

The calculation of fold change for plate reader data was done by first subtracting the background absorbance measured from paper-based reactions that did not contain sensor DNA or trigger RNA. These normalized values were smoothed to reduce measurement noise using a three-point average of the time point and the data collected 10 minutes before and after. The minimum value of each well was then adjusted to zero. For data presented in Figures 3, 4 and 6, fold change was calculated from these zero adjusted

values by dividing the wells at each time point by the average signal from the corresponding sensor-alone control wells. For our initial sensor screen, we used a more sensitive measure of fold change based on the difference in the rate of color change between control and RNA trigger wells. This was done by calculating the rate of change in normalized absorbance (570 nm) values using slope; where, at each 10 min time point, the rate was calculated using $S_n = (T_{n+1} - T_n)/10$, where T is the normalized data at a time point (T_n) and the time point 10 min later (T_{n+1}), and S_n is the slope reported for T_n. Fold change was then calculated as above. MATLAB code provided in (Pardee, Green et al. 2016)

6.8 NASBACC

Reactions were performed in a 5 µL volume containing (NASBA buffer), 1 µL of a 250 nM Cas9 nuclease (NEB, M0386) and 250 nM purified gRNA (GeneArt precision gRNA synthesis kit, ThermoFisher Scientific, A29377) mix, 3 nM NASBACC primers, and 0.4 units of RNAse inhibitor (NEB, M0314). The forward NASBACC primer is composed of the reverse complement of the trigger H sequence (5’- GTT TGA ATG AAT TGT AGG CTT GTT ATA GTT ATG TTT-3’) and the forward binding sequence of the (region 32) NASBA primers. The reverse NASBACC primer contains the T7 promoter sequence (5'-CTA ATA CGA CTC ACT ATA GG-3’) followed by the reverse binding sequence of the (region 32) NASBA primers. The assembled reaction was incubated at 37°C for 2–6 h. For toehold activation assay on freeze-dried paper, NASBACC reactions were diluted 1:10 in nuclease-free water.

6.9 Zika virus challenge of macaques, plasma collection and processing

The virus stock was thawed, diluted in PBS to the appropriate concentration for each challenge, and loaded into a 1 mL syringe that was kept on ice until challenge. Animals were anesthetized as described above, and 1 mL of inocula was administered subcutaneously over the cranial dorsum. At the conclusion of the procedure, animals were closely monitored by veterinary and animal care staff for adverse reactions and signs of disease. Fresh plasma and PBMC were isolated from EDTA-treated whole blood by Ficoll density centrifugation at 1860 rcf for 30 min. The plasma layer was collected and centrifuged for an additional 8 min at 670 rcf to remove residual cells. The supernatant plasma was then filtered over a 0.45 µm syringe filter. Collected plasma was diluted 1:10 in nuclease free water. Diluted samples were heated to 95°C for two minutes and immediately added to a NASBA reaction as described above. NASBA was run for three hours.

BIBLIOGRAPHY

(2013). Antibiotic resistance threats in the United States, 2013. Centers for Disease Control and Prevention, U.S. Department of Health and Human Services, Office of Infectious Diseases.

Andrews, J. M. (2001). "Determination of minimum inhibitory concentrations." Journal of Antimicrobial Chemotherapy **48**(suppl 1): 5–16.

Archer, E. J., A. B. Robinson, et al. (2012). "Engineered E. coli that detect and respond to gut inflammation through nitric oxide sensing." ACS Synthetic Biology **1**(10): 451–457.

Barczak, A. K., J. E. Gomez, et al. (2012). "RNA signatures allow rapid identification of pathogens and antibiotic susceptibilities." Proceedings of the National Academy of Sciences of the United States of America **109**(16): 6217–6222.

Basu, S., Y. Gerchman, et al. (2005). "A synthetic multicellular system for programmed pattern formation." Nature **434**(7037): 1130–1134.

Braff, D., D. Shis, et al. (2016). "Synthetic biology platform technologies for antimicrobial applications." Advanced Drug Delivery Reviews **105**: 35–43.

Callura, J. M., C. R. Cantor, et al. (2012). "Genetic switchboard for synthetic biology applications." Proceedings of the National Academy of Sciences of the United States of America **109**(15): 5850–5855.

Callura, J. M., D. J. Dwyer, et al. (2010). "Tracking, tuning, and terminating microbial physiology using synthetic riboregulators." Proceedings of the National Academy of Sciences of the United States of America **107**(36): 15898–15903.

Cameron, D. E., C. J. Bashor, et al. (2014). "A brief history of synthetic biology." Nature Reviews. Microbiology **12**(5): 381–390.

Canton, B., A. Labno, et al. (2008). "Refinement and standardization of synthetic biological parts and devices." Nature Biotechnology **26**(7): 787–793.

Carlson, E. D., R. Gan, et al. (2012). "Cell-Free Protein Synthesis: Applications Come of Age." Biotechnology Advances **30**(5): 1185–1194.

Carroll, M. W., D. A. Matthews, et al. (2015). "Temporal and spatial analysis of the 2014–2015 Ebola virus outbreak in West Africa." Nature **524**(7563): 97–101.

Casini, A., M. Storch, et al. (2015). "Bricks and blueprints: methods and standards for DNA assembly." Nature Reviews. Molecular Cell Biology **16**(9): 568–576.

Chan, C. T., J. W. Lee, et al. (2016). "'Deadman'and'Passcode'microbial kill switches for bacterial containment." Nature Chemical Biology **12**(2): 82–86.

Chavez, A., J. Scheiman, et al. (2015). "Highly efficient Cas9-mediated transcriptional programming." Nature Methods **12**(4): 326–328.

Chen, Y., J. K. Kim, et al. (2015). "Emergent genetic oscillations in a synthetic microbial consortium." Science **349**(6251): 986–989.

Danino, T., O. Mondragon-Palomino, et al. (2010). "A synchronized quorum of genetic clocks." Nature **463**(7279): 326–330.

Dwyer, D. J., M. A. Kohanski, et al. (2007). "Gyrase inhibitors induce an oxidative damage cellular death pathway in Escherichia coli." Molecular Systems Biology **3**(1): 91.

Edgar, R., M. McKinstry, et al. (2006). "High-sensitivity bacterial detection using biotin-tagged phage and quantum-dot nanocomplexes." Proceedings of the National Academy of Sciences of the United States of America **103**(13): 4841–4845.

Egbert, R. G. and E. Klavins (2012). "Fine-tuning gene networks using simple sequence repeats." Proceedings of the National Academy of Sciences of the United States of America **109**(42): 16817–16822.

Elowitz, M. B. and S. Leibler (2000). "A synthetic oscillatory network of transcriptional regulators." Nature **403**(6767): 335–338.

Endo, Y. and T. Sawasaki (2006). "Cell-free expression systems for eukaryotic protein production." Current Opinion in Biotechnology **17**(4): 373–380.

Farzadfard, F. and T. K. Lu (2014). "Synthetic biology. Genomically encoded analog memory with precise in vivo DNA writing in living cell populations." Science **346**(6211): 1256272.

Friedland, A. E., T. K. Lu, et al. (2009). "Synthetic gene networks that count." Science **324**(5931): 1199–1202.

Galanie, S., K. Thodey, et al. (2015). "Complete biosynthesis of opioids in yeast." Science **349**(6252): 1095–1100.

Gardner, T. S., C. R. Cantor, et al. (2000). "Construction of a genetic toggle switch in Escherichia coli." Nature **403**(6767): 339–342.

Gibson, D. G., L. Young, et al. (2009). "Enzymatic assembly of DNA molecules up to several hundred kilobases." Nature Methods **6**(5): 343–345.

Gootenberg, J. S., O. O. Abudayyeh, et al. (2017). "Nucleic acid detection with CRISPR-Cas13a/C2c2." Science **356**(6336):438–442.

Green, A. A., P. A. Silver, et al. (2014). "Toehold switches: de-novo-designed regulators of gene expression." Cell **159**(4): 925–939.

Hasty, J., M. Dolnik, et al. (2002). "Synthetic Gene Network for Entraining and Amplifying Cellular Oscillations." Physical Review Letters **88**(14): 148101.

Hodgman, C. E. and M. C. Jewett (2012). "Cell-free synthetic biology: thinking outside the cell." Metabolic Engineering **14**(3): 261–269.

Holmes, E., J. Kinross, et al. (2012). "Therapeutic modulation of microbiota-host metabolic interactions." Science Translational Medicine **4**(137): 137rv136–137rv136.

Hwang, T. J., J. H. Powers, et al. (2015). "Accelerating innovation in rapid diagnostics and targeted antibacterials." Nature Biotechnology **33**(6): 589–590.

Isaacs, F. J., D. J. Dwyer, et al. (2004). "Engineered riboregulators enable post-transcriptional control of gene expression." Nature Biotechnology **22**(7): 841–847.

Kalghatgi, S., C. S. Spina, et al. (2013). "Bactericidal Antibiotics Induce Mitochondrial Dysfunction and Oxidative Damage in Mammalian Cells." Science Translational Medicine **5**(192): 192ra185–192ra185.

Kessel, M. (2015). "Why microbial diagnostics need more than money." Nature Biotechnology **33**(9): 898–900.

Khalil, A. S. and J. J. Collins (2010). "Synthetic biology: applications come of age." Nature Reviews. Genetics **11**(5): 367–379.

Khalil, Ahmad S., Timothy K. Lu, et al. (2012). "A Synthetic Biology Framework for Programming Eukaryotic Transcription Functions." Cell **150**(3): 647–658.

Kobayashi, H., M. Kærn, et al. (2004). "Programmable cells: interfacing natural and engineered gene networks." Proceedings of the National Academy of Sciences of the United States of America **101**(22): 8414–8419.

Kohanski, M. A., D. J. Dwyer, et al. (2007). "A common mechanism of cellular death induced by bactericidal antibiotics." Cell **130**(5): 797–810.

Kotula, J. W., S. J. Kerns, et al. (2014). "Programmable bacteria detect and record an environmental signal in the mammalian gut." Proceedings of the National Academy of Sciences of the United States of America **111**(13): 4838–4843.

Kwon, Y.-C. and M. C. Jewett (2015). "High-throughput preparation methods of crude extract for robust cell-free protein synthesis." Scientific Reports **5**.

Loessner, M. J., C. E. Rees, et al. (1996). "Construction of luciferase reporter bacteriophage A511::luxAB for rapid and sensitive detection of viable Listeria cells." Applied and Environmental Microbiology **62**(4): 1133–1140.

Lu, T. K., J. Bowers, et al. (2013). "Advancing bacteriophage-based microbial diagnostics with synthetic biology." Trends in Biotechnology **31**(6): 325–327.

Lu, T. K., A. S. Khalil, et al. (2009). "Next-generation synthetic gene networks." Nature Biotechnology **27**(12): 1139–1150.

Lu, T. K. and M. S. Koeris (2011). "The next generation of bacteriophage therapy." Current Opinion in Microbiology **14**(5): 524–531.

Mimee, M., Alex C. Tucker, et al. (2015). "Programming a Human Commensal Bacterium, Bacteroides thetaiotaomicron, to Sense and Respond to Stimuli in the Murine Gut Microbiota." Cell Systems **1**(1): 62–71.

Modi, S. R., J. J. Collins, et al. (2014). "Antibiotics and the gut microbiota." Journal of Clinical Investigation **124**(10): 4212–4218.

Mutalik, V. K., J. C. Guimaraes, et al. (2013). "Precise and reliable gene expression via standard transcription and translation initiation elements." Nature Methods **10**(4): 354–360.

Nakonieczna, A., C. J. Cooper, et al. (2015). "Bacteriophages and bacteriophage-derived endolysins as potential therapeutics to combat Gram-positive spore forming bacteria." Journal of Applied Microbiology **119**(3): 620–631.

Ng, K. M., J. A. Ferreyra, et al. (2013). "Microbiota-liberated host sugars facilitate post-antibiotic expansion of enteric pathogens." Nature **502**(7469): 96–99.

Pardee, K., A. A. Green, et al. (2014). "Paper-based synthetic gene networks." Cell **159**(4): 940–954.

Pardee, K., A. A. Green, et al. (2016). "Rapid, low-cost detection of Zika virus using programmable biomolecular components." Cell **165**(5): 1255–1266.

Qi, Lei S., Matthew H. Larson, et al. "Repurposing CRISPR as an RNA-Guided Platform for Sequence-Specific Control of Gene Expression." Cell **152**(5): 1173–1183.

Ro, D. K., E. M. Paradise, et al. (2006). "Production of the antimalarial drug precursor artemisinic acid in engineered yeast." Nature **440**(7086): 940–943.

Roberts, B. E. and B. M. Paterson (1973). "Efficient translation of tobacco mosaic virus RNA and rabbit globin 9S RNA in a cell-free system from commercial wheat germ." Proceedings of the National Academy of Sciences of the United States of America **70**(8): 2330–2334.

Ruder, W. C., T. Lu, et al. (2011). "Synthetic biology moving into the clinic." Science **333**(6047): 1248–1252.

Salis, H. M., E. A. Mirsky, et al. (2009). "Automated design of synthetic ribosome binding sites to control protein expression." Nature Biotechnology **27**(10): 946–950.

Schofield, D. A., C. T. Bull, et al. (2012). "Development of an Engineered Bioluminescent Reporter Phage for Detection of Bacterial Blight of Crucifers." Applied and Environmental Microbiology **78**(10): 3592–3598.

Schofield, D. A., I. J. Molineux, et al. (2009). "Diagnostic Bioluminescent Phage for Detection of Yersinia pestis." Journal of Clinical Microbiology **47**(12): 3887–3894.

Schofield, D. A., N. J. Sharp, et al. (2012). "Phage-based platforms for the clinical detection of human bacterial pathogens." Bacteriophage **2**(2): 105–283.

Shis, D. L., F. Hussain, et al. (2014). "Modular, multi-input transcriptional logic gating with orthogonal LacI/GalR family chimeras." ACS Synthetic Biology **3**(9): 645–651.

Slomovic, S. and J. J. Collins (2015). "DNA sense-and-respond protein modules for mammalian cells." Nature Methods **12**: 1085–1090.

Slomovic, S., K. Pardee, et al. (2015). "Synthetic biology devices for in vitro and in vivo diagnostics." Proceedings of the National Academy of Sciences of the United States of America **112**(47): 14429–14435.

Smartt, A. E. and S. Ripp (2011). "Bacteriophage reporter technology for sensing and detecting microbial targets." Analytical and Bioanalytical Chemistry **400**(4): 991–1007.

Smith, M. T., K. M. Wilding, et al. (2014). "The emerging age of cell-free synthetic biology." FEBS Letters **588**(17): 2755–2761.

Stricker, J., S. Cookson, et al. (2008). "A fast, robust and tunable synthetic gene oscillator." Nature **456**(7221): 516–519.

Sun, Z. Z., C. A. Hayes, et al. (2013). "Protocols for implementing an Escherichia coli based TX-TL cell-free expression system for synthetic biology." Journal of Visualized Experiments: JoVE(79).

Sun, Z. Z., E. Yeung, et al. (2013). "Linear DNA for rapid prototyping of synthetic biological circuits in an Escherichia coli based TX-TL cell-free system." ACS Synthetic Biology **3**(6): 387–397.

Tabor, J. J., H. M. Salis, et al. (2009). "A synthetic genetic edge detection program." Cell **137**(7): 1272–1281.

Tanji, Y., C. Furukawa, et al. (2004). "Escherichia coli detection by GFP-labeled lysozyme-inactivated T4 bacteriophage." Journal of Biotechnology **114**(1–2): 11–20.

Tawil, N., E. Sacher, et al. (2014). "Bacteriophages: biosensing tools for multi-drug resistant pathogens." Analyst **139**(6): 1224–1236.

Utsumi, R., R. E. Brissette, et al. (1989). "Activation of bacterial porin gene expression by a chimeric signal transducer in response to aspartate." Science **245**(4923): 1246–1249.

Weber, W. and M. Fussenegger (2012). "Emerging biomedical applications of synthetic biology." Nature Reviews. Genetics **13**(1): 21–35.

Yang, L., A. A. K. Nielsen, et al. (2014). "Permanent genetic memory with >1-byte capacity." Nature Methods **11**(12): 1261–1266.

CURRICULUM VITAE